UNIVERSITY OF THE WITWATERSRAND, JOHANNESBURG

Application of Multiple Point Statistics and Direct Sampling Simulation for Resource and Reserve Estimation Under Grade Uncertainty

Student Name: Mahlomola Isaac Mabala

(Student Number: 0312836R)

School of Mining Engineering

Johannesburg, South Africa.

MSc (50/50)	MSc by Research Only	PhD
X		

Supervisors: Prof. Richard Minnitt, Prof. Christina Dohm

A research dissertation submitted to the Faculty of Engineering and the Built Environment, University of the Witwatersrand, in fulfilment of the requirements for the degree of Masters in Engineering

Date: 22 September 2021

DECLARATION

I declare that this report is my own, unaided work. I have read the University Policy on Plagiarism and hereby confirm that no plagiarism exists in this report. I also confirm that there is no copying nor is there any copyright infringement. I willingly submit to any investigation in this regard by the School of Mining Engineering and I undertake to abide by the decision of any such investigation.

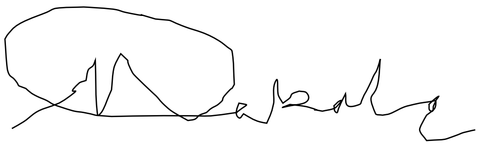

Signature of Candidate

22/09/2021

Date

ABSTRACT

Traditional grade estimation techniques produce single versions of grade distribution of a Mineral Resource. These approaches do not sufficiently provide a means to quantify the uncertainty around the estimates. Furthermore, the application of these methods when the sampling density is low such as in mine/pit extension areas results in the underrepresentation of spatial variation and generates unsatisfactory results. The research project aims to test and provide a proof of concept about the applicability of direct sampling simulation (DeeSse) in grade estimations and related uncertainty quantification, particularly in areas with sparsely spaced drill holes. The area with scarce data at Tarkwa mine is in the pit extension area (EA) where diamond drill holes are at 200 m x 100 m x 3 m spacing. However, there is sufficient closely spaced grade control data in the nearby Akontansi pit at a grid spacing of 25 m x 25 m x 3 m. These closely spaced samples were used to create a training image (TI) on 10 m x 10 m x 3 m blocks using simple kriging. All subsequent simulations were run on the same support. The TI was validated by comparing it to the etype estimate of 50 Sequential Gaussian Simulations (SGSIM) which were conditioned to the same data as the TI. Fifty DeeSse simulations were then run in the TI area using data spaced on a 50 m x 50 m x 3 grid. The DeeSse etype estimate was then validated by comparing it to a SGSIM etype estimate of 50 SGSIM simulations conditioned to the same data as DeeSse. DeeSse was found to be generally comparable with SGSIM with some minor bias. DeeSse reproduced a larger range of grade values while SGSIM showed more local variability. Several opportunities for possible improvement of the TI and simulations were identified. Nonetheless, the TI and the application of DeeSse were deemed valid for the purpose of the study.

Following the application of DeeSse within the TI area, it was then implemented and validated using SGSIM in the EA. The subsequent DeeSse simulations from the EA were then used to quantify the uncertainty around the grades, tonnages, metal, and revenue estimates. DeeSse was found to provide a more robust approach that offered more confidence in the estimates. It was therefore concluded that DeeSse can be successfully applied in areas with sparse data to generate resource models with more confidence. However, its success largely dependent on the ability to produce a representative TI.

DEDICATION

I would like to dedicate this work to my wife Cindy Mabala and our daughter Niara Mabala. Thank you for your unwavering support and encouragement as well as allowing me to spent hours away from our family while I pursue my studies. Above all, I would like to dedicate this work to the Lord All Mighty who through His grace has given me the ability to finish this task. May He receive all glory, forever and ever, Amen!

ACKNOWLEDGEMENTS

I would firstly like to acknowledge and thank my supervisors Prof. Richard Minnitt and Prof. Christina Dohm for their willingness and patience in imparting the necessary knowledge and providing the much-needed guidance throughout this project. I would also like to thank Dr. Winfred Assibey-Bonsu, Mr. Matthew Aboagye and Mr. Tyson Mutobvu from Goldfields for their assistance during the completion of this study. Thirdly, I would like to acknowledge and thank Dr. Julien Straubhaar and Prof. Phillipe Renard from the University of Neuchatel for the training and assistance provided regarding the use of DeeSse algorithm and the Ar2Gems software. Finally, I owe my sincere gratitude to Goldfields and the University of the Witwatersrand's School of Mining Engineering for allowing me to participate in this project and for providing the necessary resources to make this study possible.

TABLE OF CONTENTS

LIST OF FIGURES

LIST OF TABLES

LIST OF SYMBOLS

x	coordinate location vector
$E[Z(x)]$	expected value of a random function
h	lag distance
z	sample or observation of Z
$Z\ (x)$	random variable Z at location x
$\gamma\ (h)$	semi-variance
λ	Lagrangian multiplier
$d\{dn(x), dn(y)\}$	distance between data events in the training image and simulation grid
σ^2	variance

LIST OF ACRONYMS AND ABBREVIATIONS

Block Variance	BV
Central Processing Unit	CPU
Conditional Cumulative Probability Distribution Function	ccdf
Cross-Correlation Based Simulation	CCSIM
Cross-Correlation Function	CCF
Cumulative Distribution Function	cdf
Direct Sampling	DeeSse
Exploratory Data Analysis	EDA
Extended Normal Equation Simulation	ENESIM
Extension Area	EA
Filter-based Simulation	FILTERSIM
Gold	Au
High-order Simulation Algorithm	HOSIM
Hybrid Pixel- and Pattern-Based Simulation	HYPPS
Improved Parallel Multiple-point Algorithm	IMPALA
Inverse Distance Weighting	IDW
Kriging Efficiency	KE
Kriging Neighbourhood Analysis	KNA
Kriging Variance	KV
Mean Absolute Percentage Error	MAE%

Mine Call Factor	MCF
Multiple-Point Statistics	MPS
Net Present Value	NPV
Normal Score	NSCORE
Ordinary kriging	OK
Quality Assurance and Quality Control	QA/QC
Reverse Circulation	RC
Single Normal Equation Simulation	SNESIM
Selective Mining Unit	SMU
Sequential Gaussian Simulation	SGSIM
Sequential Indicator Simulation	SISIM
Simple Kriging	SK
Simulated Annealing	SA
Simulation Grid	SG
Simulation of Pattern	SIMPAT
Slope of Regression	SLOR
Three-Dimensional	3D
Training Image	TI
Unique Pattern-growth Algorithm	GROWTHSIM

1 CHAPTER I: INTRODUCTION

1.1 Purpose of the Study

Traditional geological modelling and grade estimation techniques produce single versions of lithological domaining and grade distribution of a Mineral Resource. These approaches do not sufficiently provide a means to quantify the uncertainty around the estimates. Uncertainty quantification should be of paramount importance in resource and reserve estimation since the size, geometry, grade, and/or spatial positions of the geological units are not perfectly known (van der Grijp & Minnitt, 2015). Furthermore, the application of current kriging methods when the sampling density is low such as in mine/pit extension areas results in the underrepresentation of spatial variation and generates unsatisfactory results (Mariethoz, 2018). As a result, alternative methods that can generate robust estimations and quantify uncertainties around the estimates, particularly in areas with sparsely spaced drill holes, need to be investigated and tested.

The purpose of this study is to investigate and evaluate the benefits of integrating grade uncertainty of an orebody into resource estimation by:

- Developing a TI for grades using closely spaced grade control data.
- Modelling and quantifying grade uncertainty in a pit extension area (EA) with low sampling density, through the use of the TI and the novel Direct Sampling (DeeSse) Multiple Point Statistics (MPS) algorithm.
- Integrating the subsequent uncertainty models into grade/tonnage curves and metal content calculations.

The study aims to provide a proof of concept for the application of DeeSse for stochastic resource modelling in areas where the sample size is small. This research study is confined to a geological domain of the Akontansi pit at Tarkwa mine and specifically the A1 reef horizon. The simulations are based in section of the pit and within a portion of the extension area of the mine. The locality maps of the pit and the mine are shown in Figures 1.1 and 1.2. The Tarkwa gold mine is located four kilometres west of the town of Tarkwa which is in the south-western region of Ghana, 300 km from the capital city Accra.

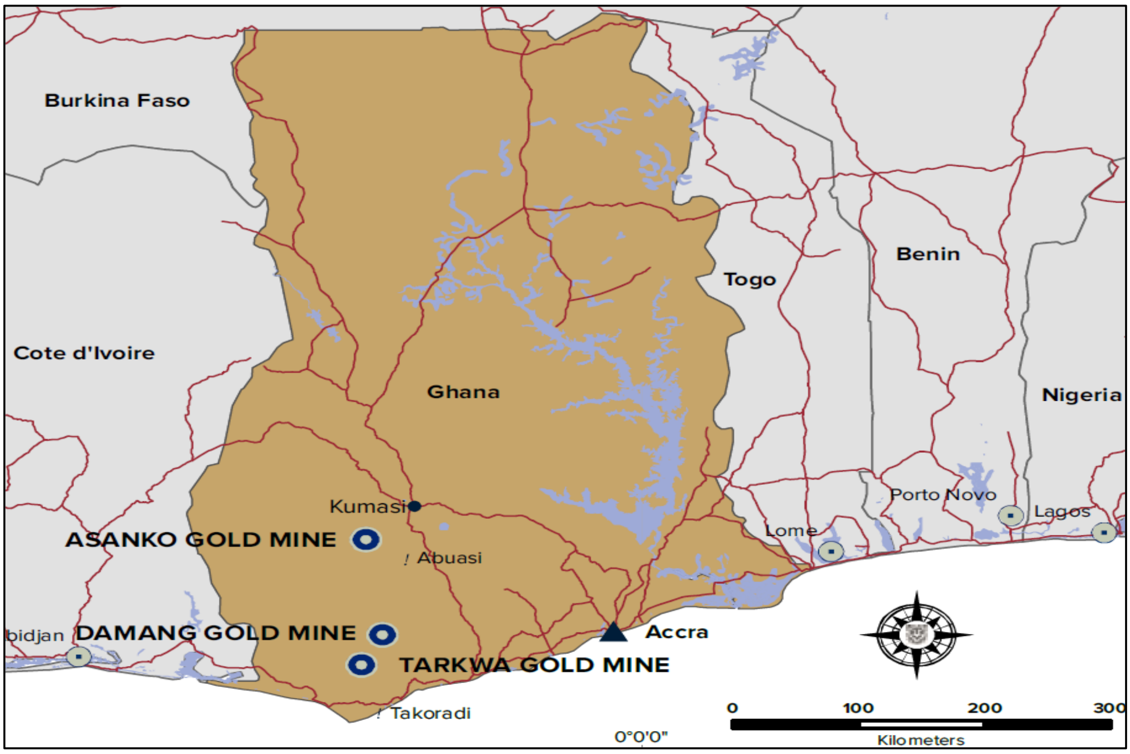

Figure 1.1: Tarkwa mine location map (Goldfields, 2019)

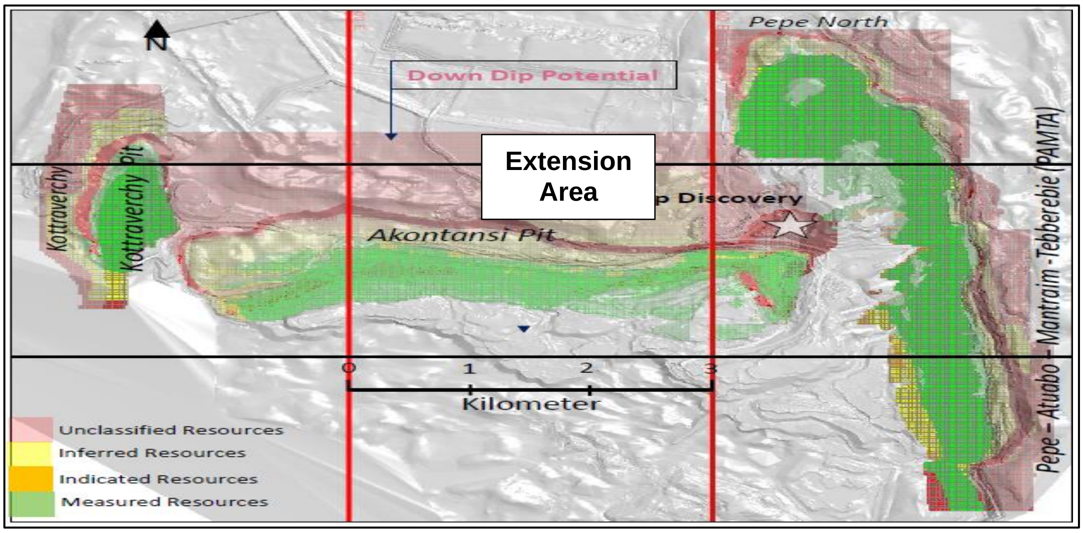

Figure 1.2: Location of the Akontansi pit (Holland, 2020)

1.2 Regional Geology

The Tarkwa ore bodies are located within the Tarkwaian system. This system dominates the stratigraphy of the Ashanti belt in south-west Ghana. The Ashanti belt strikes north-easterly. It is primarily a synclinal structure made of Lower Proterozoic sediments and volcanics. These are underlain by metavolcanics and metasediments of the Birimian system. The contact between the Birimian and the Tarkwaian is marked by zones of intense shearing. This contact is host to a large number of gold deposits. The Tarkwaian is characterised by lower intensity metamorphism and is predominated by coarse grained immature sedimentary units (van der Westhuizen, et al., 2011). The regional geology of the Tarkwa orebody is summarised in Table 1.1:

Table 1.1: Regional geology of Tarkwa mine (van der Westhuizen, et al., 2011)

Group	Series	Thickness (m)	Lithology
Tarkwaian (youngest)	Huni	1370	Minor phyllites, quartzites
	Tarkwa Phyllite	120-400	Schist, chloritic and sericitic phyllites
	Banket	120-160	Conglomerates, grits and quartzites.
	Kawere	250-700	Conglomerates, grits and quartzites.
Birimian (oldest)	Birimian		Sediments, volcaniclastics and meta-volcanics

1.3 Local Geology

The local geology at Tarkwa is dominated by the Banket series, separated by a sequence of mineralised conglomerates and pebbly quartz. The Banket series varies in thickness between 32 m to 270 m (van der Westhuizen, et al., 2011). The diagram in Figure 1.3 represents the stratigraphy of the Tarkwa deposit:

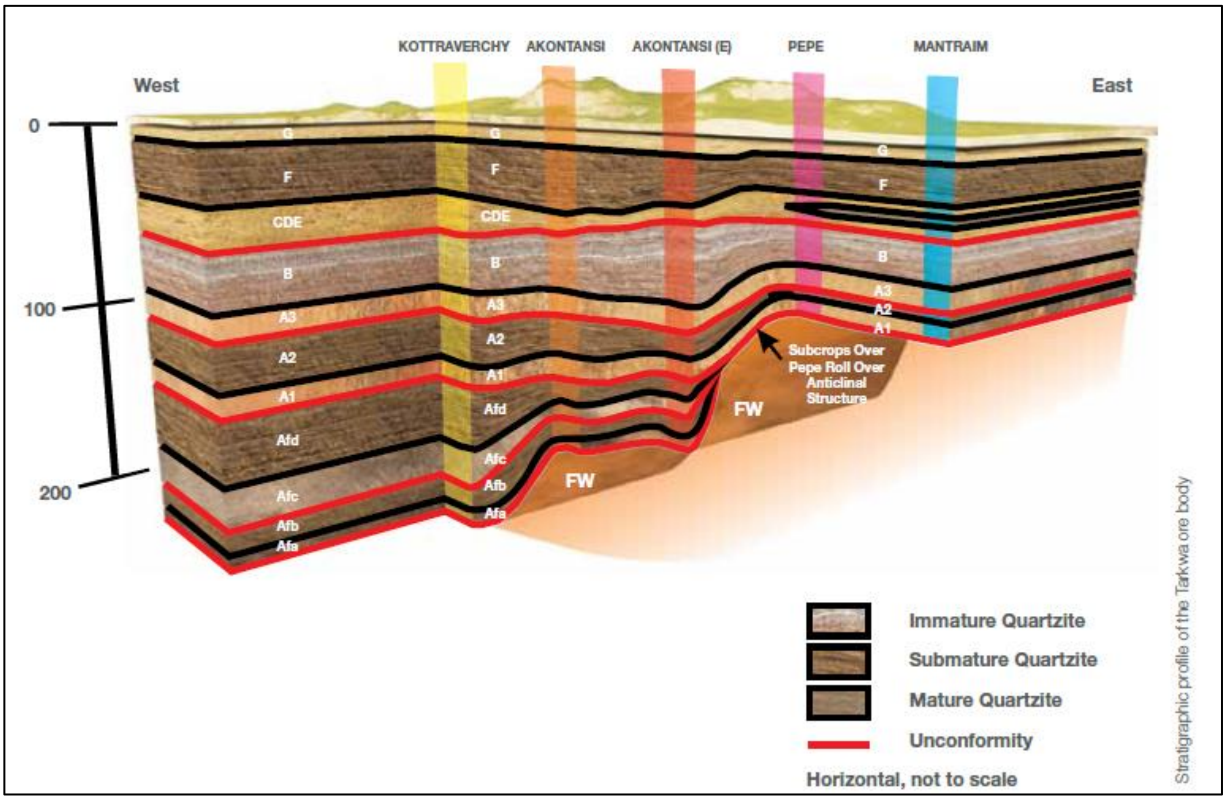

Figure 1.3: Stratigraphic profile of the Tarkwa orebody (van der Westhuizen, et al., 2011)

The gold is mineralised as free particles with an average size of between 50-150 μm. The mineralised reefs are categorised as follows (from the base going upwards) (van der Westhuizen, et al., 2011):

- AFc — 0.2 m and 3.0 m thick, only occurs in the west and is scoured by the A1 in the east.
- A1 — between 2.0 m and 7.0 m thick, moderately to poorly sorted conglomerate and thin quartzites with occasional visible gold. This research will be conducted within the A1 reef horizon. The simulation is limited within this layer as it is the only layer with a rotated training image dataset and conditioning data available at the time of the research. The A1 reef zone dips between 12 and 18 degrees.
- A3 — occurs up to 7.0 m thick and is moderately sorted.
- B2 (or B) — up to 3.0 m thick and is made up of very coarse quartzites with thin layers of sub-rounded pebble conglomerate.

- CDE — up to 8.0 m thick and can be subdivided into the lower C reef and upper E reef both of which are conglomeratic and are separated by the D reef quartzite.
- G — varies from 2.0 m to 6.0 m thick poorly sorted conglomerate with clasts of quartzite and phyllite.

1.4 Research Background

The development and application of geostatistics for resource evaluation can be summarised into four categories: Classical methods, two-point linear geostatistics, non-linear geostatistics and multi-point geostatistics:

<u>Classical Methods (pre-1945):</u>

Watermeyer (1919) and Truscott (1929) as cited in Krige (1999), were the pioneers of Mineral Resource estimation in South African gold mines by applying classical statistics for gold ore evaluation. These methods were primarily based on the symmetrical normal distribution of gold grades. However, the gold grade distributions were later shown to be positively skewed instead. As a result, large discrepancies between the estimates and Mine Call Factor (MCF) were observed (Krige, 1999).

The major classical estimation techniques developed over time from then onwards included the polygonal -, triangulation -, cross sectional - and inverse distance weighting (IDW) - methods. The major limitations of these approaches are lack of definitive ways to address estimation confidence, decision on number of samples to use, choice of a search radius, change of support and anisotropy (Clark & Harper, 2000; Dohm, 2019).

<u>Two-point Linear Geostatistics (1945-1965):</u>

Sichel (as cited in Matheron & Kleingeld, 1987) pioneered the application of a lognormal distribution of gold grades. Krige followed Sichel's work by applying a regression analysis between sampling and mining blocks for resource estimation

(Krige, 1951). Krige (1960) also played a major role in the development of the 3-parameter lognormal model to deal with long tailed positively skewed distributions. Matheron (as cited in Matheron & Kleingeld, 1987), subsequently developed the use of the variogram to define the spatial structure in his 1965 PhD thesis. Matheron further developed mathematical equations for kriging based on earlier work by Krige and De Wijs. Kriging is a variant of the basic linear regression techniques allowing estimation of a single regionalised variable at unsampled locations. Kriging provides the best unbiased linear estimate because the estimate minimises the estimation error (Matheron, 1971).

During this period, Ross (1950) cited in Krige (1999), introduced the concept of the role of support in geostatistics. Support refers to the physical ore parcel which supports the ore grade being studied as a variable (Krige, 1999).

The following two-point linear geostatistical methods are currently in use (Rossi & Deutsch, 2014):

- Simple kriging (SK): Allows for the determination of optimal weights that minimise the expected error variance. The mean is a known constant inferred from samples for the entire domain.
- Ordinary kriging (OK): Also based on the minimum error variance for the linear estimate by constraining the sum of the weights to 1. Unlike the simple kriging method, the mean does not have to be known, but a covariance of a stationary variable is required.
- Universal kriging (Kriging with a trend model): Estimates residuals from a specified location-dependent mean.
- Kriging with an external drift: This is a variant of kriging with a trend wherein the trend model is scaled from a secondary variable.
- Factorial kriging: The random function model is split into independent components which are then separately estimated. Factorial kriging is of value to researchers interested in imagery analysis.

- Block kriging: The mean value of a variable over a local area is estimated instead of a point location by discretising a block into many points which are estimated using the point kriging and then averaged within the block.

The major drawbacks of these methods are the over-smoothing of the results and the inability to satisfactorily quantify uncertainty of the estimates for reserve modelling (Albor Consuegra & Dimitrakopoulos, 2010).

<u>Two-point Non-linear Geostatistics (1966-1994)</u>:

In order to attach some reliable measures of uncertainty to block estimates, non-linear methods were developed. Non-linear geostatistics involve directly predicting the variability/uncertainty in the mining blocks based on a probability distribution model (Rossi & Deutsch, 2014). These methods attempt to estimate the conditional expectation as well as the conditional distribution of grade at a location instead of just predicting the grade itself (Vann & Guibal, 2001).

The following major non-linear geostatistical methods were developed during this period (Vann & Guibal, 2001):

- Disjunctive Kriging,
- Indicator Kriging and variants (e.g. Multiple Indicator Kriging; Median Indicator Kriging, Residual Indicator Kriging, etc.),
- Probability Kriging,
- Lognormal Kriging,
- Multi-Gaussian Kriging,
- Uniform Conditioning and

In the same period, concepts around change of support, the transfer function, parameterisation of reserves and the selectivity of distributions were introduced (Matheron & Kleingeld, 1987).

Non-linear geostatistics also allowed for the development of multivariate (cokriging) techniques such as simple cokriging, ordinary cokriging and collated cokriging. Cokriging is estimation using data defined by different attributes. For examples gold grades can be estimated from a combination of gold and copper sample values (Rossi & Deutsch, 2014).

Furthermore, conditional simulation methods were developed to quantify joint uncertainty between multiple realisations. This allows for a more complete representation of block uncertainty and the uncertainty between multiple block locations (Deutsch & Journel, 1997). Examples of popular simulation methods are sequential Gaussian simulation (SGSIM), sequential indicator simulation (SISIM), covariance (LU) decomposition, turning bands, truncated Gaussian and Plurigaussian simulations (Vann, et al., 2002). However, these methods were found to be sub-optimal for reproducing complex and heterogeneous models (Tahmasebi, 2018).

Multi-point Geostatistics (1993 – Current):

In an attempt to address the shortcomings of kriging and conditional simulations, multiple-point statistical methods were developed. Guardiano and Srivastava (1993, cited in Mariethoz and Caers, 2014) were the first to propose an idea to infer conditional probability distribution directly from a TI using Extended Normal Equation Simulation (ENESIM). This was the first MPS algorithm. MPS is an alternate approach to variogram-based geostatistics whereby TIs are used to "*estimate the conditional probability at interpolation location given the observed and the already interpolated data"*. A training image is a conceptual image (or dataset) that defines a 3D numerical rendering of interpreted geological attributes (Mariethoz & Caers, 2014; Tahmasebi, 2018).

Various MPS algorithms are continually being developed and are summarised in Section 2.7. The major advantage of these methods is their ability to quantify geological risks and integrate these risks into the resource estimation even when dealing with heterogeneous conditions. Due to the use of TIs together with hard conditioning data, MPS can be applied sufficiently in extremely under-informed conditions (Mariethoz, 2018). MPS techniques also avoid the excessive smoothing of results as compared to kriging-based simulations (Garcia, 2016).

1.5 Problem Statement

The current resource and reserve estimation methods used at Tarkwa mine do not properly account for the inherent grade uncertainty. This is because the resource model developed is deterministic. Deterministic models merely aim to provide an optimal estimate together with an associated error variance. These models do not seek to evaluate the uncertainty linked to the unknown grade. As such, they do not adequately account for geological uncertainty (Chanderman, 2017). This means that the risks associated with achieving or not achieving estimated grades, tonnages and associated metal content is not well understood. This lack of an optimal framework for uncertainty quantification limits the ability to adequately mitigate orebody risk, produce better reserve depletion plans and make more informed decisions. The kriging-based methods currently being used at Tarkwa also cause over-smoothing of results and do not adequately represent local variability, particularly where the sampling density is low.

Additionally, the EA towards the north of the Akontansi pit (see Figure 1.2) has been diamond drilled at sparsely spaced grid intervals of 200 m x 100 m x 3 m. Thus, the use of kriging-based methods in this under-informed area has proven to be sub-optimal. The scarce hard data in the extension makes it difficult to infer the parameters of a covariance model.

However, there is plenty of grade control sample data drilled at 25 m x 25 m x 3 m grid spacing available in the adjacent pit area. The abundant sample data in the pit area allows for the development of a representative training image which can be used in the application of MPS for resource estimation within the EA. MPS could address the challenges of kriging-based methods such as not being able to adequately quantify uncertainty, limitations of estimating in poorly informed areas and over-smoothing of results.

This research aims to model and quantify grade uncertainty using the direct sampling MPS algorithm in a pit EA with low sampling density. The TI required by MPS will be in the form of a 10 m x 10 m x 3 m block support kriged-model estimated from the 25 m x 25 m x 3 m grade control sample data. Consequently, the resultant uncertainty would be integrated into the calculation of grade tonnage curves and metal content calculations. The DeeSse results will be validated using another kriging-based simulation technique, i.e. SGSIM. The research is confined to a domain within the Akontansi pit at Tarkwa mine.

1.6 Assumptions

It is assumed that the data provided for the development of the TIs and conditioning data are validated representations of the geology and spatial grade distribution of the area of study. The TI and the variogram of the grade control data are assumed to both represent the underlying spatial structure in the TI and EA. It is also assumed that the data provided by the mine is the most recent and that the database has been subject to a rigorous quality assurance and quality control (QA/QC) system. It is further assumed that the only uncertainty in this study arises from natural grade variability in the deposit and is not due to bias or errors associated with sampling or analytical procedures. It is also assumed that the geological structures and contacts within the area of study are generally understood and do not require further analysis. Hence, the focus is only modelling grade uncertainty.

1.7 Research Questions

The research aims to answer the following questions:

- How can the use of direct sampling MPS techniques enhance resource modelling for the extension area of the Akontansi pit at Tarkwa mine?
- How can stochastic resource estimation be integrated into grade-tonnage curves, metal content calculations and revenue projections?

1.8 Research Objectives

The main aim of this study is to investigate and evaluate the benefits of integrating grade uncertainty of an orebody into resource estimation by using the novel Direct Sampling Multiple Point Statistics algorithm. By so doing, the study will serve as a proof of concept for the application of DeeSse for stochastic grade estimation in areas with low sampling density. The following objectives will have to be fulfilled to achieve the purpose of this study:

- Review the literature on both geological uncertainty, kriging-based and multiple-point geostatistical estimation and/or simulation methods.
- Develop and validate a TI within a pre-determined geological zone and reef horizon (A1 reef) using closely spaced grade control data.
- Model the gold deposit by using the TI and DeeSse to simulate grade distributions within the A1 reef horizon in the pit extension area which has low sampling density.
- Integrate the uncertainty grade models into calculations of grade and tonnage curves, metal content and revenue projections.
- Validate the DeeSse simulations by using SGSIM within the same area.
- Compare results from both DeeSse and SGSIM.
- Draw conclusions from the study and make recommendations for future work.

1.9 Research Methods

The area of study is divided into two parts, i.e., the TI area and the EA as shown in Figure 1.4. The TI area comprises of closely spaced 25 m x 25 m x 3 m grade control reverse circulation (RC) drill holes composited at 1 m intervals within the pit area. The RC holes were used to create 10 m x 10 m x 3 m OK and SK block estimates within a 650 m x 580 m x 72 m model block model representing possible TIs. Following the comparison of the TIs, the SK TI was subsequently chosen as a TI to be used in this study. Fifty SGSIM simulations were then run using samples from the 25 m x 25 m x 3 m input grid and on the same support as the TI. The SK TI was then validated by comparing it to the SGSIM etype estimate of the 50 simulations.

From the closely spaced RC holes within the TI area, a subset of drills holes at 50 m x 50 m x 3 m grid spacing was also extracted. Fifty DeeSse and SGSIM simulations were run on a block support of 10 m x 10 m x 3 m using the input data from the 50 m x 50 m x 3 m grid. The resultant DeeSse etype estimate was compared to the SGSIM etype estimate in order to validate the application of the DeeSse technique on a wider spaced sampling grid within the TI Area.

Following the validation of the TI and DeeSse, 50 DeeSse and SGSIM simulations were then run in the EA using exploration drill hole samples at 200 m x 100 m x 3 m grid spacing. These were vertical surface drill holes composited at 1m intervals. The DeeSse and SGSIM etype estimates were subsequently compared in order to validate the results. Since the A1 reef horizon ranges from 2m to 7m, between 2 and 7 samples are expected per drill hole.

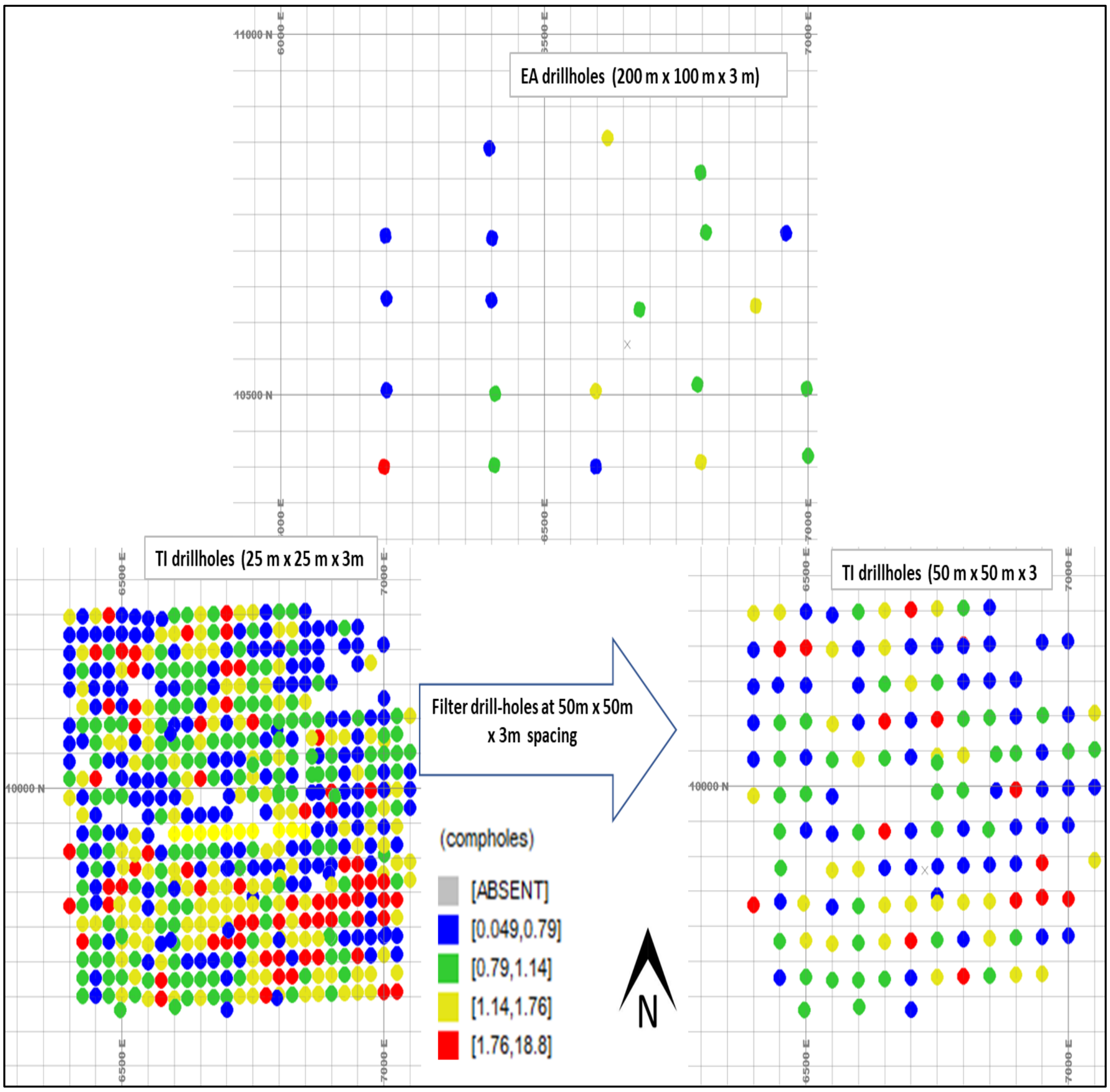

Figure 1.4: Plan view of the drill holes in the EA and the TI in the pit

Prior to using the drill hole data, it was first rotated so that the plane of the data is flat instead of inclined. This was carried out to enable the proper functioning of the DeeSse algorithm. When an inclined plane is used, DeeSse gives an error that there are too many undefined nodes. This is because DeeSse requires that either a cuboid or a cube-shaped 3D-grid is fitted to the training image data. However, just fitting either a cuboid or a cube to encompass the inclined data results in many undefined nodes above and below the plane of the data. As a result, the data had to be initially rotated before any estimations or simulation could be undertaken. In order to achieve the objectives of this report, the following methodology (which is detailed in Chapter 2 and 3) was followed:

- Literature review:
    - A review of key concepts, theories, and studies.
    - A review of key debates and controversies.
- Sample analysis:
    - Calculation of descriptive statistics for the three given datasets.
    - Cleaning and validation of data.
    - Updating descriptive statistics for the cleaned and validated data to identify and confirm any statistical changes due to the cleaning and validation process.
    - Distribution analysis.
- Geological modelling (no geo-domaining carried due to the data being extracted from pre-defined domain):
    - Wireframe implicit modelling.
    - Prototype modelling and block modelling.
- Development of training image on 10 m x 10 m x 3m block support using 25 m x 25 m x 3 m samples.
    - Variography (Experimental variogram calculations and modelling).
    - Investigation of anisotropic directions.
    - Kriging Neighbourhood Analysis (KNA).
    - Estimation (OK and SK)
    - Deciding on which model to use as final the TI.
- Training image validation:
    - Running 50 SGSIM simulations in the TI area on the same support and input data as TI.
    - Comparing SGSIM etype estimate (average) model to the TI.
- Application and Validation DeeSse in the TI Area based on 10 m x 10 m x 3 m block support and 50 m x 50 m x 3 m input data:
    - Running 50 DeeSse simulations in the TI area.
    - Running 50 SGSIM simulations in the TI area.
    - Comparing DeeSse etype estimate to the SGSIM etype estimate (average).

- Estimation using DeeSse and validating DeeSse results in EA grid based on 10 m x 10 m x 3 m block support and 200 m x 100 m x 3 m input data:
    - Estimate using DeeSse and SGSIM in the EA grid.
    - Comparing DeeSse- and SGSIM etype estimate models within the EA.
- Stochastic resource estimation using DeeSse in the EA (200 m x 100 m x 3 m input data and 10 m x 10 m x 3m block support):
    - Uncertainties around estimates of the grade realisations.
    - Probabilities above and below thresholds from the simulations.
    - Stochastic grade tonnage curves.
    - Uncertainties around metal content estimates.
    - Uncertainties around revenue estimates.

Datamine StudioRM software was used for the creation of the TIs and the running of SGSIM while Ar2Gems was used for the running the DeeSse simulations. StudioRM is chosen because it is the software being used for resource estimation at Tarkwa mine. Ar2Gems was chosen because it featured the DeeSse algorithm and was offered at no charge for research purposes.

1.10 Significance of the Study

Although kriging-based techniques are commonly being applied in Mineral Resource estimation, they have some limitations. These limitations include over-smoothing of results, inadequate quantification of uncertainty and sub-optimal estimates. These limitations are exacerbated in areas where the sample data is scarce or drill spacing is excessively sparse. Even though conditional simulation techniques were developed to overcome some of these challenges, kriging-based simulations are still limited when dealing with complex and heterogeneous conditions. These techniques also inherently carry the limitations of variogram modelling when sample data is scarce.

Stochastic resource estimation using DeeSse provides a method for resource estimation whereby the grade uncertainty at each location is quantified. The uncertainty could then be integrated into reserve modelling. The use of a training image developed from closely spaced grade control data allows for optimal resource estimation in under-informed areas such as the Akontansi pit extension area.

The following benefits can also be achieved by Tarkwa mine through the application of DeeSse:

- Better understanding of the uncertainty around the estimated grades,
- Optimal platform for practical risk analysis and ore body risk mitigation,
- Integration of the improved forecasts into short- and long-term business planning and decision making,
- Better profiling of Au kilograms at risk in operational, business, and strategic plans and,
- Improved cash flow risk analysis and sensitivities.

Application of the DeeSse algorithm for quantification of uncertainty has not been adequately tested in paleoplacer gold deposits such the one at Tarkwa mine. The motivation of this research is to test the viability of applying these stochastic methods to harness the benefits associated with risk-based resource and reserve estimation.

1.11 Structure of the Report

The report has been divided into six chapters, namely:

Chapter I: Introduction: This chapter deliberated on the purpose and significance of the study, research background, the problem statement, research objectives and critical research questions. Lastly, the chapter provided a preview of the research methods and structure of the report.

Chapter II Literature Review: This chapter guides the reader through the relevant literature that has motivated this study as well as recent works related to similar studies.

Chapter III Research Methodology: This chapter describes the methodologies developed for the study and outlines the various tests that were carried out.

Chapter IV Results and Analysis of Results: The results of the methods are presented as tables and figures in this chapter and then analysed.

Chapter V Overall interpretations of the results are discussed with a focus on answering the fundamental research questions and objectives.

Chapter VI Conclusion and Recommendations: General research conclusions are presented in this chapter which closes with recommendations for future work.

2. CHAPTER II: LITERATURE REVIEW

2.1. Introduction

In this chapter relevant literature covering key aspects of the research are detailed. Brief explanations of the techniques used in this study are given. Important practical considerations when applying these techniques are communicated in order to aid in the methodology followed. The advantages and limitations of these methods are also highlighted together with relevant case studies. The chapter also attempts to identify the need and validity for this study by analysing similar studies in literature and identifying relevant learnings and gaps. Literature review and introduction of key concepts such as geological uncertainty, theory of regionalised variables, kriging, OK, SK, SGSIM, MPS, DeeSse and stochastic modelling are discussed.

2.2. Geological Uncertainty

Geological and resource modelling is accompanied by various sources of uncertainty. Research into geological uncertainty has grown in recent years. Nevertheless, adequate quantification and reporting of these associated uncertainties are rarely carried out in practice (Kitts, 1976; Mann, 1993; Bardossy & Fodor, 2001; De Souza, et al., 2004; Pérez-Díaz, et al., 2020). Bardossy and Fodor (2001) and Pérez-Díaz, et al. (2020) highlight that uncertainty is usually confused with error in geological articles. Bardossy and Fodor (2001) define uncertainty as the recognition that the results of measurements/observations may deviate slightly from the natural reality. Alternatively, Pérez-Díaz et al., 2020, define uncertainty as the consequence of the mismatches between available knowledge and the knowledge required for decision making. On the other hand, error is defined as the difference between the true value and an estimated value (Bardossy & Fodor, 2001; Pérez-Díaz, et al., 2020). Figure 2.1 is a visual representation of the difference between uncertainty and error:

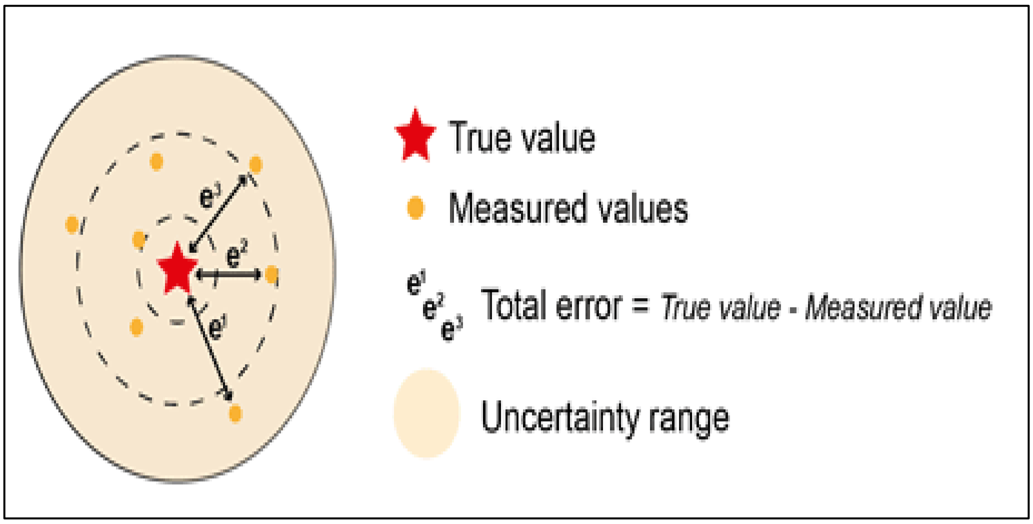

Figure 2.1: Difference between uncertainty and error (Pérez-Díaz, et al., 2020)

Since any parameter of the geological object, phenomenon or process can be a source of uncertainty, it is practically impossible to identify all of them (Bardossy & Fodor, 2001). Nonetheless, Mann (1993), classified these sources into several categories which are:

- Inherent variability of geological objects.
- Sampling-, observation-, and measurement- errors as well as the propagation of errors.
- Errors from the mathematical evaluation of geological data. The most usual source being from insufficient number of samples.
- Conceptual and model uncertainty.

Inherent variability is the only source of uncertainty that is not due to human activity. All the other types of uncertainties are part of the geological investigation. The process of geological investigation requires several stages i.e. acquisition, processing, analysis, interpretation, and modelling of geoscientific data. All of these stages are susceptible to objective (i.e. data or technique-related) and subjective (i.e. person-related) uncertainties (Pérez-Díaz, et al., 2020).

Traditional methods attempt to report on the uncertainty of the estimate by attaching confidence intervals around an estimate and the associated kriging variance (Bardossy & Fodor, 2001). However, stochastic simulations provide a better approach to assess and quantify both local and global geological uncertainties. Stochastic simulations can be used to assess and quantify the uncertainty of estimates of both grade and geological boundaries (Bardossy & Fodor, 2001; De Souza, et al., 2004; Garcia, 2016; Chanderman, 2017; Pérez-Díaz, et al., 2020). This allows for the quantification of risk through the integration of the uncertainty into decision-making, resulting in mine designs and production schedules with higher value and better risk management. Better risk management ensures that production targets are met by mining operations (Leite & Dimitrakopoulos, 2007; Dimitrakopoulos, 2011; Garcia, 2016). Additional detail regarding stochastic geostatistical methods is provided in Sections 2.6 and 2.7.

Although a broader view of geological uncertainty is discussed in this section, this study focuses primarily on the uncertainty of grade estimates within reasonably well-known geological boundaries. More discussion on relevant underlying concepts, advantages, limitations, and related case studies of deterministic and stochastic methods are discussed in subsequent sections.

2.3. Theory of Regionalised Variables

Geostatistics is based on the theory of regionalised variables (RV). A regionalised variable is a random variable (i.e. randomly generated by some probabilistic mechanism) distributed in space and represents some natural occurrence/process/property. Most natural occurrences (in this case, a geological property) can be described by a random and a structured component. The random aspect describes the local behaviour while the structured element is related to the overall distribution of the geological phenomena. The theory of regionalised variables aims to adequately describe the structural properties of a natural phenomenon and then estimate the related regionalised variable from limited sample data. This aim is achieved through the probabilistic representation provided by random functions. A random function $Z(x)$ is a set of random variables that have spatial location $(x, y \; and/or \; z)$ and whose dependence on each other is specified by some joint probabilistic mechanism (joint distribution of a set of variables). For example, two random variables $z(x_i)$ and $z(x_i + h)$ in the same area are not independent but are related by a correlation expressing the spatial structure of the geological property. The basic idea of the theory is to consider a regionalised variable $z(x_i)$ as one realisation of a random function $Z(x)$. Figure 2.2 graphically summarises the theory of regionalised variables (Matheron, 1971; David, 1977).

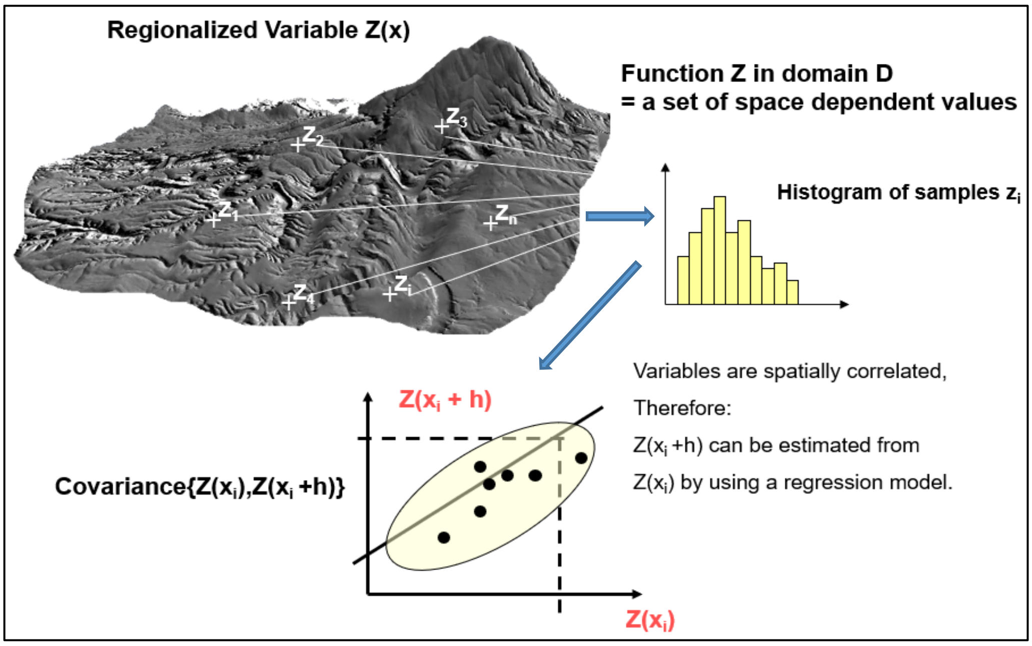

Figure 2.2: Concepts of the Theory of Regionalised Variables (Spatial Analysis Lab, 2005)

Two major assumptions are necessary in order to allow for the description of the characteristics of the random function and the consequent estimation of unknown points:

- Second-order stationarity: Means that the expected value $E[Z(x)]$ and spatial covariance of the random function $Z(x)$ are the same throughout the field of interest (i.e. domain). Additionally, spatial covariance is assumed to depend only on the distance and direction separating any two locations and not on the actual data values. This assumption requires a finite variance of $Z(x)$ (David, 1977; Bardossy, 2002).

- Intrinsic hypothesis: It was found that in many deposits (particularly gold orebodies), the assumption of a finite variance was not suitable, (Krige, 1951). However, if one considers the variations of the grades $\{Z(x+h)\} - Z(x)$ rather than the grade itself, finite variance can be achieved. This approach led to the development of the slightly weaker intrinsic stationarity. The intrinsic stationary assumes that the expected value of the random function $Z(x)$ is constant over the entire domain. Secondly, it assumes that the variance of the increment $VAR[Z(x+h) - Z(x)]$ corresponding to the difference in the regionalised at two different locations depends only on the vector h separating them (David, 1977; Bardossy, 2002).

2.4. Variography

The intrinsic stationarity assumption about $Z(x+h) - Z(x)$ allows for the definition of the theoretical variogram $2\gamma(h)$ (David, 1977):

$$\boldsymbol{VAR[Z(x+h) - Z(x] = 2\gamma(h)} \quad \textbf{2-1}$$

The semi-variogram is formulated as (David, 1977; Clark & Harper, 2000):

$$\boldsymbol{\gamma(h) = \frac{1}{2} VAR[Z(x+h) - Z(x)] = \frac{\sum[Z(x+h) - Z(x)]^2}{2N}} \quad \textbf{2-2}$$

where N is the number of pairs $(Z(x),\ Z(x+h))$. It should be noted that the phrases “variogram” and “semi-variogram” are often used interchangeably in most literature as well as in this report. Variography is the calculation and plotting of an experimental variogram and the subsequent fitting of a suitable model. An experimental semi-variogram is calculated from equation 2-2 by using pairs at different lag distance intervals and varying directions. The variogram values are then plotted against distance before an appropriate theoretical variogram model is fitted shown, as shown in Figure 2.3. Variograms are modelled in one or more orthogonal directions (i.e. the major-, semi-major- and/or minor- axes) (David, 1977; Clark & Harper, 2000).

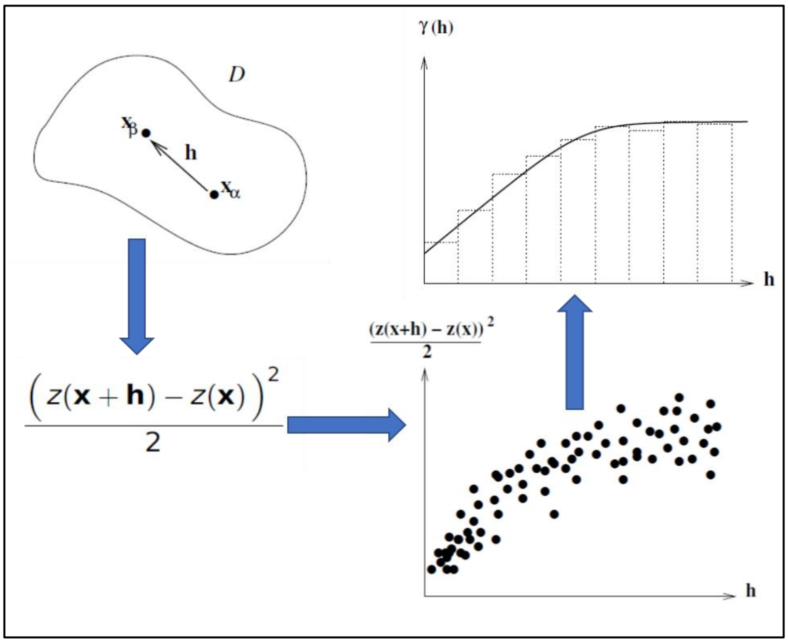

Figure 2.3: Illustration of variography (Wackernagel, 2013)

The main parameters of a typical variogram model as illustrated in Figure 2.4 are (Clark & Harper, 2000; Dohm, 2019):

- The nugget effect (C_0): Describes the variation of samples at short separation distances. The nugget can be divided into two parts, i.e. "*the inherent small scale (geological) variability and any errors in the data (e.g. sampling errors and database errors")*. C_0 is usually estimated from a downhole variogram.
- Spherical component (C_1): Describes the part of the variogram that describes spatial correlation.
- The total sill ($C_0 + C_1$): Represents the total variability inherent in the data. The sill is equivalent to the total data variance in a non-standardised variogram.
- The range (a_1) of continuity: This is the lag at which the variogram reaches the sill. There is no spatial correlation for samples separated by lags beyond the range of continuity.

There are instances where a variogram model reflects a number of components that can be modelled at different ranges of continuity. These types of models are said to have nested structures (Clark & Harper, 2000; Dohm, 2019).

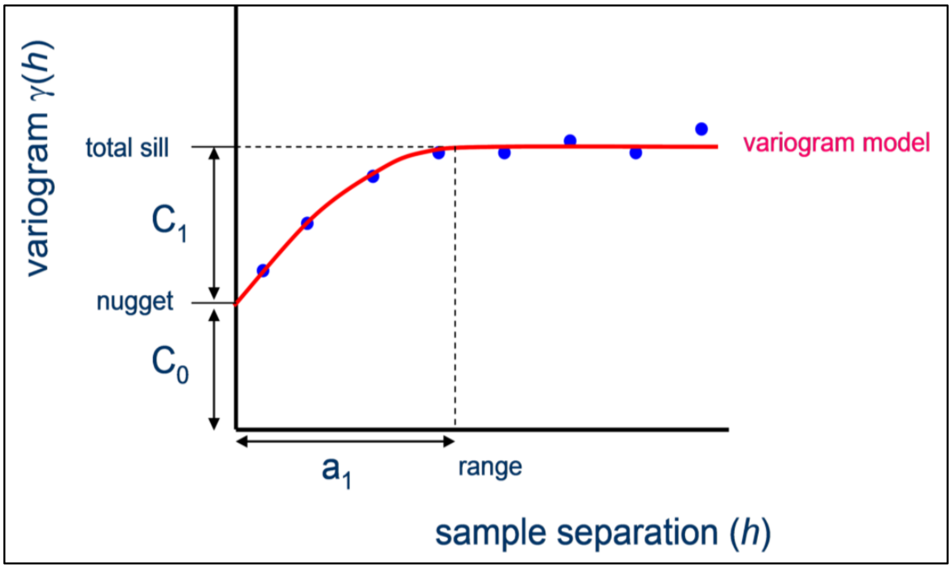

Figure 2.4: Parameters of a variogram model (Dohm, 2019)

Various types of mathematical models can be fitted to best match the shape reflected by experimental variograms. The common variogram models are spherical and exponential (Clark & Harper, 2000).

Key guidelines when calculating or modelling variograms which also underpin approaches used in Sections 3.4., 3.5 and 3.6 are (Guibal, 2001):

- The number of pairs for each lag in the experimental variogram should be at-least 30.
- The variogram can become unreliable at lags greater than one-third of the maximum sample separation.
- When noisy variograms with no obvious structure are encountered, one should consider using relative variograms or transformation e.g. log-, Gaussian -, or indicator – transformations (Rivoirard, 1987; Journel, 1989).
- When dealing with highly skewed data, the data is normally transformed using normal scores transformation prior to calculating the variograms.

This transformation is usually carried out in order to prevent the obscuring of the underlying continuity and directions by high grade outliers.

- It is critical to correctly assess the shape and slope near the origin since greater weight is generally given to the experimental points closest to the origin provided sufficient pairs are available.
- If the total sill is not clearly defined, the ‘average’ level of fluctuation is often used.
- Due to the presence of long-range trend in the data, the overall variance is not always at the total sill.
- There are a few situations when one needs to consider drifts, cyclicity and the hole effect.
- The experimental variogram should be calculated in several directions in the x-y plane, and at geologically sensible orientations in the third dimension, in order to detect anisotropies.
- In the absence of any detected anisotropy, an isotropic model can be fitted.
- 3D variogram maps are commonly used to detect anisotropies.

Variograms are essential for geostatistical estimation because (Clark & Harper, 2000):

- The use of the experimental semi-variogram forms the basis for a ‘model semi-variogram' that becomes the best available distance function for a given set of sample measurements.
- The nugget effect gives a measure of the random “uncorrelatable” variability inherent in the material being sampled.
- The ability to fit different variograms in different directions provides a means for accommodating differences in continuity in different directions.

However, the use of variograms is limited when the assessment of uncertainty is required, particularly when dealing with complex geological phenomena:

- The variogram describes the spatial variation between a pair of data values (i.e. two-point statistics) which cannot capture complex spatial patterns (Chanderman, 2017).
- Parameters deduced from variograms are based on incomplete measures of the spatial variability of the data and do not accurately inform the geological modelling and estimation processes. This results in the generation of high entropy models in which the heterogeneity and connectivity of the variable is misrepresented (Strebelle, 2002 & 2012).
- The subjective fitting of the variogram model (particularly the estimation of the nugget effect) introduces possible biases and consequently more uncertainty (Mariethoz & Caers, 2014).

2.5. Kriging

Kriging is a method of obtaining the best linear unbiased estimates of point values or block averages*. "It is an interpolation technique that considers both the distance and the degree of variation between known data points when estimating values in unknown areas. A kriged estimate is a weighted average of the data in its neighbourhood*". The weights allocated to the sample data are optimised to minimise the estimation variance (i.e. kriging variance) and provide an unbiased estimate (Armstrong, 1998). There are numerous types of kriging estimation techniques as summarised in Section 1.4. Kriging offers more advantages over classical methods such as IDW (Clark & Harper, 2000) i.e.:

- Measures of reliability of the estimates are possible by means of confidence intervals.
- Block kriging offers an objective way to deal with volumes.
- Lognormal data can be easily handled through transformation.
- There are kriging approaches for handling strong trend in the data.

Although kriging provides the best linear unbiased estimates, it does not attach adequate measures of uncertainty around the estimates (Rossi & Deutsch, 2014). In other words, kriging is a deterministic technique. Kriging produces resource models with one version of lithological domaining and grade distribution. These models do not adequately account for geological uncertainty as they do not capture the true complexity and in-situ variability of the geological phenomena (Chanderman, 2017). The inability for kriging to properly assess uncertainty is exacerbated when the sample density is low (Van der Grijp & Minnitt, 2015; Chanderman, 2017). This results in misleading resource estimations and poorly informed mine plans (De Souza, et al., 2004; Garcia, 2016; Chanderman, 2017). The following summarises the shortcomings of kriging as it pertains to the assessment of uncertainty:

- A single smoothed kriged model does not provide for robust decision making in mine planning and has been shown to contribute to the non-achievement of production targets and lower than expected Net Present Value (NPV) (Leite & Dimitrakopoulos, 2007; Albor Consuegra & Dimitrakopoulos, 2010; Godoy & Dimitrakopoulos, 2011; Menabde, et al., 2018).
- Kriged estimates do not correctly represent the local variability due excessive smoothing (Chilès & Delfiner, 1999; De Souza, et al., 2004).
- The local configuration of data affects the amount of smoothing. Hence, kriging realisations show more variability in densely sampled areas and less variability where the samples are scarce. The resultant smoothed kriged maps limit the ability of kriging to replicate prior geological knowledge such as spatial variation and patterns of the deposit (Srivastava, 2013).
- Underlying assumptions regarding the distribution of data distort the understanding of its natural variability. These contribute to conditional bias and resultant misclassification errors, as well as losing the ability to detect spatial patterns in the data (Chanderman, 2017).
- Kriging variance is independent of the data values leading to an incomplete measure of estimation accuracy (Cressie, 1990).

Despite these shortcomings, when there is sufficient information and uncertainty quantification is not required, conventional kriging methods provide acceptable results (Van der Grijp & Minnitt, 2015; Chanderman, 2015; Mariethoz, 2018). As a result, the use of the 25 m x 25 m x 3 m grade control data for the creation of a TI in the form of a kriged model is justified. The TI together with hard data in the extension area will be used for MPS simulation in the EA which has a low sample density (i.e. drill holes at 200 m x 100 m x 3 m spacing). Two TIs, one in the form of an OK model and the second one being a SK model were developed.

2.5.1. Ordinary Kriging

Ordinary kriging is based on the same minimum error variance linear estimation as SK. However, OK does not make any prior assumptions about the mean (m). The ordinary kriging block estimate $Z^*(u)$ is defined as (Rossi & Deutsch, 2014):

$$\boldsymbol{Z^*(u) = \sum_{i=1}^{n} w_i z(u_i)} \qquad \textbf{2-3}$$

where w_i denotes weights which are constrained to sum up to 1 in order to maintain global unbiasedness. $z(u_i)$ refers to sample values of a regionalised variables (e.g. grade) at locations u_i, where $i = 1,2,..,n$. n is the number of samples available. The weights are optimised in order to minimise the variance of the estimation error subject to the condition $\sum w_i = 1$. The optimisation of the weights leads to a linear system of $(n + 1)$ equations with $(n + 1)$ unknowns (Rossi & Deutsch, 2014):

$$\boldsymbol{\begin{cases} \sum_{j=1}^{n} w_j C(v_i, v_j) + \lambda = \bar{C}(V, v_i), \forall\, i = 1, 2, \ldots, n \\ \sum_j w_j = 1 \end{cases}} \qquad \textbf{2-4}$$

where C denotes the covariance and λ represents the Lagrangian multiplier. The role of λ is to balance the kriging weights. When λ is negative, it is usually due to there being too many samples or clustered samples. If there could be an improvement in the sample layout (i.e. when there are insufficient samples or samples are too far from the estimation point), λ is positive (Dohm, 2019).

The corresponding ordinary kriging variance is given by:

$$\boldsymbol{\sigma_{OK}^2 = \bar{C}(V, V) - \lambda - \sum_{\alpha=1}^{n} w_\alpha \bar{C}(V, v_\alpha)} \qquad \textbf{2-5}$$

OK is the most widely used estimation technique for Mineral Resource estimation. It is said to be more robust than SK due to its ability to rescale to a different mean value locally. However, the stationary covariance requirement means that the OK variance does not properly recognise local variability, especially in heterogeneous mineral deposits with higher and poorer grade zones (De Souza, et al., 2004; Rossi & Deutsch, 2014).

2.5.2. Simple Kriging

Simple kriging is a minimum error variance estimator, and it is by definition unbiased since stationary mean (m) is assumed known. The stationary mean is usually inferred from the average value of the samples within the stationary domain. A generalised form for SK block estimator is shown below (Rossi & Deutsch, 2014):

$$\boldsymbol{Z_{sk}}^*(\boldsymbol{u}) - \boldsymbol{m}\,(\boldsymbol{u}) = \sum_{i=1}^{n} \boldsymbol{w_i} \cdot [\boldsymbol{z_v}\,(\boldsymbol{u_i}) - \boldsymbol{m}(\boldsymbol{u_i})] \quad \textbf{2-6}$$

SK's weights are unconstrained, and the minimisation of the estimation variance leads to the SK system equations (Rossi & Deutsch, 2014):

$$\sum_{j=1}^{n} \boldsymbol{w_j}\overline{\boldsymbol{C}}(\boldsymbol{v_i},\boldsymbol{v_j}) = \overline{\boldsymbol{C}}(\boldsymbol{v_i},\boldsymbol{V}), \forall\, \boldsymbol{i} = \boldsymbol{1},\boldsymbol{2},\dots,\boldsymbol{n} \quad \textbf{2-7}$$

The corresponding simple kriging variance is given by (Rossi & Deutsch):

$$\boldsymbol{\sigma_{SK}^2} = \overline{\boldsymbol{C}}(\boldsymbol{V},\boldsymbol{V}) - \sum_{i=1}^{n} \boldsymbol{w_i}\overline{\boldsymbol{C}}(\boldsymbol{v_i},\boldsymbol{V}) \quad \textbf{2-8}$$

Although the use of SK in practical applications is limited, SK is commonly used to obtain simulations (Rossi & Deutsch, 2014).

2.5.3. Practical considerations for the application of kriging

Since two kriged TIs will be developed, it is important to give a summary of some practical considerations when developing kriging-based models so as to ensure accurate estimation results. These considerations will guide the creation of TIs in Section 3.4.3. According to Armstrong (1998), the accuracy of the estimate depends on:

- The number and quality of the sample data at each point,
- The location of samples within a deposit,
- The distance between samples and the point or block to be estimated and,
- The spatial continuity of the variable under consideration.

It is critical to be aware of the influence of the information -, support- and regression effect on the estimate. The information effect is the reduction in the selectivity of estimated blocks compared to reality due to limited information during estimation. Support effect (also known as volume-variance effect or change of support effect) is due to the reduction in the variance as the size and volume of a block or sample increases. The support effect causes the misclassification of ore as waste or waste as ore. The regression effect is the conditional bias due to the overestimation of high grades and underestimation of lower grades (Isaaks, 2005; Clark, 2015; Dohm, 2019). Deutsch & Deutsch (2015), list pre-requisites for ensuring accurate estimates, thus minimising the influence of these effects. These are: data quality, compositing, managing outliers, domaining, correct estimation block size selection and managing large scale trends. Once these pre-requisites are met, the optimal kriging search plan need to be selected. The kriging plan includes the number and locations of data used in the estimation. The practical considerations for optimal selection of parameters that could minimise conditional bias in grade estimation models and, by extension, the TIs in this report are summarised as follows:

Orientation and Dimensions of Search Ellipsoid:

Parameters of the search ellipsoid determine how far out to search for data to support a particular kriged estimate. The selection of a search ellipsoid should align with the variogram anisotropic orientation and ranges as well as the drill hole spacing. A local search neighbourhood excludes samples outside the search ellipsoid. When working with 3D drill hole data, there is an option of using an octant search in order to ensure that samples are taken from more than one drill hole (Deutsch & Journel, 1997). Optimal search ellipsoid parameter definition is critical because it (Deutsch & Journel, 1997):

- Optimises computing and memory requirements.
- Limits the neighbourhood conditioning data to within ranges of continuity defined by the variogram.
- Allows local rescaling of the mean when using ordinary kriging.

The selection of the optimal search ellipsoid parameters in the development of the TIs was based on the outcomes of the kriging neighbourhood analysis (KNA). Literature around the use of KNA is detailed later within this Section.

Number of Sample Data:

It is critical to select a minimum and maximum number of data points within a search ellipsoid to be used in generating kriging estimates. The objective for choosing an optimum number of search data is to minimise mean squared error (MSE) and conditional bias. The number of search data selected is a trade-off between computation time and the reliance on global stationary mean. However, the influence of computation time has decreased over time due to major improvements in computing capabilities. It has been shown that the MSE decreases with the maximum number of search data used in kriging. Though, beyond a particular number of samples, the effect on the MSE is minimal and does not necessarily worsen the accuracy of the estimate. On the other hand, limiting the number of search data may result in shadows or numerical artefacts which is undesirable for interpretation of kriging maps (Deutsch & Deutsch, 2015). Figure 2.5 shows results from a study that investigated the relationship between simple and ordinary kriging's MSE and number of search data. Common practice is to use OK with a large number of search data since SK's effectiveness is limited by the extremely large dependence on global mean. Nonetheless, in a study by Deutsch, et al (2014), it was shown that SK performs better than OK when there is a low number of search data. In the same study, OK was proven to be the better estimator when large number of search data is available. Another consideration worth noting when using OK is to restrict the number of samples to use per drill hole. This restriction is carried out in order to avoid the use of data from only one drill hole when estimating in areas with limited data (Deutsch &

Deutsch, 2015). KNA guided the choice of the optimum number of samples for the kriging process used to create the TIs for this study.

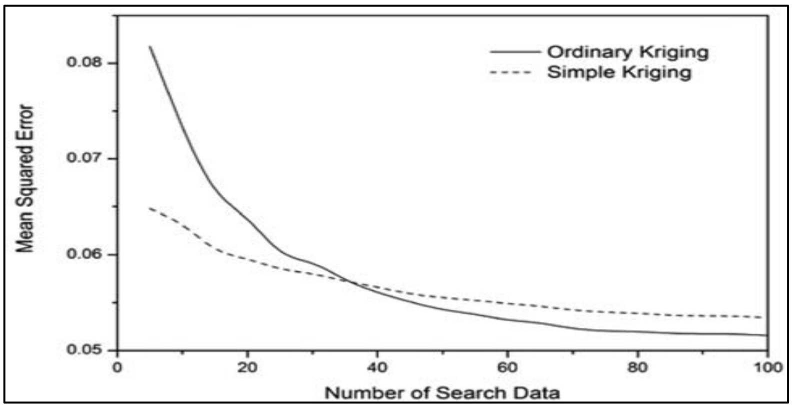

Figure 2.5: Effect of the number of search data (Deutsch, et al., 2014)

Compositing:

Compositing is the averaging of original assay/grade values to predetermined lengths in order to (Rossi & Deutsch, 2014):

- Homogenise the data scale or support, e.g. scale to bench height,
- Correct for incompletely sampled intervals,
- Improve robustness of variography and geostatistical analysis,
- Reduce random variability at small scale intervals (i.e. nugget effect) and,
- Improve overall quality of the resource model.

Once a choice to composite has been made, a number of related decisions are subsequently required. These include deciding on the method and length of compositing, truncation at geological boundaries, handling intervals with missing values and minimum compositing lengths (Rossi & Deutsch, 2014; Abzalov, 2016). Glacken and Snowden (2001) provide details about practical guidelines that can assist with these decisions. In the development of the TIs, the data provided was already composited to 1m intervals as is the practice at Tarkwa mine. Therefore, composting is not detailed in the methodology of this report.

Outliers:

Outliers are termed as values that deviate from the general tendency of the majority. Generally, in statistical analysis, outliers are due to spurious or erroneous data collection and are usually dealt with by excluding them from the analysis. However, in resource estimation, particularly in precious metal deposits, extreme high grades are valid assays and are common due to the positive skewness of the distributions (Rossi & Deutsch, 2014). Therefore, merely excluding these grades is not recommended. Common approaches are capping the extreme grades and/or domaining the high grades. The need to deal with these extreme grades is necessitated by the objective to prevent the overestimation or underestimation of the Mineral Resource (Leuangthong & Nowak, 2015). When developing the TIs, it was necessary to honour all the data and underlying trends so as to maintain the representability of the TIs. Therefore, no grade capping/cutting was carried out.

Domaining:

In order to satisfy the stationary assumptions of geostatistics, geological domaining is carried out prior to estimation. Spatial analysis of the data is carried out within the predefined domains. A geological domain is an area within the deposit which is geologically homogeneous (i.e. statistical and geological characteristics are generally similar within this zone) (Rossi & Deutsch, 2014). These geological domains are usually defined by geological properties (i.e. hard boundaries) such as lithology, mineralisation, faulting, deformation, or weathering. The domains can also be delineated by means of cut-off values of grade (Guibal, 2001). Since the data used in this research project has been extracted from a pre-defined domain, this step was not necessary in the study.

Estimation Block Sizes:

The selection of optimal estimation block sizes is critical to the quality of the resource estimate. It is ideal to estimate blocks at the scale of the envisaged selective mining unit (SMU). The SMU is conventionally defined as the smallest parcel of ground on which mining decisions (e.g. deciding ore or waste) are made. However, when drill hole spacing is sparse, decreasing the block size to fit the SMU often leads to loss of precision of individual block estimates. This then distorts the estimates and introducing conditional bias which consequently gives mine plans which are unreliable and unrealistic. Hence, it is important to select block sizes in relation to the sampling grid. There are various ways of deciding on optimum block dimensions as detailed in Krige (1996) and Jara et al. (2006). Additionally, sub-blocking may be required to increase the resolution at geological boundaries and for geotechnical and blast design applications (Collings, et al., 2001; Johnson, 2001). A block size of 10 m x 10 m x 3 m which represents the predetermined SMU at Tarkwa were selected for the development of the TIs. KNA was used to confirm the suitability of using this SMU for kriging. Sub-blocking was not carried out as the current SMU resolution was deemed sufficient for the objective of the study.

Discretisation:

Discretisation is the process of subdividing grid blocks into small scale points or nodes which represent individual volumes relative to the block size. Discretisation is crucial for block kriging since it enables the calculation of the data-to-block average covariances. The higher the level of discretisation, the better. However, with increased discretisation, computing requirements will also be increased and too many discretisation points could lead to numerical precision problems (Rossi & Deutsch, 2014; Sunday & Deutsch, 2020). KNA was used to the select the optimal number of discretisation points in the X, Y and Z directions.

Kriging Neighbourhood Analysis (KNA):

The objective of KNA is to determine the optimum combination of neighbourhood and block parameters that will minimise conditional bias. KNA provides a quantitative method of testing different input parameters for kriging and assessing their impact on the quality of the estimate. It provides a guide for the selection of optimal values for parameters such as search radius, number of samples, block sizes and number of discretisation points. The parameters depend on a number of factors which are mathematically represented by the variogram. The variogram is the most critical input to the KNA process. KNA is used in the selection of optimal values for relevant kriging neighbourhood parameters when carrying out kriging in this study. These factors include anisotropy, ranges of continuity, drill hole spacing and inherent variability (Vann, et al., 2003)

There are a number of statistics that KNA can output. The two measures of conditional bias produced by the KNA are the Kriging efficiency (KE) and the slope of regression (SLOR). KE indicates the effectiveness of the kriged estimate to accurately reproduce the local block grade. KE is reported as a ratio between 0 and 1 (or percentage 0-100%). Low kriging efficiency shows that there is a high degree of over-smoothing as shown in Figure 2.6. It is worth noting that KE can have a negative value if the kriging variance (KV) is greater than the true block variance (BV). Negative KE values occur when the kriged estimate provides the same level of reliability as compared to using the global mean as the block estimate (Krige, 1996). General practise is to exclude blocks with negative KE when reporting a Measured Resource as discussed in subsequent sub-sections (Clark, 2015). KE is calculated as follows (Krige, 1996; Deutsch, et al., 2014):

$$\boldsymbol{KE = \frac{BV-KV}{BV}} \quad \textbf{2-9}$$

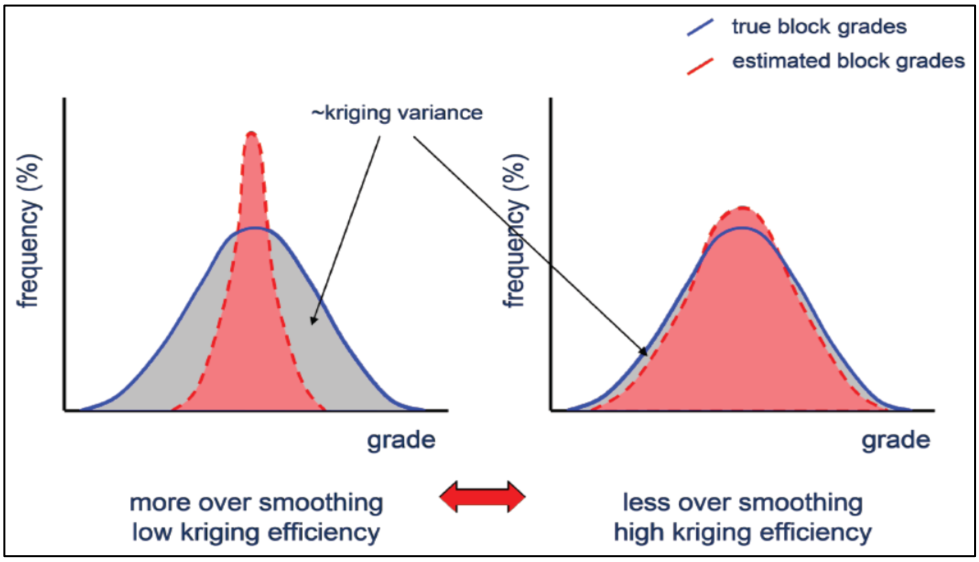

Figure 2.6: Kriging efficiency and over-smoothing

SLOR is equivalent to the regression slope of the estimated blocks against the true grades as shown in Figure 2.7. SLOR summarises the degree of over-smoothing of high and low grades. SLOR for each block can be calculated as follows (Clark, 2015):

$$SLOR = \frac{BV-KV+\lambda}{BV-KV+2\lambda} \quad \text{2-10}$$

Where λ represents the Lagrangian multiplier. A smaller value for λ, could indicate a higher SLOR. However, the actual size of λ is governed by the variogram model and sampling configuration (Dohm, 2019). The SLOR is also reported as a ratio between 0 and 1. For SK, SLOR is 1 while SLOR for OK is generally less than 1. A SLOR close to 0, shows that there is excessive smoothing and hence the estimated and actual block grades are poorly correlated as shown in Figure 2.7 (Vann, et al., 2003).

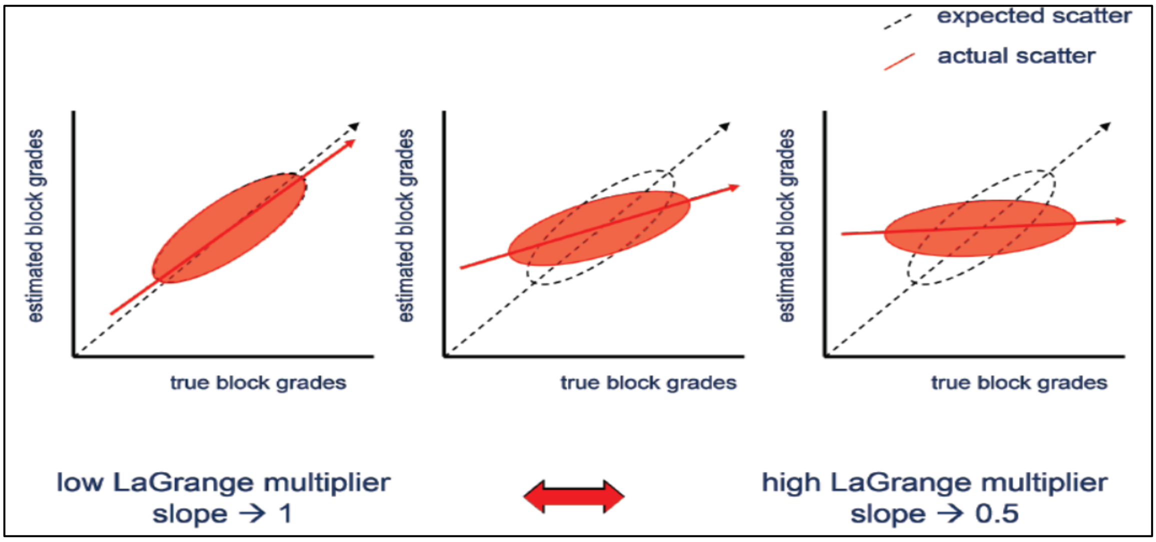

Figure 2.7: Slope of regression and over-smoothing

<u>Validation</u>:

Validation of the resource estimate is necessary to check the model's ability to reproduce the true grade distribution. It can be conducted through the use of various techniques which include comparing (Glacken & Snowden, 2001):

- Input and output mean grades within domains,

- Histograms of input and output grade distributions within domains,
- Sections/plans of input data and block grade estimates,
- Resource estimates from using alternative algorithms or approaches
- Estimates with production data, e.g. comparison of grade-tonnage curves for the resource model and the grade control model. This technique is called reconciliation and is considered the best validation tool.

Another method for validating estimated results is carrying out cross validation (also known as back estimation). Cross validation involves the removal of a data point and then using the surrounding points to estimate at the location of the "removed" data point. This is followed by the determination of the actual errors by subtracting the estimates from the actual values. The actual errors are averaged. If the estimation is unbiased, this average should be zero. The variance of the errors is then calculated and compared with the average kriging variance for all the estimations. If the estimation is correct, the ratio between these two parameters is expected to be one (Clark, 1986).

<u>Reporting of Results</u>:

Different international codes for public reporting of Mineral Resources and Mineral Reserves exist. In South Africa, the South African Code for the Reporting of Exploration Results, Mineral Resources and Mineral Reserves (SAMREC) "*provides minimum requirements, recommendations, and guidelines for public reporting of resources and reserves*". The purpose of the reporting codes is to prevent misleading, inaccurate, or fraudulent information relating to mineral properties being published and promoted on stock exchanges. According to SAMREC, Mineral Resources can be classified into Inferred, Indicated, and Measured categories according to the level of geoscientific knowledge and confidence. Similarly, Mineral Reserves can also be classified into Probable and Proved, (SAMREC, 2016). In this report, the focus is on providing a proof of concept for the application on DeeSse in a sparsely spaced area by using a TI developed from grade control data. This was carried out by extracting small portions of conditioning data from the grade control area and the extension area.

As a result, it was beyond the scope of the study to attempt to classify the Mineral Resource.

2.6. Models of Uncertainty

Since deterministic uncertainty estimates do not adequately account for the variability from one location to another, geostatistical conditional simulations were developed to better model uncertainty. Conditional simulations provide a series of equiprobable realisations that represent a range of plausible possibilities instead of one outcome. These simulations are termed "conditional" since actual data points are used for each realisation (i.e. simulations are conditioned to the data). Simulations allow for the assessment of the joint uncertainty between multiple realisations. As a result, a comprehensive representation of block uncertainty and the uncertainty between multiple block locations is possible (Journel, 1974; Journel & Huijbregts, 1978; Khosrowshahi & Shaw, 2001; Rossi & Deutsch, 2014). Although conditional simulations were first developed in the 1970s (Journel, 1974), they have become popular with the advent of more powerful computers (Khosrowshahi & Shaw, 2001; Rossi & Deutsch, 2014). They have since been applied in various applications such as:

- Grade control tools and optimisation of sampling grids (Shaw & Khosrowshahi, 1997; Boucher, et al., 2004; Vargas, 2017).
- Validating resource estimate parameters such as SMU correction factors and decisions around dealing with high grades (Glacken, 1996; Khosrowshahi & Shaw, 2001).
- Ore block optimisation (Shaw & Khosrowshahi, 1997; Everett & Grobler, 2013; Dimitrakopoulos & Godoy, 2014).
- Analysis of risk related to resource classification (Dohm, 2004; Rossi & Camacho, 2004; Wawruch & Betzhold, 2004; Emery, et al., 2006).
- Assessment of the uncertainty of mineable reserves during feasibility studies, (Rossi & Alvarado, 1998; Hosseini, et al., 2017).
- Assessment of the potential of mineralisation (Ersoy & Yunsel, 2006; Amarante, et al., 2019).

Deterministic methods such as kriging provide unbiased minimum error estimates. However, the unavoidable smoothing effect and lack of optimal means for assessing local uncertainty makes conditional simulations favourable (Rossi & Deutsch, 2014). Conditional simulations provide a number of advantages over deterministic approaches because they (Khosrowshahi & Shaw, 2001):

- Reproduce the original variability (histogram) and spatial continuity (variogram) observed in the data. This implies that extreme values of the original distribution are preserved better than deterministic models which are sensitive to outliers.
- Provide an assessment of local uncertainty.
- Are built on finer grids (point-scale) which means there is a sufficient number of nodes within the block size of interest (Rossi & Deutsch, 2014). This allows for more robust geostatistical studies. These point-scale simulations can be block averaged to get block results.
- Provide predictions about variations of the characteristics of recoverable reserves at various operational stages such as mine optimisation, design and planning including stockpiling and blending (Journel & Huijbregts, 1978). Figure 2.8 summarises the difference between deterministic and stochastic approaches in a mining project valuation process (Dimitrakopoulos, 2011).

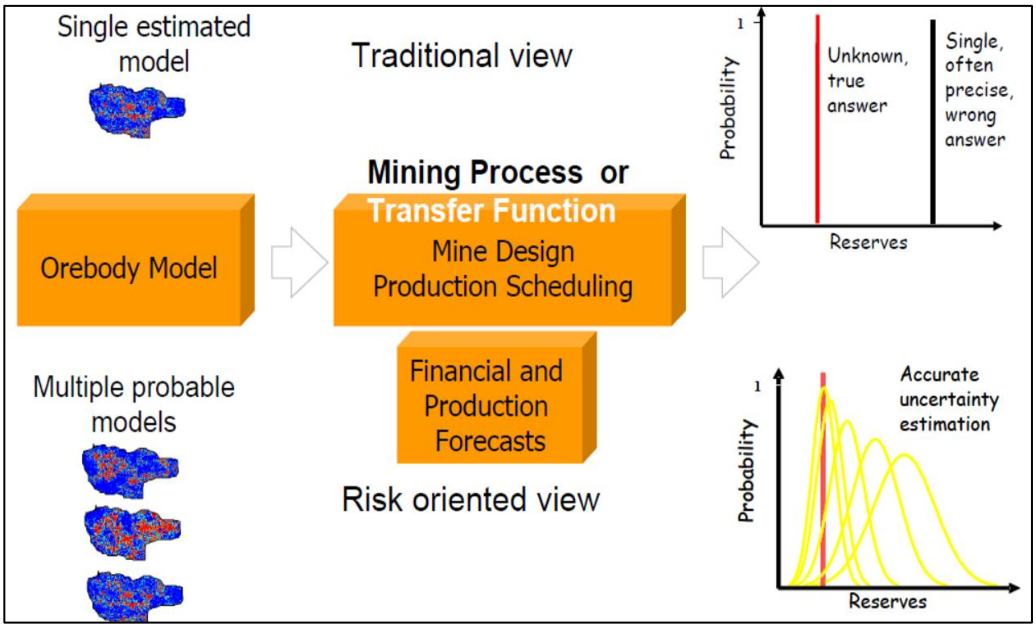

Figure 2.8: Difference between deterministic and stochastic approaches to Mineral and Reserve estimation (Dimitrakopoulos, 2011)

There are various geostatistical simulation techniques as listed in Section 1.4. Further detail regarding the derivation and underlying theories about these simulation methods can be found in Journel & Huijbregts (1978), Khosrowshahi and Shaw (2001), Vann et al. (2002) or Rossi and Deutsch (2014) among other sources. In this study, SGSIM was used as a validation method to compare to DeeSse. The choice of SGSIM was based on its popularity and easy of application. Prior to running the simulations, factors such as the number of conditioning data and the underlying random function (Gaussian or indicator-based) need to be decided upon. Selection of parameters such as grid size, random number generator, simple or ordinary kriging, multiple-grid simulation and use of irregular grids also require special attention (Rossi, 2003).These aspects guide the application of SGSIM in Sections 3.5, 3.6 and 3.7.

2.6.1. Sequential Gaussian Simulation (SGSIM)

SGSIM is a widely used algorithm based on a multi-Gaussian random function assumption. It is a simulation version of the multivariate Gaussian kriging algorithm. Thus, all conditional distributions are Gaussian, and SK is the only technique that can yield the estimated Gaussian mean and variance. As a result, simple kriging of grid nodes through a random path and conditioning data is used to generate local distributions. Some practitioners may occasionally use OK in order to avoid consequences of departing from stationarity, especially when there is a significant number of samples such as blast hole data (Vann, et al., 2002; Rossi & Deutsch, 2014).

Although traditional conditional simulation methods such as SGSIM solve the uncertainty quantification problem posed by kriging, they still possess a number of limitations. A summary of these limitations is given below:

- Where the risk of mining high-grade shoots is being investigated, SGSIM is suboptimal. SISIM is usually used as an alternative in order to model a number of spatial dispersions through variograms at various cut-offs (Khosrowshahi & Shaw, 2001).
- When simulations are carried-out where there is sparse or poor-quality data, the short-range variability is poorly characterised (Khosrowshahi & Shaw, 2001).
- SGSIM is based on second-order statistics, i.e. the mean and covariance. However, a large number of spatially distributed geological attributes are represented by non-Gaussian and non-linear connectivity of low and high grades. Hence, conditional simulations do not fully describe complex geological attributes (Strebelle, 2012; Tahmasebi, 2018; de Carvalho & Dimitrakopoulos, 2019).
- Gaussian simulation methods maximise spatial disorder (maximum entropy) beyond the imposed variogram in the realisations generated. This results in unrealistic quantification of the connectivity of high grades (Journel & Deutsch, 1993; de Carvalho & Dimitrakopoulos, 2019).

2.7. Multiple Point Statistics

Multiple-point statistics (MPS) was inspired largely by the pioneering of conditional algorithms at Stanford University and the use of outcrop studies by several oil companies in the late 1980s and early 1990s. The interest by oil companies to use conditional simulation was hampered by wells typically being spaced sparsely at several hundreds to thousands of metres apart. This makes it difficult to get the closely spaced data required to calculate experimental variograms. As a result, oil companies relied on outcrop studies to provide the data required to support the parametrisation of object- or variogram- based approaches. Object based modelling uses predefined geometries as well as conditioning data to make inferences about geometrical parameters. From then onwards, digital images of outcrops or other similar phenomena began to be used for calculating experimental variograms and multi-point statistics. This gave birth to MPS, where TIs are used to estimate the conditional probability at each location given observed and already interpolated data. A TI is a conceptual image that defines a 3D numerical rendering of interpreted geological attributes (Srivastava, 2018; Tahmasebi, 2018).

MPS algorithms offer a number of advantages over traditional variogram- and object- based approaches. The use of TIs in MPS allows for the direct and simultaneous inference of multivariate distributions. Traditional geostatistical tools are limited in this regard as the variogram cannot represent all the structural information of the random function model. Hence, MPS handles heterogeneity of the attribute and complex features better than traditional approaches (Strebelle, 2002; Hu & Chugunova, 2008; Peredo & Ortiz, 2011; Hosseini, et al., 2017). Since all statistics are directly provided by the TIs, it is expected that MPS would be a more robust approach than kriging-based methods in areas where the data is sparsely spaced. TIs make the integration of actual local data to the prior structural interpretation by geologist possible, thus ensuring results that represent reality better. Although object-based alternatives can reproduce the geology accurately, conditioning to dense or borehole data requires extensive computation and has proven to be difficult (Srivastava, 2018; Tahmasebi, 2018). The smoothing effect of kriging is consequently avoided by using MPS (Journel, 2003; Journel & Zhang, 2005). It should also be noted that MPS still provides all the other advantages of conditional simulation discussed in Section 2.6 such as the assessment and quantification of uncertainty. However, MPS approaches are not without their challenges which include (Tahmasebi, 2018):

- Conditioning the model to dense point/secondary datasets is usually difficult (e.g. well and seismic data),
- Lack of similarity between the internal patterns in the TI and the conditioning data,
- Deficiency of the current similarity functions for quantitative modelling,
- Lack of better and more realistic validation methods.

In addition to these challenges there are still arguments against the use of MPS in Mineral Resource estimation, (Journel & Zhang, 2005):

- MPS' little theoretical pedigree. "*For example, there is no real model inference, the uncertainty that can be estimated based on a set of MPS realisations is poorly defined, and extreme events cannot be produced beyond those found in the training image*" (Mariethoz, 2018). The counter argument for this is that today, due computation advances, pedigree does not only come from analytical derivations.
- MPS relies on TIs which are subjective and difficult to obtain in order to deliver the necessary structural information. The counter is that covariance-based algorithms are similarly subjective.
- It has also been argued that MPS only produces random fields when the size of the training image tends to infinity. MPS algorithms do not approximate a random function when finite training image are used. Their value lies in the ability to produce realistic realisations. Therefore, using MPS requires some compromises with function theory and model consistency (Mariethoz, 2018).

The first published example of an MPS simulation was by Guardiano and Srivastava (1992) as shown Figure 2.9. The algorithm developed by Guardiano and Srivastava (1992) was called Extended Normal Equation Simulation (ENESIM) and is not in use anymore due its high computing costs. There are numerous MPS algorithms that currently exist, and new ones are constantly being developed. Following the development of ENESIM, the first efficient implementation of MPS was the Single Normal Equation Simulation (SNESIM) proposed by Strebelle (2002). Brief descriptions of commonly used MPS algorithms are summarised in Table 2.1. For further explanation about the theory of MPS and detailed descriptions of various MPS algorithms, see Mariethoz & Caers (2014).

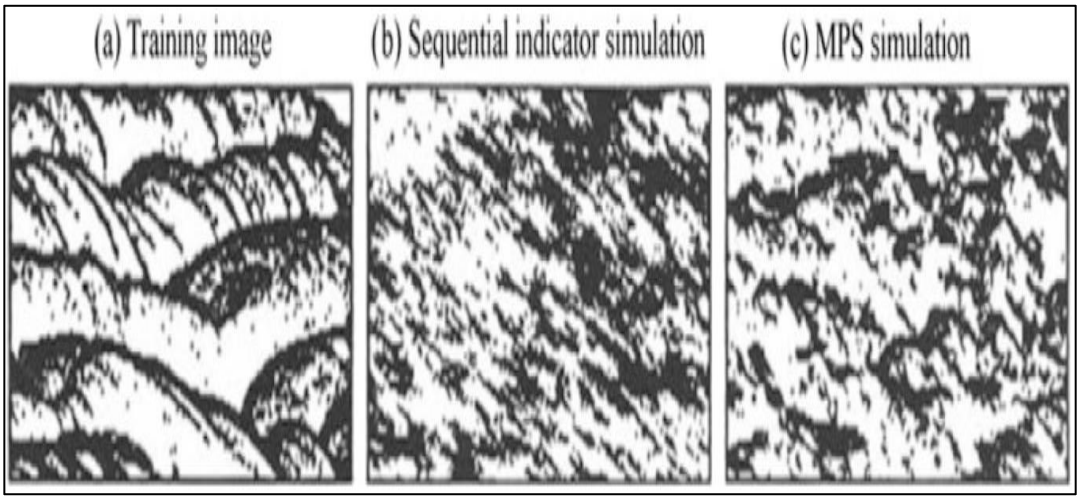

Figure 2.9: First published example of MPS (Guardiano & Srivastava, 1992)

MPS simulation are classified into pixel- and pattern- based methods. The difference between pixel-based and pattern-based methods is that the former is based on pixels/points that represent various geological properties. On the other hand, pattern-based algorithms do not paste one pixel at a time, instead they simulate entire patches (Mariethoz & Caers, 2014; Tahmasebi, 2018).

Table 2.1: Summary of MPS algorithms (Mariethoz & Caers, 2014; Tahmasebi, 2018)

Algorithm	Description
Extended Normal Equation Simulation (ENESIM)	A pixel-based method, which is an extension of indicator kriging allowing for the reproduction of multiple events inferred from a TI (Guardiano & Srivastava, 1992). One of the main drawbacks of this algorithm is scanning the TI for each point visited, which makes it impractical for large simulation grids (SGs) and TIs.

Algorithm	Description
Single Normal Equation Simulation (SNESIM)	This is also a pixel-based method. It is an improved version of ENESIM by introducing a search tree to prevent the rescanning of the TI for each point visited. The algorithm scans the input TI once before simulation begins and then stores the frequency/probability of all pattern occurrences in a search tree (Strebelle, 2002). However, the inability to produce realistic, highly connected, and large-scale geological features is a major disadvantage. Other variations of SNESIM include: • Improved parallel multiple-point algorithm using a list approach (IMPALA) which uses a list instead of a tree to store data events. This reduces computer memory requirements and thus decreases CPU costs (Straubhaar, et al., 2011). • High-order simulation algorithm (HOSIM) which uses cumulants to store patterns instead of frequencies (Mustapha & Dimitrakopoulos, 2011). • Unique pattern-growth algorithm (GROWTHSIM) which uses a random-neighbour path (Eskandari & Srinivasan, 2010).
Direct Sampling (DeeSse)	A pixel-based method that only scans a part of the TI and pastes one single pixel. Less RAM is required since no database is created. This method can be used for both categorical and continuous variables (Mariethoz, et al., 2010).
Simulated Annealing (SA)	A pixel-based method which is a popular method in optimisation and is used to find the global minima. Drawbacks include large central processing unit (CPU)

Algorithm	Description
	time and a large number of trial-and-error iterations to achieve optimal values (Peredo & Ortiz, 2011).
Simulation of Pattern (SIMPAT)	A pattern-based method initially developed to address some of the limitations in the SNESIM algorithm. This method replaces probability with a distance for finding most similar patterns (Arpat & Caers, 2007). Drawbacks include high computational costs, underestimating the spatial uncertainty and serious issues with 3D modelling.
Filter-based Simulation (FILTERSIM)	A pattern-based method that summarises both the TI and data-event by applying various filters to reduce the spatial complexity and dimension (Zhang, et al., 2006). Main challenges include the use of a limited set of linear filters that cannot always convey all the information and variability in the TI and difficulties with the proper selection of the appropriate filters.
Cross-Correlation based Simulation (CCSIM)	This is a pattern-based method that uses a cross-correlation function (CCF) along a 1D-raster path. The algorithm can realistically reproduce the large-scale structures in a short time (Tahmasebi, et al., 2012). However, the realisations produced do not fully match the orebody.
Hybrid Sequential Gaussian/Indicator Simulation and TI	This involves integration of indicator simulation methods with MPS. The properties of MPS are obtained by integrating the results of indicator kriging and a variogram (Ortiz & Deutsch, 2004). The main problem is that initial results of indicator kriging highly influence the final realisation.

Algorithm	Description
Hybrid Pixel- and Pattern-based Simulation (HYPPS)	This method combines the strengths of both the pixel and pattern-based algorithms by discretising the simulated grid into regions with or without conditioning data (Tahmasebi, 2017).

Core concepts of MPS are the TI and simulation path. The basic MPS method can be summarised as follows for each node ($\mathbf{x}$) to be simulated (Mariethoz, et al., 2010; Meerschman, et al., 2013):

- Get the conditioning data around the node $\mathbf{x}$ to form local data events $\mathbf{d_n} = \{\mathbf{Z}(\mathbf{x_1}) \cdots \mathbf{Z}(\mathbf{x_n}),\}$ for conditioning the random variable $\mathbf{Z}(\mathbf{x})$.
- Scan and analyse the TI and compute a conditional cumulative probability distribution function (ccdf):

  $$\mathbf{F}(\mathbf{z}, \mathbf{x}, \mathbf{d_n}) \ = \ \mathbf{Prob}\{\mathbf{Z}(\mathbf{x}) \leq \mathbf{z} | \mathbf{d_n}\}$$

- Randomly sample a value from the ccdf and copy the value to node $\mathbf{x}$ in the SG.
- Go to the next node following the predetermined simulation path. At each successive location, the ccdf is conditioned to both previously simulated nodes and the actual data.

2.7.1. Training image

The TI is a conceptual image that defines a 3D numerical rendering of interpreted geological attributes. The TI provides information from multiple points, thus allowing simulations conditioned to the occurrence of two or more points simultaneously. "*TIs can be generated using the physics derived from process-based methods or statistical methods or by using the extracted and observed rules for each geological system. The TI can be of any type, ranging from an image to statistical properties in space and time*". Sources for data to construct

TIs include outcrops, drill hole data, seismic data, or stratigraphic analysis (Hashemi, et al., 2014). TIs are one of the most important inputs of MPS. However, providing a representative TI or set of TIs is one of the biggest challenges in multiple point geostatistics (Tahmasebi, 2018). Although TIs are considered a reasonable representation of reality, they are not necessarily always statistically representative. This is because of the complexities of natural processes and associated subjective interpretations. As a result, there is usually a trade-off between statistical representations and empirical realism. Sometimes more than one TI may be necessary. Further reading on the selection of representative TIs and debates around some concepts regarding TIs will be found in Journel (2003); Journel and Zhang (2005); Boisvert, et al. (2007); Emery and Lantuéjoul (2014); and Mariethoz and Caers (2014). In this study, two TIs are created by kriging grade control data using OK and SK. The data used to krige the TIs was simply extracted from an existing domain. The actual selection and testing of alternative TIs are beyond the scope of this report.

2.7.2. Simulation path

Geostatistical techniques are conducted on a SG. A SG is a 2D/3D computation grid and is composed of several cells, depending on the size of the domain and simulation. "*These cells are visited in diverse ways on a predefined path, either in a random or in a structural manner (i.e. raster path). In the random path, a series of random numbers equal to the number of unknown cells, based on a random seed, is generated for each realisation and the unvisited points on SG are simulated accordingly"*. A random path is mainly used in sequential simulation algorithms. In the raster path, the simulation cells are visited systematically, and one can predict the next point to be visited. Raster paths are mainly used in stochastic modelling. These paths produce higher quality realisations, and the small number of constraints assists the algorithms to better identify the matching data (or patterns) (Tahmasebi, 2018). In this study a random simulation path is used.

2.7.3. Direct sampling algorithm (DeeSse)

In this study, DeeSse has been selected as the MPS simulation method to test its application in the simulation of grades in areas where the data is sparse. The DeeSse algorithm is one of the recent MPS techniques developed at the University of Neuchâtel in Switzerland. It was primarily selected because there is limited literature about its application in mining. It also offers several advantages over major MPS algorithms because it (Mariethoz, et al., 2010):

- Respects the conditional probability distribution from the TI without actually computing it. This means that DeeSse can be applied where traditional MPS approaches have failed such as in instances where there is a large dataset.
- Can simulate continuous variables and multivariate conditions.
- Provides for the use of the distance between two data points and an acceptable predefined error range in dealing with differences between the TI and simulation. Traditional MPS techniques deal with this problem arbitrarily by dropping the successive data points from a data event until a match is found.
- Offers possibilities of using TIs that can be categorical, continuous, univariate, or multivariate, stationary, or non-stationary.
- Allows for realistic modelling in cases which are highly influenced by heterogeneity and connectivity of geological structures.
- Exploits non-parametric relationships of variables of a different nature e.g. categorical and continuous relationships.
- Delivers a higher computation advantage than traditional MPS methods because it reduces memory usage since no catalogue of events need to be stored.

- Does not require a fixed geometry of data events. The shape of the data event and search window can change at each simulated node.

- Avoids the use of use multigrids, thus abandoning related problems such as the migration of conditioning data within coarse multigrids. It still ensures that all different sizes of structures are simulated by applying a progressive decrease of the size of data event as a function of the density of simulated nodes.

- Is easier to implement and parameterise.

Table 2.2 also summarises how DeeSse outranks standard approaches to MPS. Nonetheless, it has been reported that the choice of the data event in DeeSse can lead to uncertainty due to the less constraining conditional data. DeeSse also struggles to reflect changes in sediment patterns as the location of depositions changes (Yin & Feng, 2017).

Table 2.2: Comparison of DeeSse against major MPS algorithms (Renard, et al., 2019)

METRIC	**SNESIM**	**FILTERSIM**	**IMPALA**	**DeeSse**
Categorical variable	√	√	√	√
Continuous variables	X	√	X	√
Joint multivariate simulation	X	X	X	√
Global proportion	√	√	√	√
Local proportion maps	√	√	√	√
Mean values over blocks	X	X	X	√
Connectivity conditioning	X	X	√	√
Affinity and rotation trends	zone	zone	zone	continuous
Nonstationary TI with auxiliary variable	X	X	√	√
Tolerance on rotation / affinity	X	X	X	√
Multiresolution (Pyramid)	X	X	X	√

The aim of the DeeSse algorithm is to simulate a random function $\mathbf{Z}(\mathbf{x})$. The input data into DeeSse includes (Mariethoz, et al., 2010):

- TI: Nodes are denoted by $\mathbf{y}$
- SG: A set of $\mathbf{N}$ conditioning data $\mathbf{Z}(\mathbf{x_i}), \mathbf{i} \in [\mathbf{1}, \cdots, \mathbf{N}]$.(If available)

The DeeSse algorithm is illustrated Figure 2.10 below:

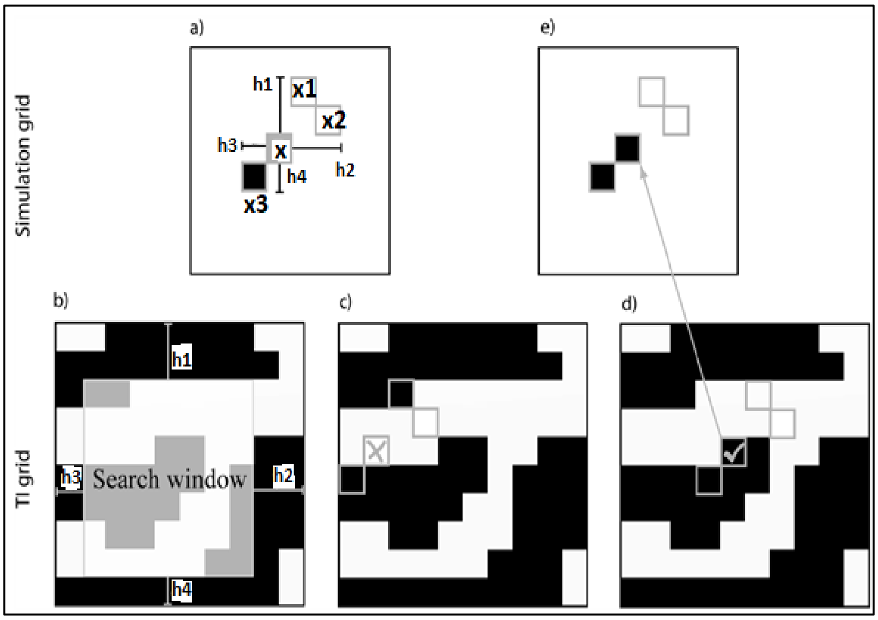

Figure 2.10: Direct sampling algorithm description (Mariethoz, et al., 2010)

There are limited applications of DeeSse in mining; examples of published literature on the application of DeeSse across various industries include:

- Simulation of ore boundaries for a lateritic bauxite deposit (Dagasan, et al., 2019).
- 3D geological modelling using cutting-edge Multiple-Point Statistics technology (Pluyaud, et al., 2019).
- Simulating rainfall time-series (Oriani, et al., 2018).
- A geostatistical approach to the simulation of stacked channels (Rongier, et al., 2017).
- Modelling uncertainty in gold deposits (Van der Grijp & Minnitt, 2015).

- Geological resources modelling in mining at Escondida Norte mine (Perez, et al., 2015).
- Simulation of log-permeability field conditioned to block data in a braided river environment (Straubhaar, et al., 2016).
- Conditioning of multiple-point statistics facies simulations to tomographic images (Lochbühler, et al., 2014).
- Simulation of flow and transport properties (Mariethoz, et al., 2010; Meerschman, et al., 2013).
- Conditional Simulation of Complex Geological Structures Using Multiple-Point Statistics (Strebelle, 2002).

2.8. Chapter Summary

This chapter provided a comprehensive review of literature concerning geological uncertainty, theory of regionalised variables, kriging, OK, SK, SGSIM, MPS and DeeSse. It highlighted the advantages, limitations and practical considerations for techniques used in this study. Case studies and debates around key concepts were highlighted.

3. CHAPTER III: RESEARCH METHODOLOGY

3.1. Introduction

The approach of this study is to investigate a proof of concept for the application of DeeSse for grade estimation, particularly when drill hole spacing is sparse. OK and SK TIs were developed using closely spaced 25 m x 25 m x 3 m grade control data for the A1 reef horizon within the pit area (TI area). The TI were developed on a support of 10 m x 10 m x 3 m SMU blocks. Only the SK TI was eventually selected and used for all DeeSse simulations to make it comparable with the SK-based SGSIM simulations used for validation. All SGSIM simulations used an NSCORE variogram developed from the 25 m x 25 m x 3m grade control data. The TI was then validated by comparing it to the SGSIM etype estimate of 50 simulations developed using input data spaced at 25 m x 25 m x 3 m.

Following the validation of the TI, 50 DeeSse simulations were run in the TI area and the resultant etype estimate was validated by comparing it to a SGSIM etype estimate of 50 SGSIM simulations within the same area. These DeeSse and SGSIM were conditioned to the same input data at 50 m x 50 m x 3 m grid spacing which is greater than the data spacing used for the development of the TIs. This moderately spaced 50 m x 50 m x 3 m drill hole data were extracted by filtering them from the closely spaced 25 m x 25 m x 3 m set.

After the validation of the application of DeeSse within the better "known" grade control (TI) area, DeeSse and SGSIM grade simulations were then run in the lesser "known" extension area. The simulations within the EA were developed using input drill hole data spaced at a grid size of 200 m x 100 m x 3 m. The subsequent DeeSse and SGSIM etype estimates were also compared as part of the validation process. Drill holes in the EA are sparsely drilled diamond exploration holes. The drill hole grid configuration showing the TI area and EA is shown in Figure 1.4.

Prior to using the drill hole dataset, it was rotated from being originally along an inclined plane in order to get the data to lie along a flat plane. This was necessary for the functioning of DeeSse so as to limit the number of uninformed nodes within the 3D cuboid grid encompassing the data. The data was given as 1 m composites. The successive workflow in the methodology included:

- Sample analysis,
- Geological (wireframe) modelling,
- Training image creation and validation.
- Application and validation of DeeSse within the TI area.
- Application and validation of DeeSse within the EA.
- Stochastic resource modelling which included uncertainty quantification and stochastic grade-tonnage curves.
- Determination of uncertainties and distributions of the metal content estimates and revenue projections.

No geological domaining was required since the data used in the study was extracted from an already defined domain of the A1 reef horizon. The data given was already composited at 1 m intervals as per the mine's practice. Thus, borehole length analysis and additional decisions about composite lengths was not necessary. Grade capping or cutting was also not applied in order to preserve the patterns in the TI and also to honour the original conditional data. The major assumption of the methodology is that the TI and the variogram of the grade control data both represent the underlying spatial structure in the TI and EA.

3.2. Sample Analysis

The first step in sample analysis was to visualise the drill holes on plan view and comment on the spatial distribution of grades. The visualisation enabled the identification of changes in grade distribution in different directions. This was used to confirm anisotropic investigations from variogram maps.

Exploratory Data Analysis (EDA) on gold (Au) grades was carried out on each of the three sample data sets (i.e. 25 m x 25 m x 3 m, 50 m x 50 m x 3 m and 200 m x 100m) for the A1 reef. The EDA on grades will guide decisions around geological domaining and compositing. For this particular study, EDA was carried out to depict any grade trends within the domain and assist in identifying underlying data distributions. EDA statistics calculated included the number of samples, mean, mode, skewness, kurtosis, variance, standard deviation, coefficient of variation and quantiles of Au grades.

Data -preparation, -cleaning and -validation were implemented to prevent any errors and possible biases. Data preparation started by confirming whether the relevant database is subject to a quality control protocol. It was also verified that the QA/QC procedures are in place and are being implemented during assaying. During data validation and cleaning, any missing records were identified, and blank assay values were deleted. Drill holes were also visualised in Datamine StudioRM and checked for any apparent errors. Examples of possible errors could include overlaps, incorrect positioning of collars or mismatches between data and hole traces (Dohm, 2019). Data tables were checked for format compatibility required by Datamine StudioRM and Ar2Gems. The samples were regarded as representative of the underlying distribution and there was no clustering of samples identified. As a result, declustering was unnecessary. It was essential to update EDA results when any data changes were made during the data - cleaning - and validation - processes. This was done to assess how these changes could have affected the original summary statistics and distributions.

Analysis and identification of the underlying distribution was carried out. The use of histograms and summary statistics aided the identification of the underlying probability distributions. Log transformation of sample data was necessary to test for lognormality. Sampling analysis was carried out using SAS Enterprise Guide as well as Datamine StudioRM. The results, analysis of the EDA and of the distribution assessments are discussed in Section 4.2.

3.3. Geological Modelling

Two wireframe geological models were developed for the TI and EA by creating vein surfaces defined by the respective drill hole samples encompassing the A1 reef zone. The wireframe models were created using the radial interpolation function within the Datamine StudioRM implicit geological modelling tool. Radial interpolation generates bounding circles around samples. The size of the discs is defined by a predetermined extension radius. The limiting boundary is subsequently constructed by bounding arc segments of the discs. These circles, together with the extension radius and arc segments, model changes of direction around the structure. The main advantage of using radial interpolation is that the continuity or search radius can be adjusted to control the "dimple-ness" of the hanging wall and footwall without causing unexpected "blow outs" in the surface, (Datamine, 2020). The geological model was created using the following control parameters, (Datamine, 2020):

- Uncertainty – how strictly should the samples (FROM-TO) should be honoured.
- Extension radius – radius of interpolation discs created around a sample.
- Continuity –radial distance over which a sample will exert an influence
- Resolution – resolution of wireframe surface.
- Trend smoothness – how "bumpy" or "wavy" the surface appears.

No pitchouts were permitted and drill holes with gaps were ignored in the processing of the wireframe. Various inputs were tested and the ones that provided the most realistic model honouring both the drill holes and the expected geology were chosen. The control parameters selected through trial and error for the creation of the TI and SG geological models are shown in Table 3.1. The subsequent wireframes produced were cleaned by removing planar holes, crossovers, interior and hanging triangles.

Table 3.1 : Geological modelling input parameters

Parameter	TI	SG
Uncertainty	0.01	0.001
Extension radius	35.6 m	200 m
Continuity	50 m	260 m
Resolution	High	High
Trend smoothness	50%	50%

The TI and SG wireframe geological models were then populated with blocks within which estimation will be carried out. The resultant models are referred herein as block models. The block model boundaries are limited by the extents of the sample data and wireframes. A considerable amount of work has already been carried out by the mine to establish the optimal estimation block sizes which also correspond to the smallest mining unit (SMU). The sizes of these SMU blocks are s (X) 10 m x (Y) 10 m x (Z) 3 m (personal communication, Aboagye, 2019). The resultant geological and block model including the relevant parameters are shown and analysed in Section 4.3.

3.4. Training Image Creation

A training image for the grade was constructed in the form of kriged grade models using closely spaced 25 m x 25 m x 3 m spaced data for the A1 reef zone. Two training models were developed using both SK and OK within Datamine StudioRM. One model was subsequently chosen based on a predetermined criterion as shown later in Section 4.4. To create kriged training models, the steps followed included variography, KNA and estimation.

3.4.1. Variography

Variography included experimental variogram calculations, anisotropy investigations and fitting variogram models using 25 m x 25 m x 3 m grade control data for the A1 reef. Downhole and standard variograms were calculated using StudioRM for the directions and dips shown below.

- Initial direction: 0.00 + or - 15.00 degrees
- Initial dip: 0.00 + or - 7.50 degrees
- Increment between successive directions: 30.00 degrees
- Increment between successive dips: 15.00 degrees
- Number of directions: 6
- Number of dips: 12

The lag distances were selected based on the maximum distance between samples of 871 m, average drill hole spacing of 25 m, composites lengths of 1 m and the A1 reef thickness being between 3 – 7 m. The subsequent lag intervals were defined as summarised in Table 3.2:

Table 3.2 : Variogram lag parameters applied to the 25 m x 25 m x 3 m grade control data

Parameter	**Downhole**	**Standard variogram**
Number of lags	7	18
Minimum lag distance (m)	1	25
Lag tolerance (m)	0.5	12.5
Maximum lag distance (m)	7	436

The selection of the variography input parameters was guided by the considerations discussed in Section 2.4. The nugget effect was estimated from a downhole variogram. Variogram maps for experimental variograms which displayed adequate description of spatial continuity and sufficient number of pairs were calculated. These variograms maps were assessed individually to investigate the experimental variogram/s which showed the largest ranges of continuity. The directions at which these variogram/s were calculated were noted and the corresponding variogram/s were modelled. The variograms and variogram maps are shown and analysed in Section 4.4.1.

3.4.2. Kriging neighbourhood analysis (KNA)

KNA was implemented using Datamine StudioRM to optimise the discretisation points and search parameters used in the estimation process. The parameters at which the block covariance approached a constant value, gave the highest KE, or resulted in the highest SLOR were selected. Section 4.4.2 details the results and analysis of KNA.

3.4.3. Estimation

Before the OK and SK TI models could be estimated, important aspects regarding the DeeSse requirements and software constraints needed to be addressed. These aspects primarily had to do with the choice of the type of estimation boundary for training image models. Common practice in kriging is to estimate within blocks bound by a geological model in the form of a wireframe. However, this wireframe can be dipping and undulating in nature. A best fit cuboid (i.e. prototype) is normally generated to engulf the wireframe and subsequent grade model as shown in Figure 3.1.

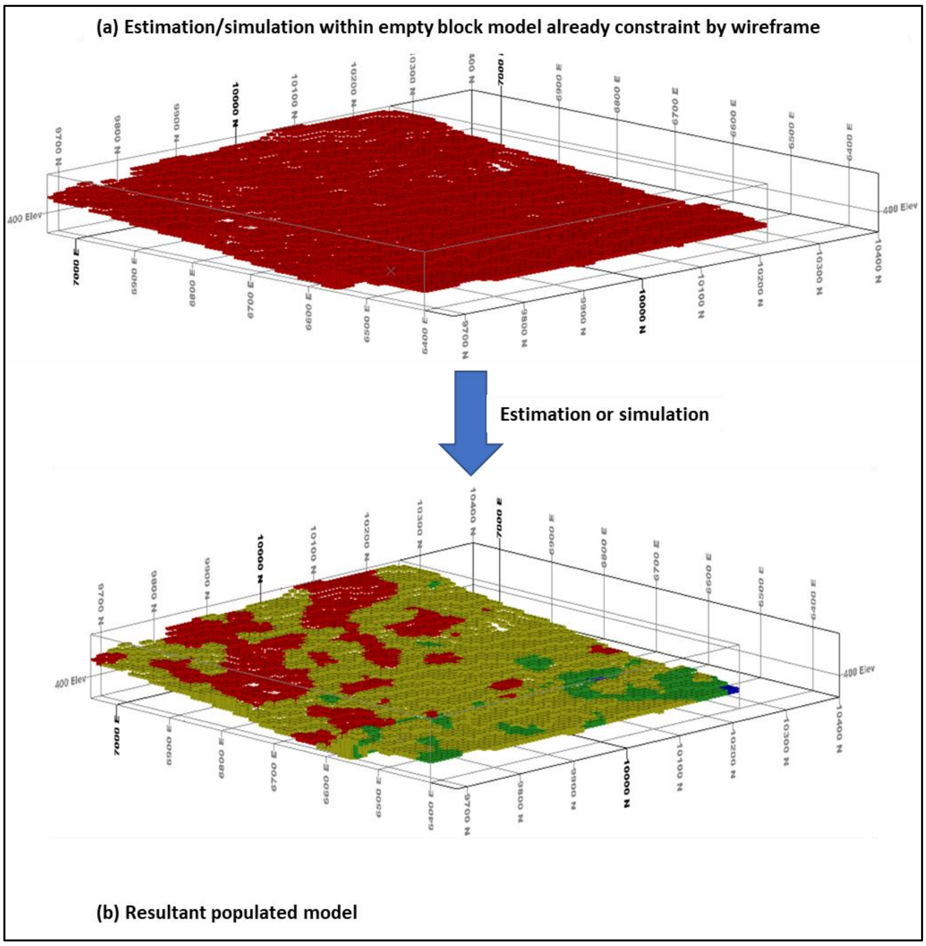

Figure 3.1 : Diagram showing estimation within 10 m x 10 m x 3 m blocks bound by a wireframe

As shown in Figure 3.1, the only locations containing data would then be located within the wireframe region. This posed a problem when attempting to use DeeSse because the algorithm requires that data be within a regular grid filled with blocks covering most of the cuboid/prototype. As a result, the DeeSse application returned errors specifying that there were too many uniformed nodes. An attempt to select portions of the TI which would have fewer uninformed nodes was tested. However, this method is cumbersome and significantly reduced the size of TI, making it non-representative. Another option would have been to fit a rotated prototype, however importing data in the Ar2Gems only allowed rotation by one axis i.e. the vertical axis.

Hence, the original data used by the mine was subsequently rotated for the A1 reef to test whether the “uninformed nodes” problem will persist. This rotated data is the sample information subsequently used in this study. Attempting to import a training image created from the rotated data did not yield desired results. The error resulting from too many uninformed nodes persisted. When small portions of the TIs which form a cuboid with fewer uninformed nodes were selected, the training image became smaller and non-representative. This then required that the simulation grid (SG) be reduced as well. Another concern was that, even when smaller portions of the TI were successfully imported, Ar2gems flattened the view of the TI. This flattened view provided uncertainty about the true locations of the estimation blocks. This approach remained cumbersome and suboptimal.

Another approach was further investigated. This tactic involved estimating blocks that fill the entire cuboid or prototype without constraining the estimation to wireframe boundaries. The idea was then to split the blocks using a wireframe later during the post-processing stage as shown in Figure 3.2. This approach was tested using both the rotated and unrotated data. With both data sets, the TIs could be successfully used for DeeSse simulations. However, using the unrotated data meant that a bigger prototype with significantly more unnecessary blocks would be needed. Around 1.2 million blocks would be created when estimating within a cuboid which encompasses unrotated data. This required more computing time and computer storage space. On the other hand, the cuboid from rotated data contained just over 90 thousand blocks and resulted in faster simulations being achieved. Furthermore, the cuboid model from unrotated data had lower averages for KE and SLOR. Although these KE and SLOR values improved following the splitting of the cuboid with wireframes, these measures were still significantly lower than when using rotated data.

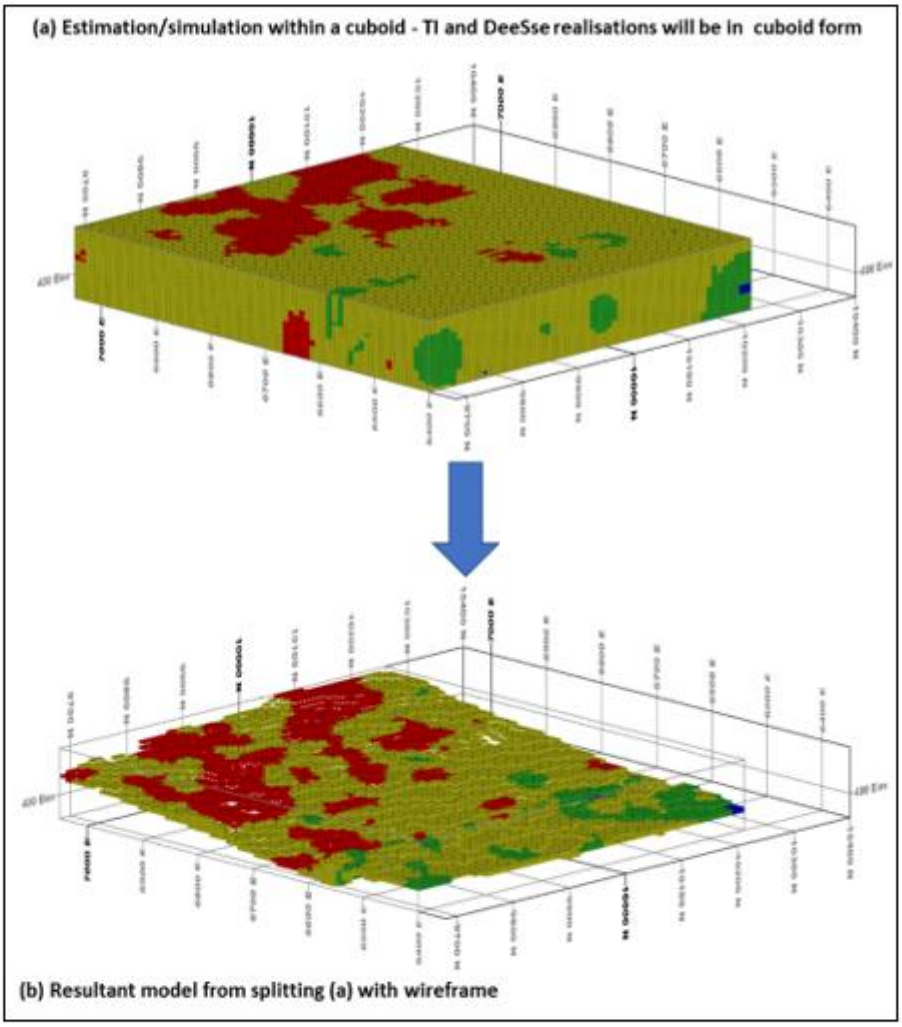

Figure 3.2 : Diagram showing estimation within a cuboid which is later split by a wireframe (10 m x 10 m x 3 m blocks)

As a result, the TIs' creation approach in this report involved kriging into the entire cuboids using the rotated data and then splitting the cuboids with wireframes during post-processing. The splitting allowed for the extraction of only the relevant blocks which were within with the geological unit. A comparison between grade block models developed within wireframes and the ones from splitting cuboids after estimation was necessary. This assessment was critical in order to investigate whether the cuboid estimation approach would be sufficiently robust. The cuboid and wireframe-based models for OK and SK were compared by looking at their means, variances, ranges, KEs and SLORs. This comparison and relevant results are detailed and discussed in Section 4.4.3. Finally, only one TI between the SK and OK models would be chosen for DeeSse simulations as explained in Section 4.4.3. The parameters used for the kriging of the TIs are summarised in Table 3.3. The choice of the parameters used was guided by the KNA and considerations highlighted in Section 2.5.3.

Table 3.3 : Parameters for kriging using 25 m x 25 m x 3 m data

Parameter	**Values**
Grid parameters	As per prototype model in Table 4.3
Block sizes	(X) 10 m x (Y) 10 m x (Z) 3 m
Variogram model	Parameters as selected in Section 4.4.1 and shown in Table 4.4
Discretisation in the X direction	4
Discretisation in the Y direction	4
Discretisation in the Z direction	2
Search distance X (m)	302
Search distance Y (m)	353
Search distance Z (m)	302
Minimum number of samples	1
Maximum number of samples	50

3.5. Training Image Validation Using SGSIM (25 m x 25 m x 3 m Input Data)

SGSIM involves the following steps and practical considerations (Rossi & Deutsch, 2014):

1) EDA of sample data, including variography and domain definition. Conditional simulations are very sensitive to departures from stationarity; therefore, domain definition is critical so as to obtain representative simulations. Best practice is to first implement the simulation on a small area, while fine-tuning the parameters that give a better reproduction of histograms and variograms. Only after that can “complete” multiple simulations be run.
2) De-trending of data if necessary.
3) Normal scores (NSCORE) transformation of sample data to obtain the corresponding Gaussian distribution. Declustering may be necessary if samples are preferentially located. Despiking may also be necessary in

order to remove ties presented by the original variable (Deutsch & Journel, 1997; Rossi & Deutsch, 2014).

4) Calculating and modelling variograms in the Gaussian space.
5) Defining a random path through each domain to be simulated in order to avoid artefacts. It is important to ensure that nodes are visited only once. Nodes that are already simulated are skipped.
6) Using simple kriging to estimate the conditional distribution for each node to be simulated in Gaussian space. "*The estimated simple kriging value* $Y^*(u)$ *is the mean of the conditional distribution at that node, and its variance is the simple kriging variance* $\sigma_{sk}\ (u)$".
7) Assigning the closest data to grid nodes can significantly speed up the simulation but some information may be lost. It also important to ensure that when there are vertical drill holes, the node spacing is equivalent to the sample composite lengths to ensure that most of the drill hole data is used. This is not applicable when dealing with inclined-, sub-horizontal-, twinned- or closely spaced- holes. The use of more data provides better estimates of conditional mean and variance but will take longer to run.
8) Generating a simulated value for the node $Y_s(u)$ by randomly drawing a value from the conditional simulated distribution obtained in the previous step.
9) Incorporating the simulated value $Y_{\ s}\ (u)$ as conditioning data for nodes to be subsequently simulated, thereby ensuring variogram reproduction.
10) Repeating and continuing the process until all nodes and all domains have been simulated. The number of realisations needed is a defined by how many are necessary to model the uncertainty. It has been suggested that 20 to 50 simulations are generally sufficient to characterise the range of possible values for the simulated variables (Deutsch & Journel, 1997; Goovaerts, 1999; Rossi & Deutsch, 2014).
11) Verifying that the histogram of the simulated values is Gaussian; also checking that the simulated values reproduce well the Gaussian variogram model used in the simulation.

12) Back transforming the Gaussian simulated values to the original variable space.
13) Adding back the trend if the simulation was performed on residuals.
14) Verifying that the histogram of the back-transformed data is similar to the original distribution (Leuangthong, et al., 2004).
15) Verifying that the variogram obtained from the simulated values is similar to the variogram of the original values (Leuangthong, et al., 2004).
16) Verifying that the model presents a reasonable spatial distribution (Leuangthong, et al., 2004).
17) Checking for any other errors or omissions.

Following the creation of the TI, 50 SGSIM simulations were run using 25 m x25 m x 3 m input data and an NSCORE variogram based on the same dataset. These simulations are referred as SGSIM25 simulations in this report. The SGSIM25 were run in the same area as the TI into 10 m x 10 m x 3 m block sizes. NSCORE variograms were calculated using Datamine StudioRM for the directions and dips shown below.

- Initial direction: 0.00 + or - 15.00 degrees
- Initial dip: 0.00 + or - 7.50 degrees
- Increment between successive directions: 30.00 degrees
- Increment between successive dips: 15.00 degrees
- Number of directions: 6
- Number of dips: 12

The lag distances were selected based on the maximum distance between samples of 871 m, composites lengths of 1 m and the A1 reef thickness being between 3 – 7 m. The subsequent lag intervals were similar to those defined in Table 3.2. The input parameters for variography and SGSIM were guided by aspects discussed in Sections 2.4 and 2.6.1 respectively. SGSIM inputs are summarised in Table 3.4.

Table 3.4 : NSCORE SGSIM parameters for 25 m x 25 m x 3 m input data

Parameter	**Values**
Grid parameters	As per prototype model in Table 4.3.
Variogram Model	Parameters as shown in Section 4.5 and Table 4.8.
Minimum conditioning data	1
Maximum conditioning data	12
Search distances X (m)	378
Search distances Y (m)	436
Search distances Z (m)	30
Number of simulated points per parent cell in the X direction	2
Number of simulated points per parent cell in the Y direction	2
Number of simulated points per parent cell in the Z direction	1

Post SGSIM simulations, the points in each parent cell were block averaged to create a simulation block model of all the realisations. Etype estimate (average) estimates for both DeeSse and SGSIM25 simulations were calculated; and their statistics, variograms, block grades and cdfs were compared. For the application of DeeSse to be valid, its results should not differ significantly from the SGSIM's. The subsequent validation results are presented and analysed in Section 4.5.

3.6. Application and Validation of DeeSse in the TI Area Using a 50 m x 50 m x 3 m Drilling Grid

The basic operation of DeeSse is as follows (Mariethoz, et al., 2010):

- Each conditioning data is assigned to its closest grid node in the SG. This is followed by defining a simulation path within the SG. For each unknown location $\mathbf{x}$ in the path, its corresponding neighbours is then found. The neighbours of $\mathbf{x}$ are comprised of a maximum number of $\boldsymbol{n}$ closest grid nodes $\{\mathbf{x_1},\ \mathbf{x_2}, \cdots, \mathbf{x_n}\}$ that were either already assigned or simulated in the SG. Then lag vectors $\mathbf{L} = \{\mathbf{h_1}, \cdots, \mathbf{h_n}\} = \{\mathbf{x_1} - \mathbf{x}, \cdots, \mathbf{x_n} - \mathbf{x}\}$ are computed. If no neighbour is found for $\mathbf{x}$, a value of $\mathbf{Z}(\mathbf{y})$ from a random node $\mathbf{y}$ in the TI is assigned to $\mathbf{Z}(\mathbf{x})$ in the SG. Afterwards, data events are defined. Data events are vectors containing the values of the variable of interest at all neighbourhood nodes, and are denoted as:

  $$\mathbf{d_n}(\mathbf{x}, \mathbf{L}) = \{\mathbf{Z}(\mathbf{x} + \mathbf{h_1}), \cdots, \mathbf{Z}(\mathbf{x} + \mathbf{h_n})\}.$$

- The search window in the TI is defined by constraining the search to the maximum and minimum values of the lag vectors.
- The search window is systematically scanned from a random location $\mathbf{y}$. For each value of $\mathbf{y}$, the data event $\mathbf{d_n}(\mathbf{y}, \mathbf{L})$ is found. Then the distance $\mathbf{d}\{\mathbf{d_n}(\mathbf{x}, \mathbf{L}),\ \mathbf{d_n}(\mathbf{y}, \mathbf{L})\}$ between the data event in the SG and the one found in the TI is computed. This is followed by storing $\mathbf{y}, \mathbf{Z}(\mathbf{y})$ and $\mathbf{d}\{\mathbf{d_n}\{\mathbf{x}, \mathbf{L}, \mathbf{d_n}(\mathbf{y}, \mathbf{L})\}\}$ if the nearest distance is obtained. This distance is computed differently for continuous and categorical variables as shown below:

  Continuous Variable (Weighted Euclidian distance):

$$\mathbf{d}\{\mathbf{d_n}(\mathbf{x}), \mathbf{d_n}(\mathbf{y})\} = \sqrt{\sum_{i=1}^{n} \boldsymbol{\alpha}_\mathbf{i}[\mathbf{Z}(\mathbf{x_i}) - \mathbf{Z}(\mathbf{y_i})]^2} \in [\mathbf{0}, \mathbf{1}] \quad \textbf{3-1}$$

  where some power distance weighting can be applied to the lag vector $\mathbf{h_i}$ using a power function of order $\boldsymbol{\delta}$ as follows:

$$\boldsymbol{\alpha}_\mathbf{i} = \frac{\|\mathbf{h_i}\|^{-\delta}}{\mathbf{d_{max}}^2 \sum_{i=1}^{n} \|\mathbf{h_i}\|^{-\delta}}, \quad \mathbf{d_{max}} = \mathbf{max}\,\mathbf{Z}(\mathbf{y}) - \mathbf{min}\,\mathbf{Z}(\mathbf{y})_{\mathbf{y} \in \mathbf{TI}} \quad \textbf{3-2}$$

  Categorical variables:

$$\mathbf{d}\{\mathbf{d_n}(\mathbf{x}), \mathbf{d_n}(\mathbf{y})\} = \frac{\mathbf{1}}{\mathbf{n}} \sum_{i=1}^{n} \mathbf{a_i} \quad \in [\mathbf{0}, \mathbf{1}] \quad \textbf{3-3}$$

where $\mathbf{a_i} = \begin{cases} \mathbf{0} & \mathbf{if\ Z(x_i) = Z(y)} \\ \mathbf{1} & \mathbf{if\ Z(x_i) \neq Z(y)} \end{cases}$

The variable $\mathbf{a_i}$ is an indicator variable symbolising the fraction of nonmatching nodes.

- If $\mathbf{d\{d_n(x, L), d_n(y, L)\}}$ is smaller than the acceptable threshold $\boldsymbol{t}$, the value $\mathbf{Z(y)}$ is sampled and assigned to $\mathbf{Z(x)}$.
- When the TI matches the data event exactly, the distance is zero and $\mathbf{Z(y)} = \mathbf{1}$ is assigned to $\mathbf{Z(x)}$. Should the specified maximum scan fraction $\boldsymbol{f}$ be reached before finding an exact match between TI and data event, the node $\mathbf{y}$ with the lowest distance is accepted and its value $\mathbf{Z(y)}$ is assigned to $\mathbf{Z(x)}$.

The parameters (1) threshold position (***t***) (2) maximum fraction of the TI to be scanned (***f***), and (3) maximum number of points in a neighbourhood (***n***); should be chosen carefully to balance simulation quality and CPU time. Alternatively, other options such as parallelisation or using multi-core processors can reduce CPU time. Nonetheless, even without these attempts to improve speed, DeeSse takes about the same time as SGSIM to obtain the same simulation quality (Mariethoz, et al., 2010). The threshold ***t*** needs to be defined because it is usually not possible to find a TI pattern that matches $\boldsymbol{d_n}$ exactly. An exponent can be given to the distance function in order to calculate the distances by weighting nodes according to their proximity to the central node. All distances are normalised to be between 0 and 1 such that $\mathbf{d\{d_n(x), d_n(y)\}} = \mathbf{0}$ means an exact match and $\mathbf{d\{d_n(x), d_n(y)\}} = \mathbf{1}$ indicates no match. The maximum fraction ***f*** tells DeeSse when to stop searching the TI for patterns. Large ***f*** values may result in extremely long searches and may present a verbatim copy of the TI. Low ***f*** values may result in unrealistic realisations. The number $\boldsymbol{n}$ of grid nodes closest to $\boldsymbol{x}$ are chosen so that they are not positioned at more than half the maximum neighbourhood size from $\boldsymbol{x}$. All these parameters are usually tested through trail-and error. Followed by choosing values which give the best simulation quality at a practical simulation time (Meerschman, et al., 2013). All these considerations guide how DeeSse is parameterised.

DeeSse offers a variety of other options to enhance the use of TIs, improve simulation quality and address non-stationarity as detailed in Mariethoz, et al. (2010). For simulating a continuous variable, four Manhattan distance options are available depending on how the ranges and means of the conditioning data and the TI compare. Manhattan relative distance (Distance 4) was used in this study in order to ensure that the range of simulated values is not constraint to the range of the TI. Distance 4 allows for trends to be implicitly given by conditioning data. When calculating distance 4, the variable is not normalised, but patterns centred to the mean value are considered instead. That is, the value at a node of the pattern is the difference between the value of the variable at that node and the mean of the variable over the pattern nodes (Renard, et al., 2019).

DeeSse results can be validated by visual inspections of simulation quality and assessing simulation indicators. Visual inspection entails comparing patterns between TIs and simulations from plans and sections. Simulation indicators include the three error indices, i.e. histogram-, variogram - and connectivity – errors. For details on how these indices can be calculated and assessed see Meerschman, et al. (2013). An alternative to calculating these indices is to plot and compare the histograms, variograms and connectivity plots of the simulations against the TIs. In this study, the latter approach was implemented together with visual inspections and comparison to SGSIM results. This validation was carried out by comparing the etype estimates of the simulation methods instead of each individual realisation.

In order to validate the application of DeeSse, it was first applied in the better “known” TI area using conditioning data from the same area but at a wider grid of 50 m x 50 m x 3 m. DeeSse simulations were run into 10 m x 10 m x 3 m block sizes. The DeeSse parameters used are summarised in Table 3.5. These parameters were selected through trial and error by testing different combinations that would result in realisations that visually resemble the TI and its statistics. A balance of reproducibility and computer performance was sought.

Table 3.5 : DeeSse parameters for 50 m x 50 m x 3 m data

Parameter	**Value**
Maximum number of nodes	50
Acceptance threshold	0,000001
Distance type	Manhattan Relative Distance (4)
Max scan fraction	0.5
Simulation path	Random (0)

50 SGSIM simulations were run using 50 m x 50 m x 3 m input data. However, the NSCORE variogram based on the 25 m x 25 m x 3 m input data was used. This is the same NSCORE variogram parametrised in Table 3.4 and discussed in Section 4.5. The reason for using a more robust variogram was to ensure that SGSIM simulations are more easily compared to the DeeSse realisations given that DeeSse will also be conditioned to a TI created using the same variogram input data. Using a variogram of the 50 m x 50 m x 3 m samples would have immediately disadvantaged SGSIM and made the results less comparable to DeeSse. These 50 SGSIM simulations are referred as SGSIM50 simulations in this report. The SGSIM50 were run in the same area as the DeeSse (TI Area) into 10 m x 10 m x 3 m block sizes.

Post SGSIM simulations, the points in each parent cell were block averaged to create a simulation block model of all the realisations. Etype (average) estimates for both DeeSse and SGSIM50 simulations were calculated; and their statistics, variograms, block grades and cdfs were compared. For the application of DeeSse to be valid, its results should not differ significantly from the SGSIM's. The subsequent results are presented and analysed in Sections 4.6 and 4.7.

3.7. Application and Validation of DeeSse in the EA Using a 200 m x 100 m x 3 m Drilling Grid

Once the TI and the application of DeeSse for grade simulation was proven to be valid within the TI area, simulations were then run within the extension area. Fifty (50) DeeSse simulations were carried out using the sparsely spaced drill hole data at 200 m x 100 m x 3 m grid intervals. The choice of DeeSse parameters used was guided by considerations highlighted in Section 2.7.3 and the parameters are summarised in Table 3.6. These parameters were selected through trial and error by testing different combinations that would result in realisations that visually resemble the TI and its statistics. A balance of reproducibility and computer performance was sought.

Table 3.6 : DeeSse parameters for the 200 m x 100 m x 3 m data

Parameter	Value
Maximum number of nodes	35
Acceptance threshold	0,16
Distance type	Manhattan Relative Distance (4)
Max scan fraction	0.5
Simulation path	Random (0)

Following DeeSse implementation in the EA, another 50 SGSIM simulations were run using the 200 m x 100 m x 3 m dataset within the same area. For similar reasons given in Section 3.6, the NSCORE variogram used was on the 25 m x 25 m x 3 m input data. This NSCORE variogram has already been parametrised in Table 3.4 and is discussed in Section 4.5. These 50 SGSIM simulations are referred as SGSIM200 simulations in this report. The SGSIM200 were run in the same area as the DeeSse EA) into 10 m x 10 m x 3 m blocks. The input parameters for variography and SGSIM were guided by aspects discussed in Sections 2.4 and 2.6.1 respectively. SGSIM inputs are summarised in Table 3.7.

Table 3.7 : SGSIM parameters for 200 m x 100m data

Parameter	Values
Grid parameters	As per prototype model in Table 4.3.
Variogram Model	Parameters as shown in Section 4.5 and Table 4.8.
Minimum conditioning data	1
Maximum conditioning data	12
Search distances X (m)	162
Search distances Y (m)	92
Search distances Z (m)	17
Number of simulated points per parent cell in the X direction	2
Number of simulated points per parent cell in the Y direction	2
Number of simulated points per parent cell in the Z direction	1

Post SGSIM simulations, the points in each parent cell were block averaged to create a simulation block model of all the realisations. Etype estimate (average) estimates for both DeeSse and SGSIM200 simulations were calculated; and their statistics, variograms, block grades and cdfs were compared. For the application of DeeSse to be valid, its results should not differ significantly from the SGSIM's. The subsequent results are presented and analysed in Sections 4.8 and 4.9.

3.8. Stochastic Resource Estimation Using DeeSse in the Extension Area

Following the execution and validation of DeeSse simulations, the uncertainties around the estimations were quantified. The benefits of this stochastic estimation were then detailed by showing its applicability in:

- Presenting and quantifying the uncertainty around the estimates.
- Determining probabilities above and below thresholds.
- Calculating stochastic grade tonnage curves.
- Presenting uncertainties for estimates of metal content and revenues.

3.9. Chapter Summary

In this chapter, a detailed methodology on how the study was conducted is discussed. This included details about how sample analysis, geological modelling, TI creation, DeeSse simulation and validation as well as uncertainty quantification were carried out. It was further explained how uncertainty is integrated to better understand grade-tonnages, metal content and revenue projections.

4. CHAPTER IV: RESULTS AND ANALYSIS

4.1. Introduction

This chapter presents the results and analysis of the research activities described in CHAPTER III: RESEARCH METHODOLOGY. The results from the following activities are detailed and analysed:

- Sample analysis.
- Geological modelling.
- Training image creation and validation.
- Application and validation of DeeSse within the TI area.
- Application and validation of DeeSse within the EA.
- Stochastic resource modelling which included uncertainty quantification and stochastic grade-tonnage curves.
- Determination of uncertainties and distributions of the metal content estimates and revenue projections.

4.2. Sample Analysis

4.2.1. Locality map of drill hole samples

Plan views of three rotated datasets which are colour coded by their individual drill hole average grade values are shown in Figure 4.1. It can be noted from the locality maps that higher grades are more predominant in the southern eastern quadrant and decrease towards the north-west. There also seems to be greater ranges of continuity towards the west-eastern direction than in the orthogonal direction. Geometric anisotropy is presumed and will be further investigated and confirmed by using variogram maps in Section 4.4.1.

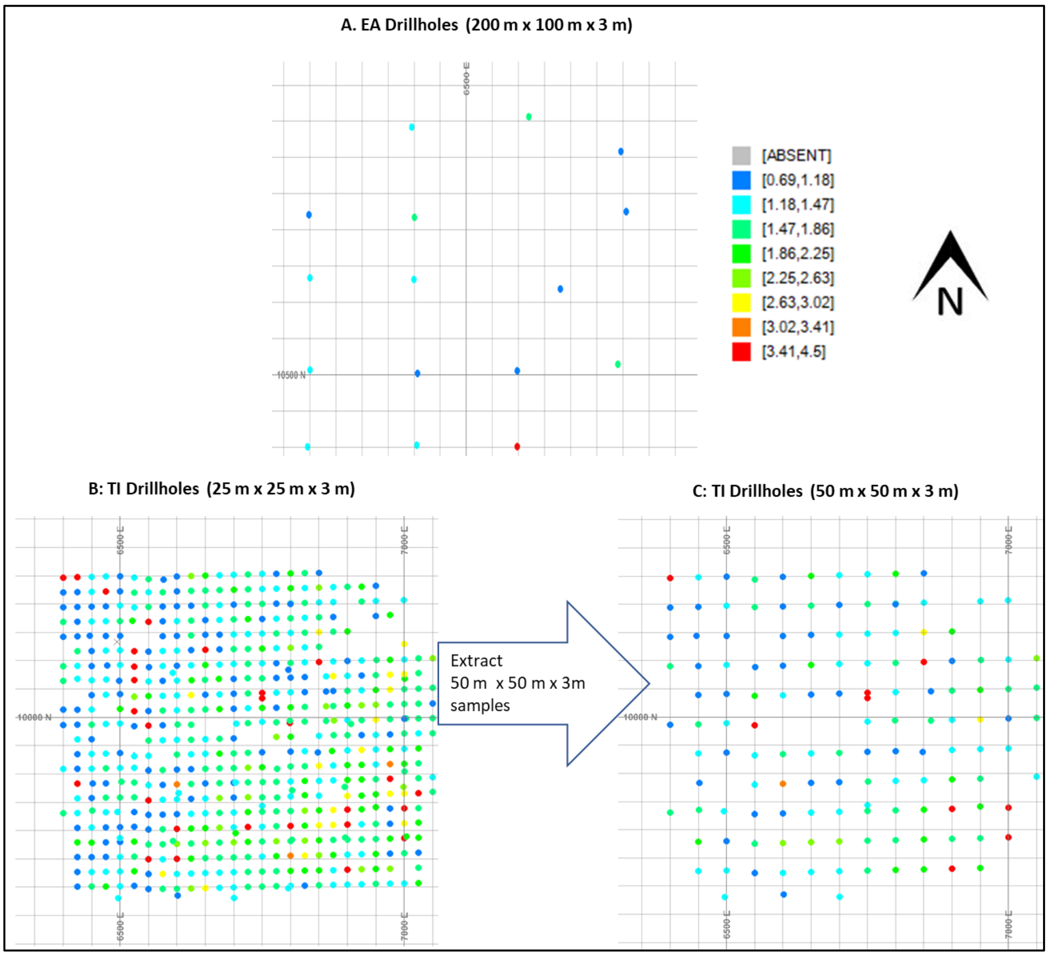

Figure 4.1 : Locality map of the drill holes (plan-view)

4.2.2. Data cleaning and validation

The 25 m x 25 m x 3 m and 50 m x 50 m x 3 m composites had one sample each with missing assay values. The 200 m x 100 m x 3 m composites had about six samples with no grade value. The samples without assay values were subsequently removed from the datasets. The reason for removing these samples was to avoid the missing data being replaced with "zero" values for grade, thereby leading to incorrect calculations. This was particularly important because at the time of the study it was not clear how Ar2Gems and Datamine StudioRM treated missing data. Examination of drill hole location plots and sections did not show any apparent sample positioning errors.

4.2.3. Exploratory data analysis

Table 4.1 summarises the EDA statistics for the three datasets before and after data validation and cleaning. Although several missing assay values were identified and deleted, the statistics did not change. That meant that StudioRM correctly treated the missing samples values as absent values instead of zeros.

Table 4.1: Summary statistics for Au (g/t) samples data (A1 reef)

Statistic	Drill hole Spacing					
	25 m x 25 m x 3 m		50 m x 50 m x 3 m		200 m x 100 m x 3 m	
	Original	Clean	Original	Clean	Original	Clean
Mean (g/t)	1.54	1.54	1.49	1.49	1.24	1.24
Standard Deviation (g/t)	1.35	1.35	1.38	1.38	0.99	0.99
Standard Error (g/t)	0.03	0.03	0.05	0.05	0.10	0.10
Variance $(g/t)^2$	1.82	1.82	1.90	1.90	0.99	0.98
Minimum (g/t)	0.01	0.01	0.05	0.05	0.03	0.03
Maximum (g/t)	22.60	22.60	18.80	18.80	4.98	4.98
Mode (g/t)	0.80	0.80	0.93	0.93	0.90	0.90
Range (g/t)	22.60	22.60	18.75	18.75	4.95	4.95
Number of samples	2857	2856	710	709	108	102
Number of missing values	1	0	1	0	6	0
Lower Quartile (g/t)	0.81	0.81	0.79	0.79	0.53	0.53
Median (g/t)	1.22	1.22	1.14	1.14	0.94	0.94
Upper Quartile (g/t)	1.86	1.86	1.76	1.76	1.67	1.67
Coefficient of Variation (CoV) %	87.46	87.46	92.36	92.36	79.96	79.96
Skewness	5.31	5.31	5.24	5.24	1.43	1.43
Excess Kurtosis	54.61	54.61	43.59	43.59	2.12	2.12

The mean grade for the 25 m x 25 m x 3 m data is 1.54 g/t and it is slightly greater (~3%) than that of the 50 m x 50 m x 3 m drill holes which is 1.49 g/t. The mean grade for the 200 m x 100 m x 3 m (i.e. 1.24 g/t) samples is considerably less than the averages of the other two datasets. It is about 19 % and 17 % less than the average grades of the 25 m x 25 m x 3 m and 50 m x 50 m x 3 m samples, respectively. This was expected since the extension area drill holes are in the north-western quadrant. It has been shown in Figure 4.1 that the grades decrease towards the north-western direction. The variances of the two datasets which are within the TI differ slightly by about 4%. This was also expected since the 50 m x 50 m x 3 m samples are a subset of the 25 m x 25 m x 3 m dataset. The variance of the 200 m x 100 m x 3 m (i.e. 0.98 $(g/t)^2$) samples is almost half the variances of the 25 m x 25 m x 3 m (i.e. 1.82 $(g/t)^2$) and 50 x 50m (i.e. 1.90 $(g/t)^2$) datasets. It is also important to note the significant differences in the number of samples within the TI area as compared to the EA. The 25 m x 25 m x 3 m dataset has 2856 samples as compared to only 102 samples for the 200 m x 100m drill holes. The mode of the 200 m x 100 m x 3 m data could not be calculated directly from the dataset. As a result, the mode was estimated graphically as shown in Figure 4.4 to be 0.90 g/t. The CoVs for all three datasets are significantly larger than 25%. This demonstrates that there is a high dispersion around the mean that will cause problems during estimation. The differences in the TI and EA grid datasets were noted because it would influence the type of distance function used when running DeeSse simulations. Histograms for the three datasets are shown in Figure 4.2, Figure 4.3 and Figure 4.4.

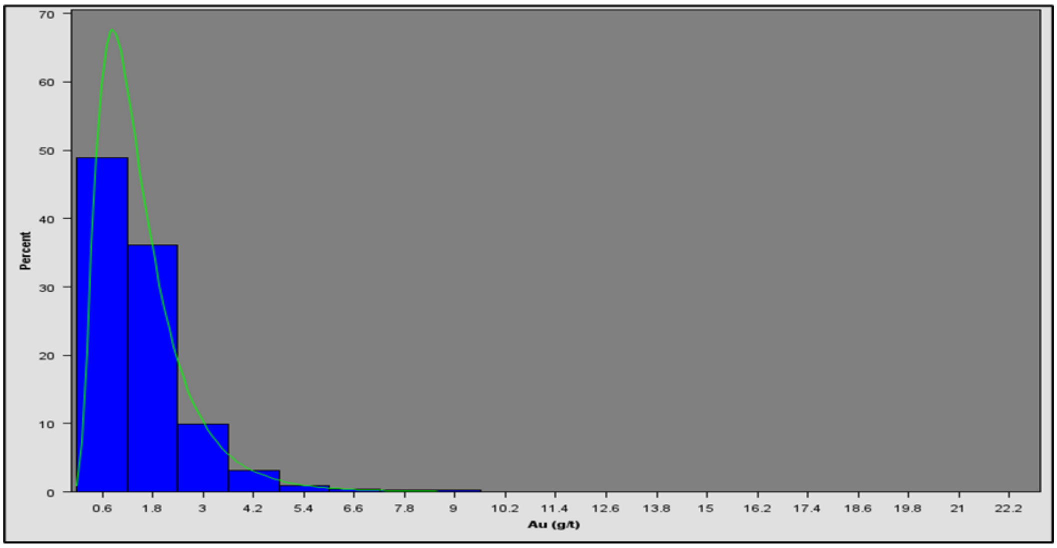

Figure 4.2: Histogram of cleaned 25 m x 25 m x 3 m Au (g/t) sample data (A1 reef)

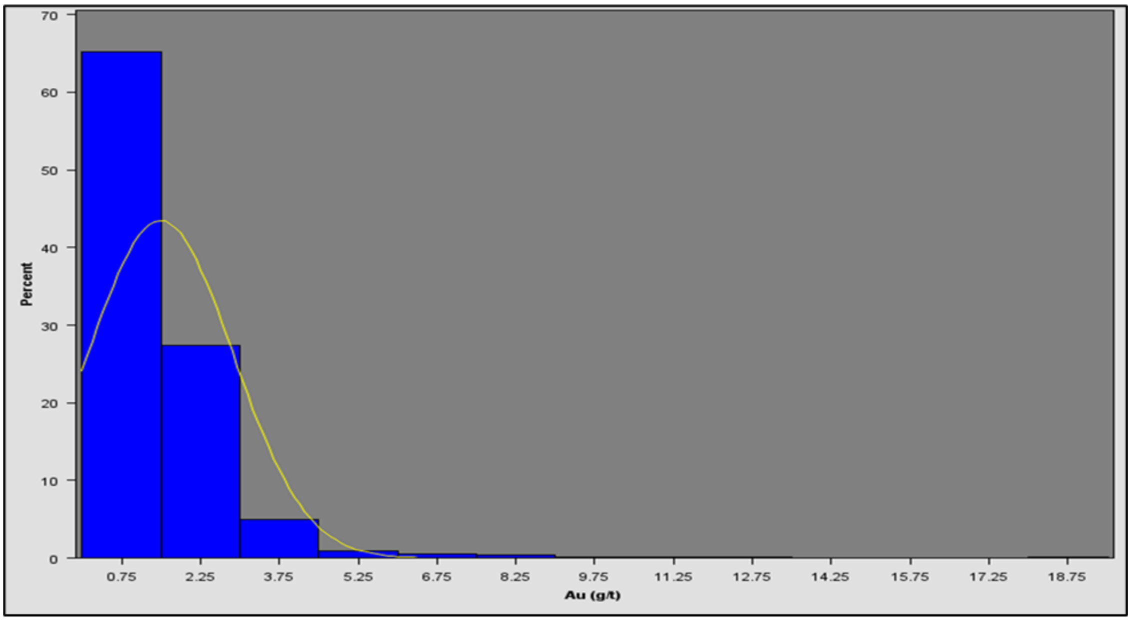

Figure 4.3 : Histogram of cleaned 50 m x 50 m x 3 m Au (g/t) sample data (A1 reef)

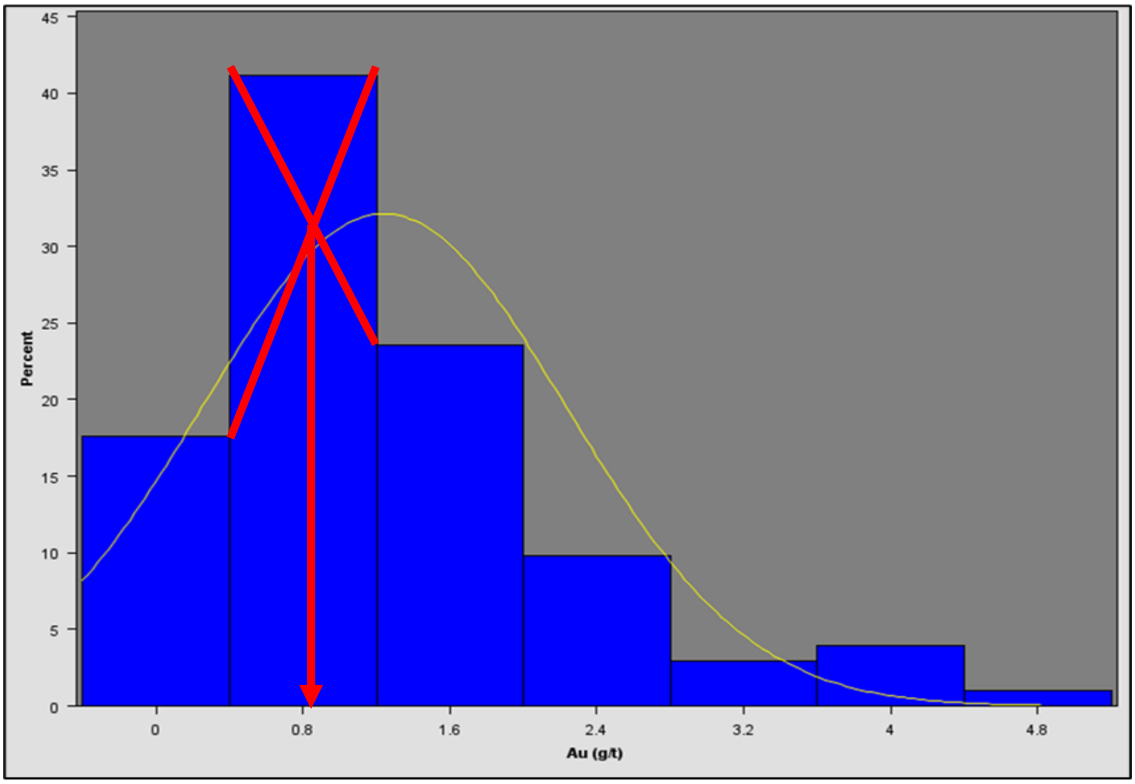

Figure 4.4 : Histogram of cleaned 200 m x 100 m x 3 m Au (g/t) sample data (A1 reef)

It is apparent from the histograms that the grade distributions for all three data sets are highly positively skewed. This is confirmed by the means being greater than the medians which are in turn greater than the modes (mean > median > mode) for all three datasets. The skewness of all three datasets also confirm that their distributions are highly positively skewed. The log-transformation of grades was then necessary to further analyse the underlying distribution by investigating the possibility of lognormality.

4.2.4. Distribution analysis

The distribution analysis was carried out on log-transformed data in order to investigate the three datasets for lognormality. The summary statistics for the transformed cleaned data are summarised in Table 4.2.

Table 4.2 : Summary statistics for log-transformed ln (Au g/t) samples data (A1 reef)

Statistic	**Drill hole Spacing**		
	25 m x 25 m x 3 m	**50 m x 50 m x 3 m**	**200 m x 100 m x 3 m**
Mean (g/t)	0.186	0.148	-0.130
Standard Deviation ln (g/t)	0.737	0.711	0.931
Standard Error ln (g/t)	0.014	0.027	0.092
Variance ln $(g/t)^2$	0.543	0.506	0.867
Minimum ln (g/t)	-5.298	-3.009	-3.629
Maximum (ln g/t)	3.118	2.934	1.605
Mode ln (g/t)	-0.223	-0.073	0.200
Range ln (g/t)	8.416	5.943	5.233
Number of samples	2856	709	102
Lower Quartile ln (g/t)	-0.217	-0.236	-0.643
Median ln (g/t)	0.199	0.131	-0.066
Upper Quartile ln (g/t)	0.621	0.565	0.513
Coefficient of Variation %	395.940	481.055	-717.207
Skewness	-1.046	-0.353	-0.353
Excess Kurtosis	3.897	2.336	2.336

The difference between the log values for the mean and median of the 25 m x 25 m x 3 m dataset is not significant, i.e. about 6 % difference. Similarly, log mean and median values for the 50 m x 50 m x 3 m samples vary moderately by about 10%. The approximate similarities of the mean and median values highlight probable symmetrical distributions of data. However, the log - mean and - median values for the 200 m x 100 m x 3 m vary greatly by just over 50%. The log values of the modes for all datasets vary significantly from the respective means and medians. The mode of the 200 m x 100 m x 3 m dataset was estimated graphically as shown in Figure 4.7. The skewness of log values for the 50 m x 50 m x 3 m and 200 m x 100 m x 3 m composited are between 0 and -0.5, which show slight symmetry in the distribution around the mean values. However, the skewness of the 25 m x 25 m x 3 m transformed samples (i.e. – 1.046) indicate possible skewness to the left. The kurtosis of all three ln Au datasets is moderately different from an excess kurtosis of three which will be indicative of a normal distribution. Although some summary statistics could highlight possible symmetry of the data, a few indicated that further analysis would be necessary before deciding on the probable underlying distribution. Hence, the histograms of all the log transformed datasets were constructed and shown in Figure 4.5, Figure 4.6 and Figure 4.7.

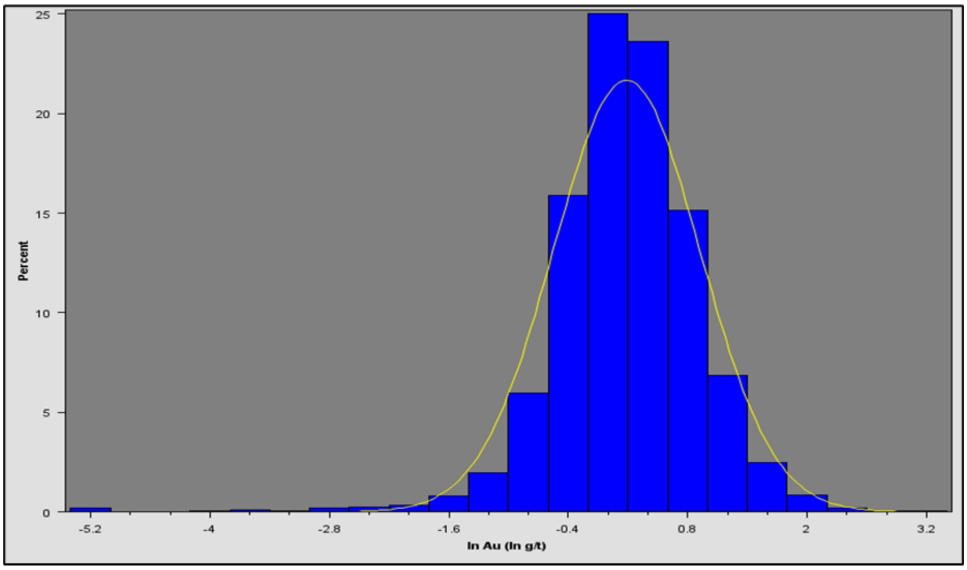

Figure 4.5 : Histogram of cleaned 25 m x 25 m x 3 m log-transformed Au sample data (A1 reef)

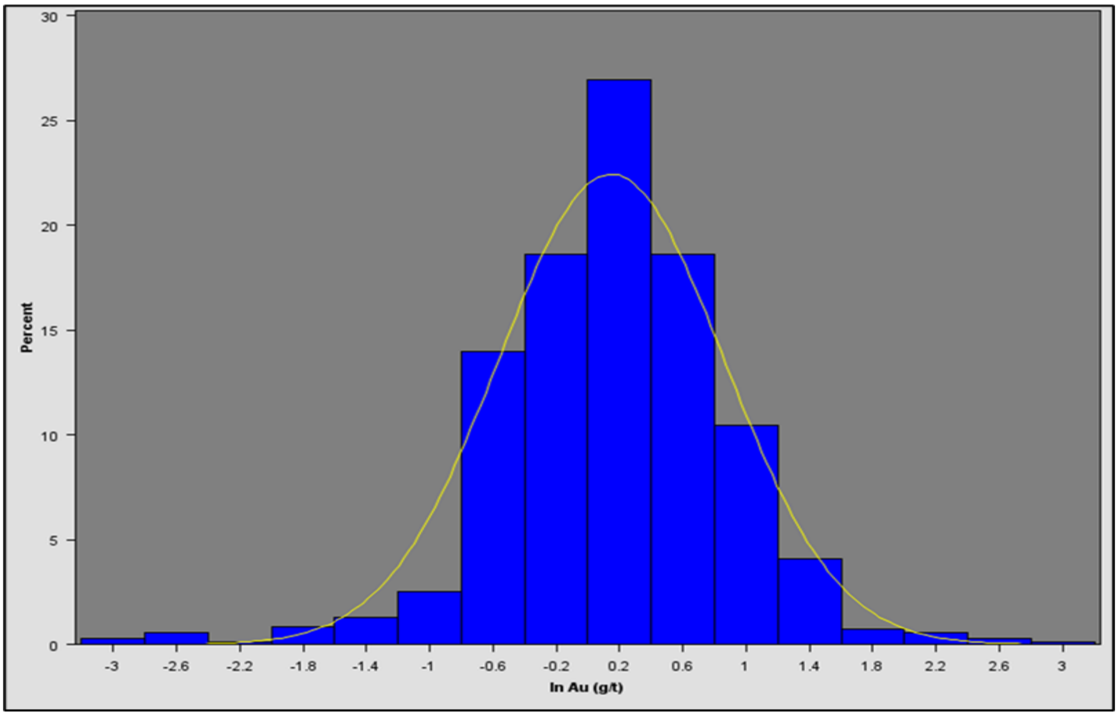

Figure 4.6 : Histogram of cleaned 50 m x 50 m x 3 m log-transformed Au sample data (A1 reef)

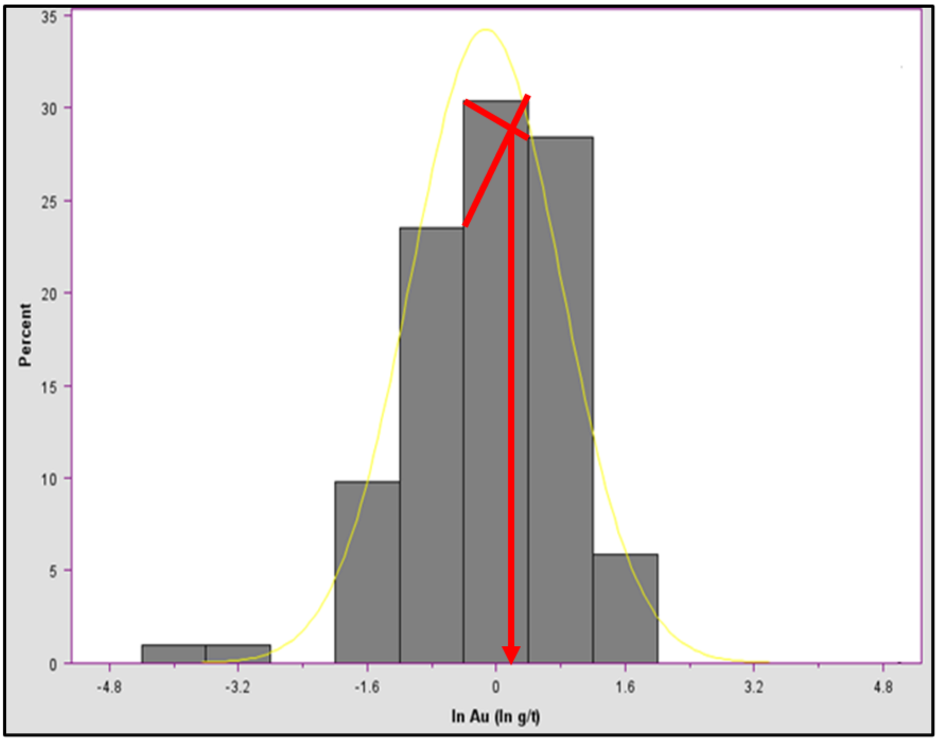

Figure 4.7 : Histogram of cleaned 200 m x 100 m x 3 m log-transformed Au sample data (A1 reef)

Fitting normal curves to the histograms of all three log transformed datasets showed that most of the data fits a normal distribution. The data seem to follow a lognormal distribution. The impact of the extreme values on the symmetry of the distributions should be noted. Outlier analysis and testing other variations of lognormal distributions (3-parameter or truncated) could provide an even better understanding of the underlying distribution. But for the purposes of this study, this was deemed unnecessary. Distribution analysis is important when calculating the unweighted global mean because the type of distribution will guide the approach for estimating the global average. In this study, the global averages were estimated from the averages of all the kriged or simulated blocks. Sample averages were used for SK estimations.

4.3. Geological Modelling

Figure 4.8 shows the TI and EA block models created from wireframes and related drill holes positions. The geological models were developed using the methodology described in Section 3.3.

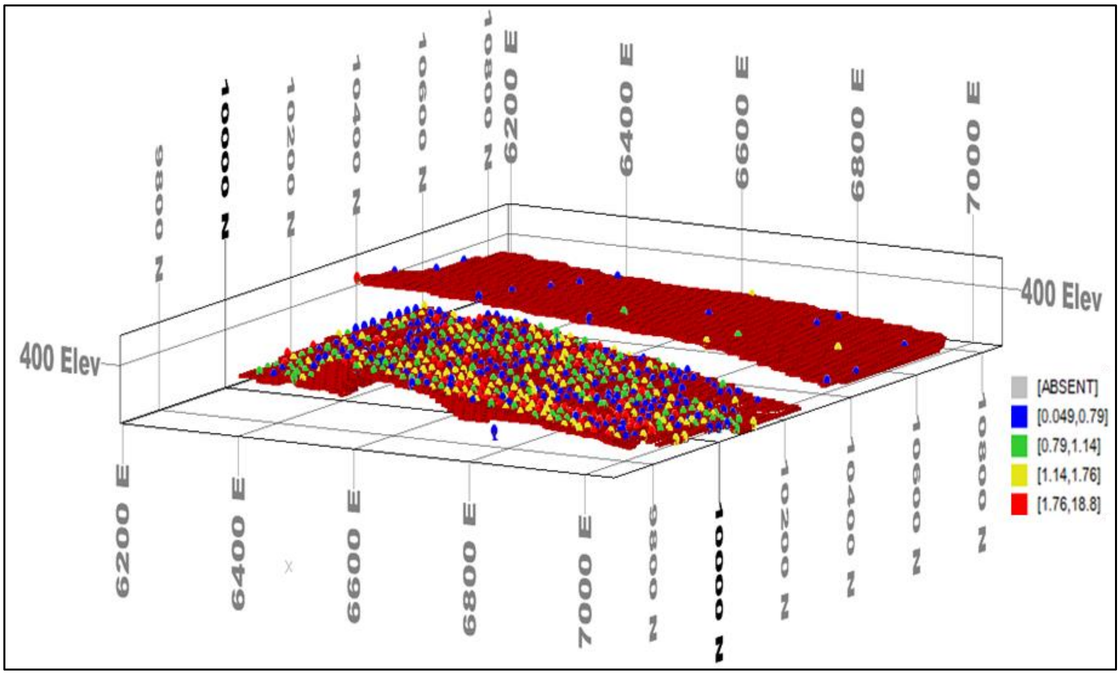

Figure 4.8: Block models within the TI area and EA

Table 4.3 summarises the associated block model parameters. The block model parameters' selection process and criteria were also described in Section 3.3.

Table 4.3 : TI and EA block parameters

TI		EA	
Parameter	**Value**	**Parameter**	**Value**
X Origin (m)	6400.001	**X Origin (m)**	6195.665
Y Origin (m)	9680.631	**Y Origin (m)**	10400.457
Z Origin (m)	352.555	**Z Origin (m)**	354.812
X Size (m)	10	**X Size (m)**	10
Y Size (m)	10	**Y Size (m)**	10
Z Size (m)	3	**Z Size (m)**	3
Number of Cells (X)	65	**Number of Cells (X)**	81
Number of Cells (Y)	58	**Number of Cells (Y)**	46
Number of Cells (Z)	24	**Number of Cells (Z)**	17

4.4. Training Image Creation

4.4.1. Variography

The nugget effect was initially estimated from the downhole variogram shown in Figure 4.9 as 0.73 $(g/t)^2$. Four variograms which displayed an adequate description of spatial continuity and sufficient number of pairs were identified, selected, modelled and respective variogram maps constructed as shown in Figure 4.10 : Variograms and variogram maps for 25 m x 25 m x 3 m samples. The spherical variogram model parameters are also summarised in Table 4.4. Variogram 3 was selected for estimation as its directions showed the longest ranges of continuity as illustrated by the ellipse fitted on the variogram map.

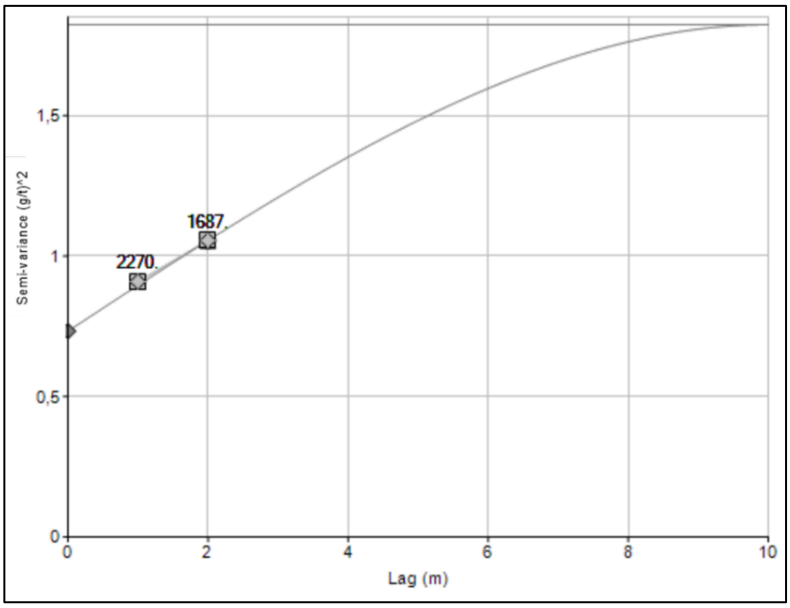

Figure 4.9 : Downhole variogram of 25 m x 25 m x 3 m samples

Table 4.4 : Variogram model (Spherical) parameters for 25 m x 25 m x 3 m samples

Model	Azimuth	Dip	C_1	Range			C_2	Range		
				X (m)	Y (m)	Z (m)		X (m)	Y (m)	Z (m)
1	Omni		1.06	162	162	162	0.03	307	307	307
2	60	0	0.01	151	289	110	1.09	192	417	230
3	***90***	***0***	***0.69***	***150***	***146***	***102***	***0.40***	***192***	***374***	***228***
4	120	0	0.81	159	144	95	0.28	262	497	243

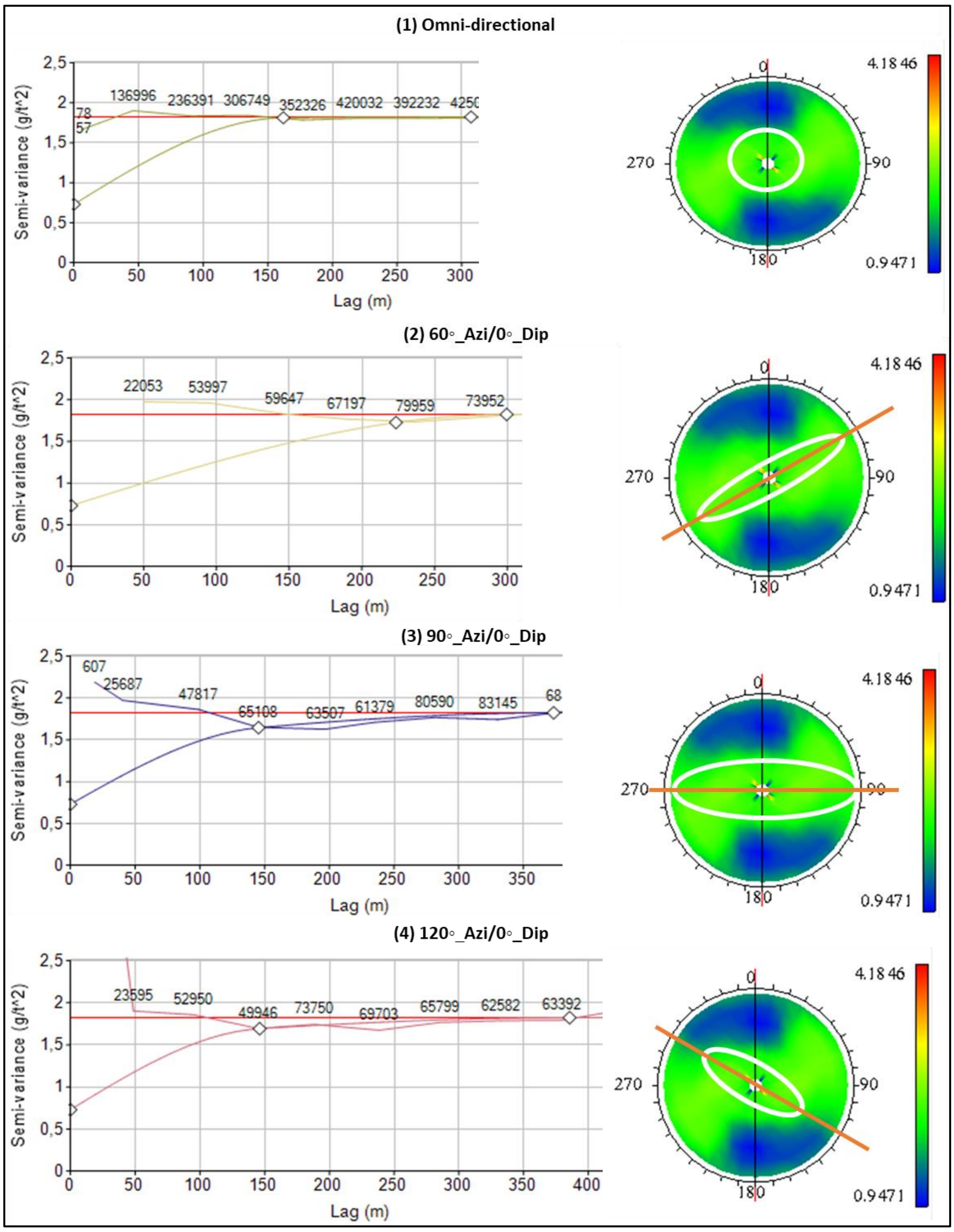

Figure 4.10 : Variograms and variogram maps for 25 m x 25 m x 3 m samples

4.4.2. Kriging neighbourhood analysis

Since it was already decided that the estimation will be carried out on the SMU (i.e. 10 m x 10 m x 3 m), the KNA was not carried out for block size selection. KNA was rather implemented to optimise the number of discretisation points, search distances, optimum and minimum number of samples. Figure 4.11 shows KNA results for the optimisation of the minimum and optimum number of samples.

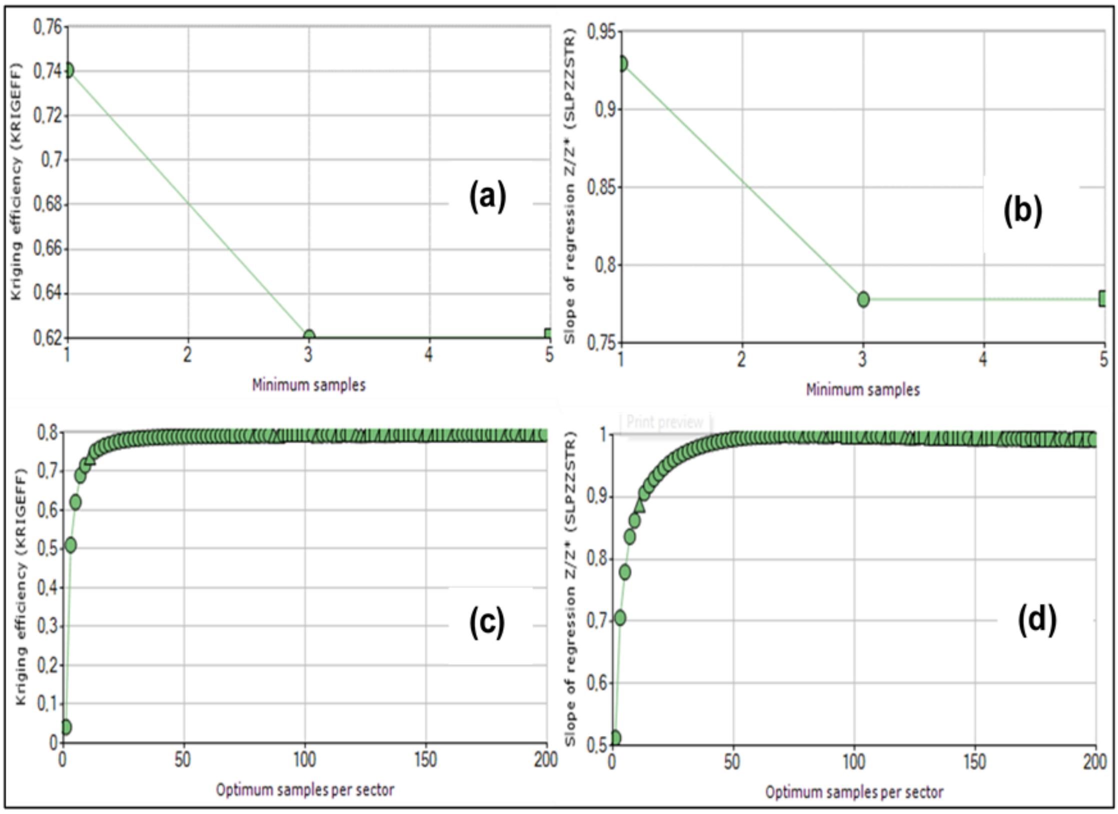

Figure 4.11 : KNA results for minimum and maximum number of samples for 25 m x 25 m x 3 m samples

From Figure 4.11 (a) and (b), the highest KE (0.74) and SLOR (0.93) is reached when a minimum number of 1 sample is used. As illustrated in Figure 4.11 (c) and (d), when 50 maximum samples are used, the highest KE (0.8) and SLOR is reached (0.99). Beyond 50 samples, there is no significant change in KE or SLOR.

Figure 4.12 shows KNA results for the optimisation of search distances. The highest KE (0.94) and SLOR (0.94) is reached when the search distances in the X, Y and Z directions are 302 m, 353 m, and 302 m, respectively.

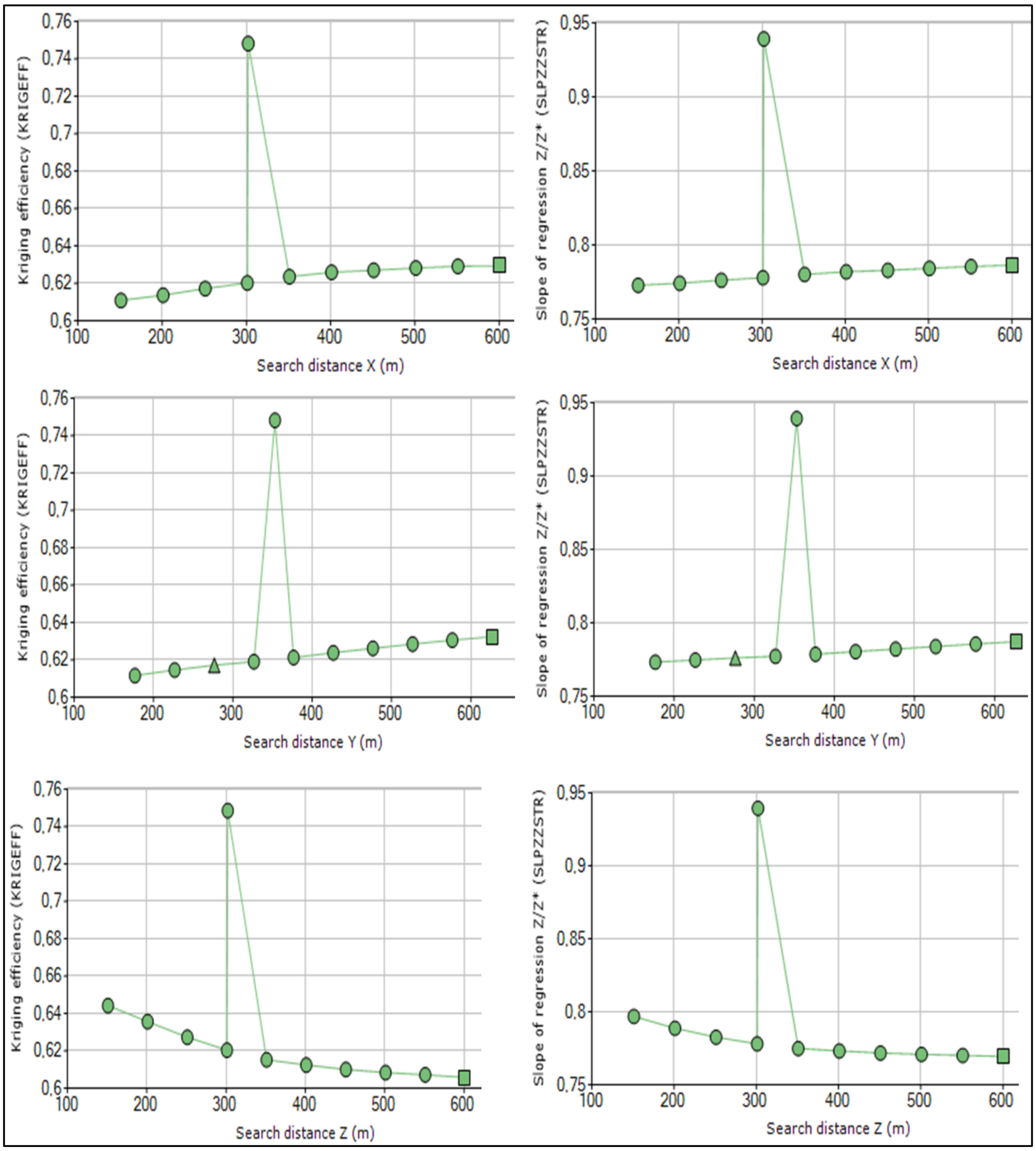

Figure 4.12 : KNA results for optimisation of search distances for 25 m x 25 m x 3 m samples

Figure 4.13 shows the results for KNA when optimising the number of discretisation points. It can be seen from Figure 4.13 that the block covariance decreases and then flattens (1.2785 $(g/t)^2$) when using 4 discretisation points in the X- and Y- directions as well as 2 points in along the Z-axis. Beyond this combination of the number of discretisation points, the change in the block covariances is insignificant.

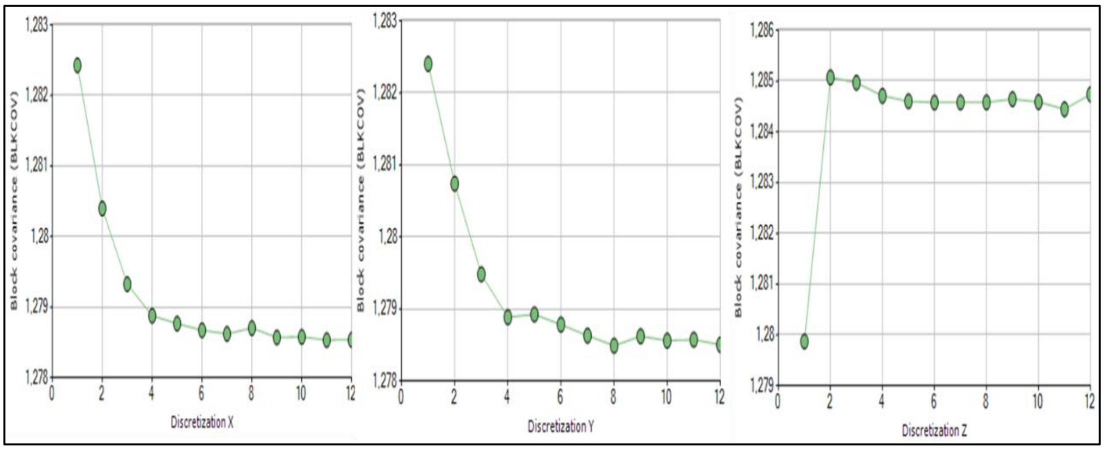

Figure 4.13: KNA results for optimisation of number of discretisation points for 25 m x 25 m x 3 m samples

The optimised parameters that gave the highest KE and SLOR or the lowest block covariance were used during kriging of the TIs and are summarised in Table 4.5.

Table 4.5 : Selected kriging parameters for 25 m x 25 m x 3 m samples

Parameter	Directions		
	X	Y	Z
Number of Discretisation Points	4	4	2
Search Distance (m)	302	353	302
Minimum Number of Samples	1		
Maximum Number of Samples	50		
Block Sizes	10 m x 10m x 3 m		

4.4.3. Estimation

Summary statistics were computed for estimation results (OK and SK) for two the two approaches, i.e. (i) estimating within a wireframe and (ii) inside a cuboid which was then split with a wireframe. These statistics are summarised in Table 4.6. There are no differences between the statistics of the two methods. It was then deduced that splitting the kriged cuboid with a wireframe produces the same results as estimating within the wireframe. To further confirm this conclusion, plan views of models from both approaches were analysed to investigate if there were any block-to-block deviations. The plans views are shown in Figure 4.14.

Table 4.6 : Comparison of ordinary - and simple - kriging grade models estimated (i) within a wireframe versus (ii) a split of a kriged cuboid with a wireframe

Parameter (10 m x 10 m x 3m blocks)	Within a wireframe		Split from a filled cuboid	
	Ordinary Kriging Training Image	Simple Kriging Training Image	Ordinary Kriging Training Image	Simple Kriging Training Image
Number of blocks	6938	6938	6938	6938
Mean (g/t)	1.513	1.512	1.513	1.512
Variance $(g/t)^2$	0.147	0.150	0.147	0.150
Kriging Efficiency Average	0.879	0.880	0.879	0.880
Slope of Regression Average	1.012	1.000	1.012	1.000
Range (g/t)	3.106	3.091	3.106	3.091

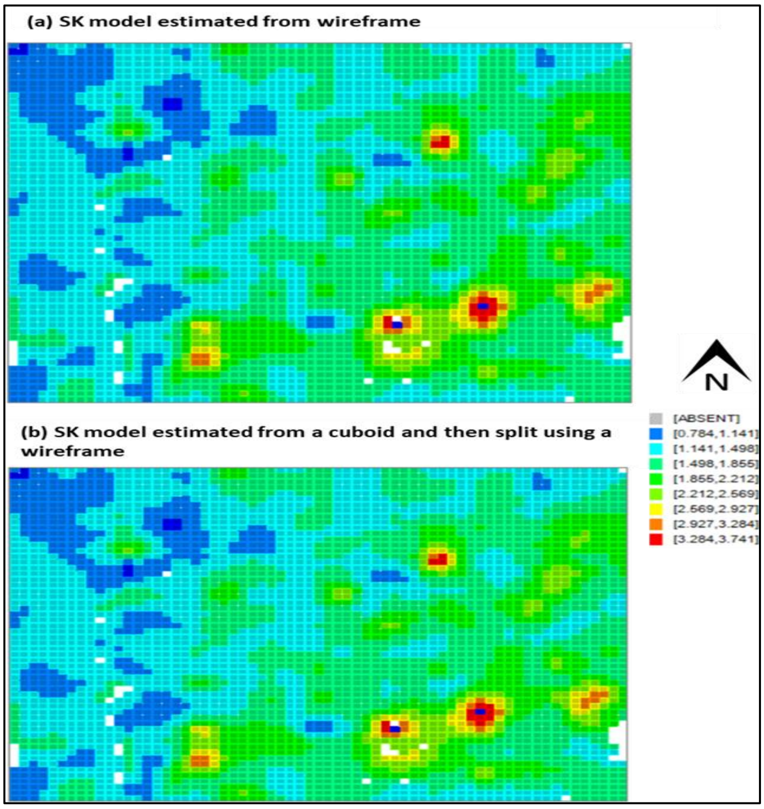

Figure 4.14 : Plan view of SK model estimated within a wireframe against split from cuboid model (10 m x 10 m x 3 m blocks)

From the plans in Figure 4.14, there were no block-by-block grade distribution differences observed. This confirmed that the two approaches produced similar results. Therefore, the cuboid could be used as a TI for DeeSse simulations as required by the algorithm, and then the resultant cuboid realisations would be split with a wireframe during post-processing. The subsequent statistical analysis and uncertainty quantification would be carried out using these splits rather the cuboids. It should also be noted that for the above models the grade distributions are decreasing towards the north-west as concluded in Section 4.2.1.

Since the SK model provides a higher KE and would be more comparable to SGSIM simulations than the OK model, the SK cuboid grade model was used as a TI for DeeSse simulations in this study. Figure 4.15 shows the SK TI's plan and 3D views. Table 4.7 summarises the selected TI's statistics.

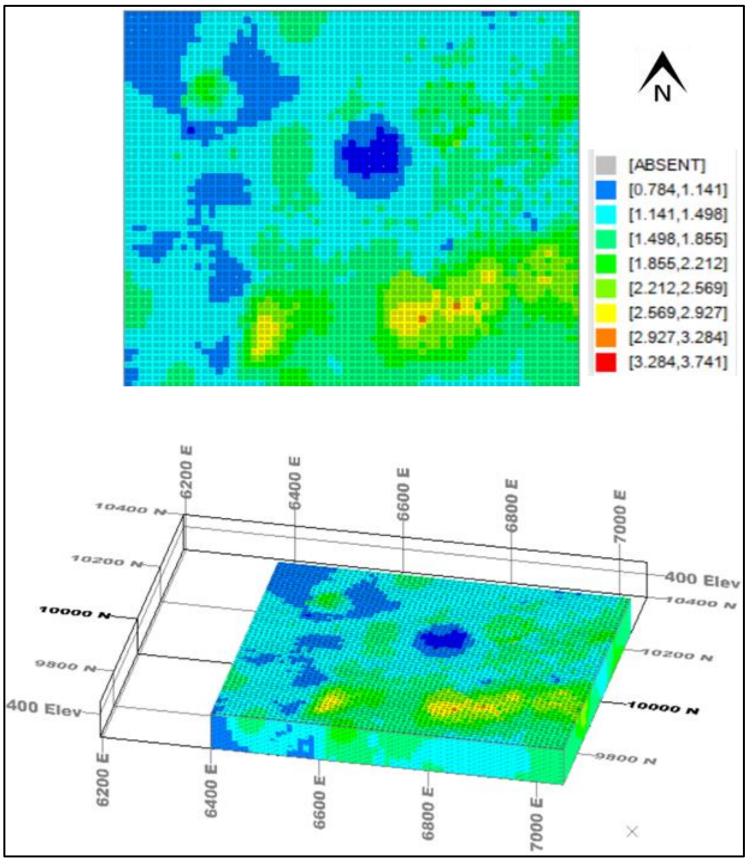

Figure 4.15 : Plan and 3D view of the SK cuboid training model to be used for DeeSse simulations (10 m x 10 m x 3 m blocks)

Table 4.7 : Selected TI (SK cuboid) statistics (10 m x 10 m x 3 m blocks)

Parameter	Value
Number of blocks	90480
Mean (g/t)	1.527
Variance $(g/t)^2$	0.115
Kriging Efficiency Average	0.655
Slope of Regression Average	1.000
Range (g/t)	3.033

The mean of the SK cuboid training model is slightly higher than the mean of the respective split. The TI grades in the cuboid TI are also about 20 % less variable than in the split model. The KE in the TI is as expected also lower than the respective wireframe model. There were also 13 times more blocks in the cuboid than the corresponding split. It is expected that all these variations will be corrected when the cuboid is split during post-processing.

4.5. Training Image Validation Using SGSIM (25 m x 25 m x 3 m Input Data)

Results of anisotropic investigations on the 25 m x 25 m x 3 m dataset have been provided already as shown Figure 4.10. Variography and subsequent SGSIM25 simulations within the TI area are summarised in this section. SGSIM25 was implemented to validate the TI. The 25 m x 25 m x 3 m dataset was used to calculate the relevant NSCORE variogram and fit a model. The methodology and parameters used are detailed in Section 3.5. The nugget effect of the NSCORE variogram for the 25 m x 25 m x 3 m samples was initially estimated from the NSCORE downhole variogram shown in Figure 4.16 as 0.71 $(g/t)^2$. The NSCORE spherical variogram model and associated parameters are illustrated and summarised in Figure 4.17 and Table 4.8 respectively.

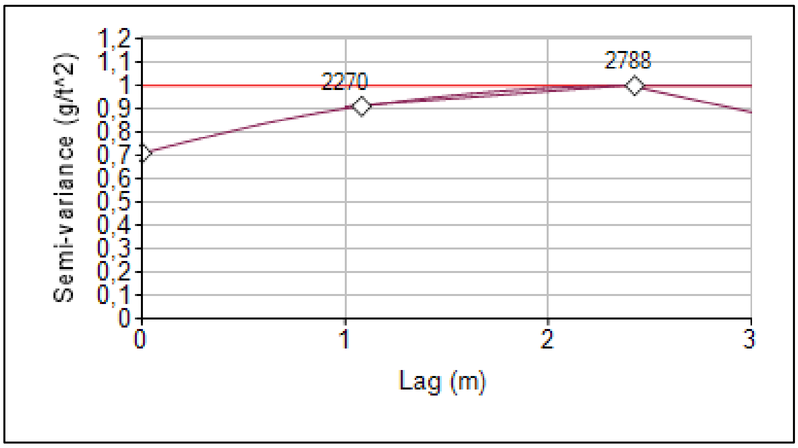

Figure 4.16: Downhole NSCORE variogram of 25 m x 25 m x 3 m samples

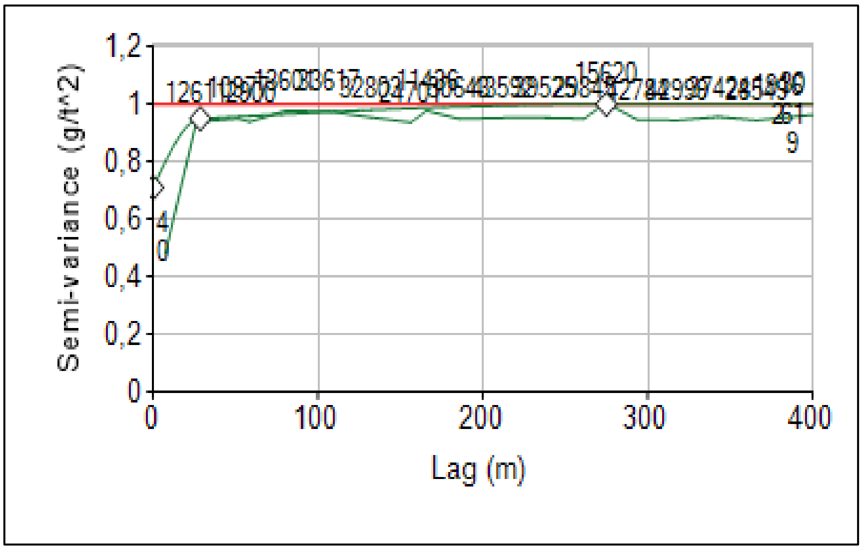

Figure 4.17: NSCORE Variogram for 25 m x 25 m x 3 m samples

Table 4.8: NSCORE Variogram model (Spherical) parameters for 25 m x 25 m x 3 m samples

Model	Azi	Dip	C_o	C_1	Range			C_2	Range		
					X (m)	Y (m)	Z (m)		X (m)	Y (m)	Z (m)
1	90	0	0.71	0.054	5.2	1.0	0.2	0.24	5.8	2.4	0.5

The means and variances of the 50 SGSIM25 simulations and their etype estimate are summarised in Table 4.9. The mean and variance of the SGSIM25 etype estimate is 1.54 g/t and 0.63 $(g/t)^2$, respectively. The minimum average grade of the realisations is 1.52 g/t while the highest average grade of the simulations is 1.60 g/t. The variances around the means of the simulations range from 0.58 $(g/t)^2$ to 0.70 $(g/t)^2$.

Table 4.9: Unweighted means and variances of 50 SGSIM25 realisations in TI area (10 m x 10 m x 3 m blocks)

Simulation	Mean (g/t)	Variance $(g/t)^2$	Simulation	Mean (g/t)	Variance $(g/t)^2$
Etype estimate	1.54	0.63			
SIM1	1.54	0.60	**SIM26**	1.53	0.59
SIM2	1.54	0.63	**SIM27**	1.56	0.65
SIM3	1.54	0.60	**SIM28**	1.56	0.70
SIM4	1.55	0.62	**SIM29**	1.52	0.61
SIM5	1.56	0.64	**SIM30**	1.54	0.59
SIM6	1.56	0.68	**SIM31**	1.54	0.63
SIM7	1.54	0.64	**SIM32**	1.53	0.65
SIM8	1.54	0.63	**SIM33**	1.52	0.58
SIM9	1.54	0.61	**SIM34**	1.55	0.59
SIM10	1.57	0.66	**SIM35**	1.54	0.61
SIM11	1.55	0.63	**SIM36**	1.54	0.68
SIM12	1.55	0.66	**SIM37**	1.56	0.60
SIM13	1.56	0.66	**SIM38**	1.60	0.70
SIM14	1.54	0.66	**SIM39**	1.54	0.65
SIM15	1.54	0.59	**SIM40**	1.55	0.60
SIM16	1.56	0.63	**SIM41**	1.52	0.62
SIM17	1.53	0.60	**SIM42**	1.53	0.64
SIM18	1.53	0.60	**SIM43**	1.52	0.58
SIM19	1.56	0.65	**SIM44**	1.55	0.62
SIM20	1.54	0.62	**SIM45**	1.55	0.62
SIM21	1.53	0.59	**SIM46**	1.54	0.62
SIM22	1.53	0.63	**SIM47**	1.54	0.64
SIM23	1.56	0.65	**SIM48**	1.52	0.58
SIM24	1.52	0.58	**SIM49**	1.54	0.59
SIM25	1.54	0.63	**SIM50**	1.56	0.70

Descriptive statistics, cdf, block grade values, variograms, plans and sections between the TI and SGSIM25 etype estimates are compared in order to validate the TI. Table 4.10 summarises the comparison of the descriptive statistics. From Table 4.10, it appears that SGSIM25 etype estimate produces a slightly higher global grade mean estimate than the TI (~2% higher). The TI's mean is also only 2% lower than the mean of sample data. However, the SGSIM25 etype estimates' variance differs significantly from the TI's by around 76 %. There is more inherent block-to-block variability within the SGSIM etype estimate than the TI grades which tend to be smoother locally. The TI's range is, however, moderately larger (~16%) than the SGSIM etype estimate. Therefore, the TI captured the statistical grade variability better than the SGSIM25 etype estimates. However, the spatial variability is more realistic for SGSIM25 etype estimate as highlighted by the comparison in variography of the two estimates in Figure 4.19. To investigate this difference in variability further, the cdfs for the TI and SGSIM were analysed.

Table 4.10: Descriptive statistics between SGSIM25 etype estimate, TI, and 25 m x 25 m x 3 m input sample data within the TI boundary (10 m x 10 m x 3 m Blocks)

Description	**Count**	**Mean (g/t) (Unweighted)**	**Variance $(g/t)^2$**	**Minimum (g/t)**	**Maximum (g/t)**	**Range (g/t)**
25 m x 25 m x 3 m samples	2856	1.54	1.82	0.01	22.60	22.60
TI	6938	1.51	0.15	0.71	3.80	3.09
SGSIM25 etype estimate	6938	1.54	0.63	0.57	3.23	2.66

Figure 4.18 shows the cdf plots of the TI and SGSIM25 etype estimates. From the cdfs, it can be observed that between cut-off grades of 0.80 g/t to 1.51 g/t

some bias exists. That is, the TI mostly underestimates the proportion above cut-off grade. At cut-off grades below 0.80 g/t and above 1.51 g/t, the cdfs are generally similar. The cdfs also confirm that the spread of the TI is greater than that of the SGSIM25 etype estimate.

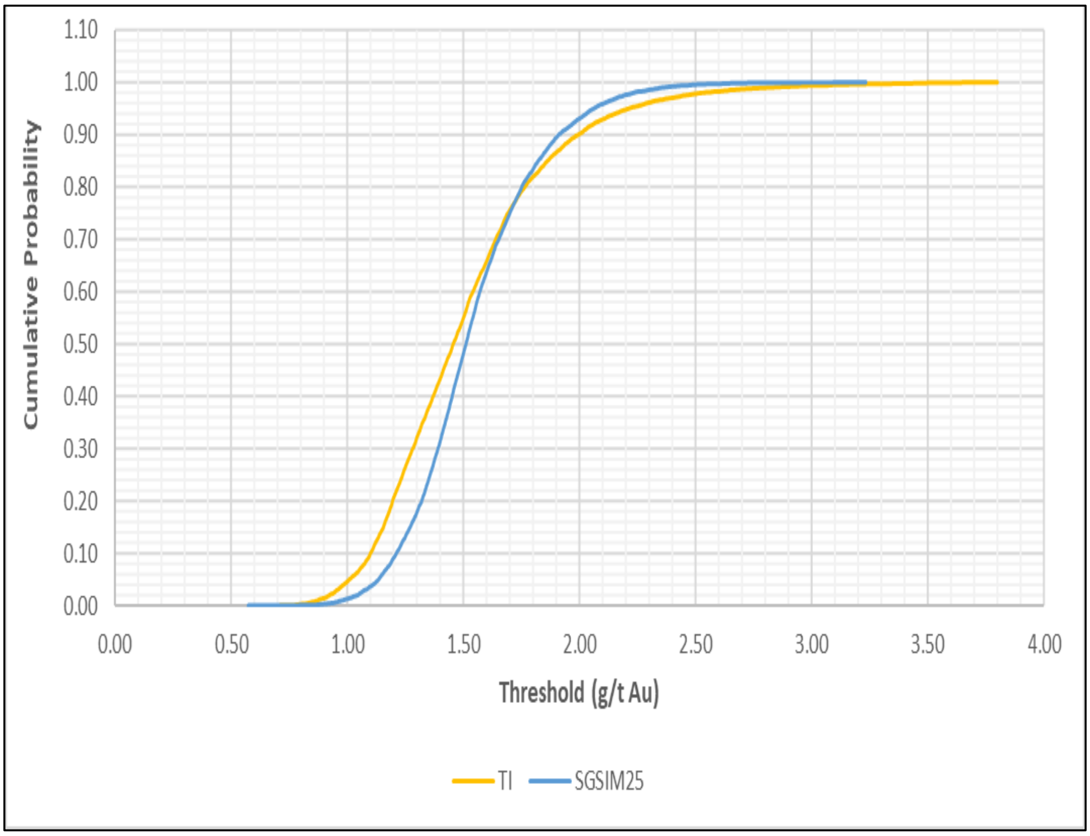

Figure 4.18: Cumulative distribution functions of TI and SGSIM25 etype estimate grades for 10 m x 10m x 3 m blocks in the TI Area

In order to compare the spatial variability of the TI and SGSIM25 etype estimates, their NSCORE variograms were calculated and modelled as shown in Figure 4.19. The variograms confirm that the SGSIM25 etype estimate is more spatially variable than the TI as shown by the higher nugget effect.

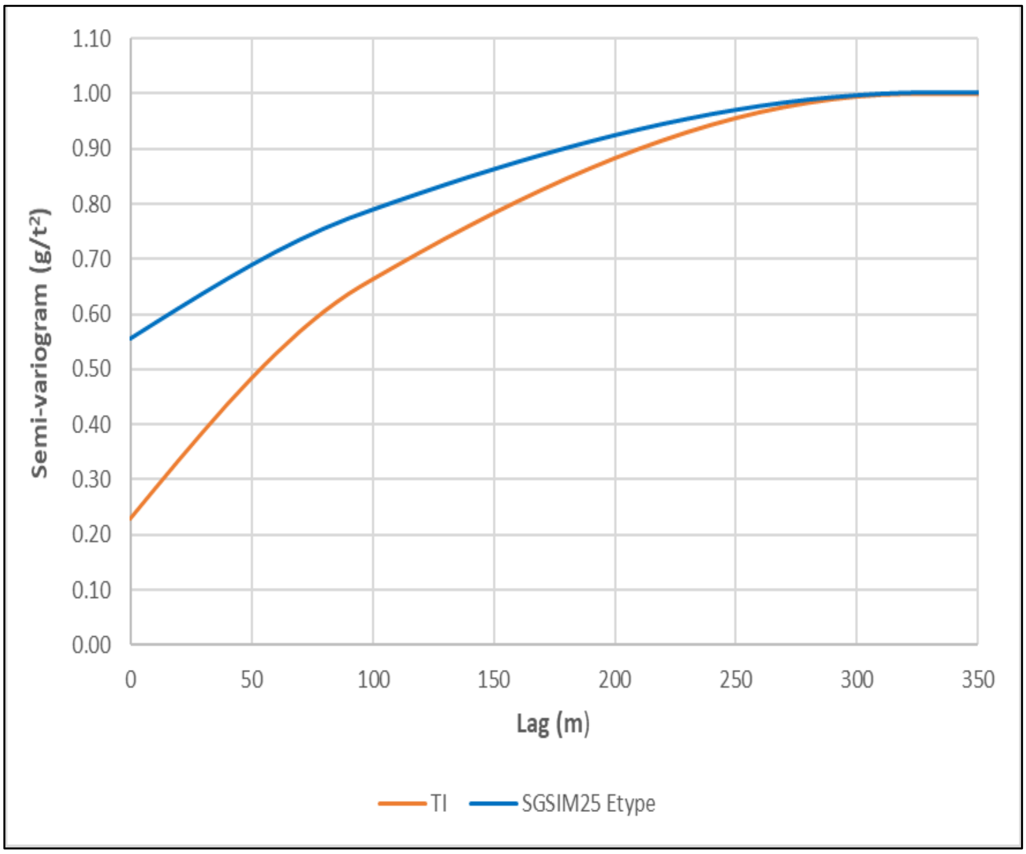

Figure 4.19 : NSCORE variograms of the TI and SGSIM25 etype estimate in the TI area (10 m x 10 m x 3 m blocks)

Figure 4.20 compares the plan views of the 25 m x 25 m x 3 m samples, TI and SGSIM25 etype estimates. From Figure 4.20, it can be observed that the spatial grade distributions of the TI and SGSIM25 etype estimate blocks are generally comparable. It should be noted how the TI's map is more smoothed than the SGSIM25's plan but shows a large range of grade values than the etype estimate. This confirms that the deductions made from descriptive statistics, cdfs and NSCORE variograms are correct.

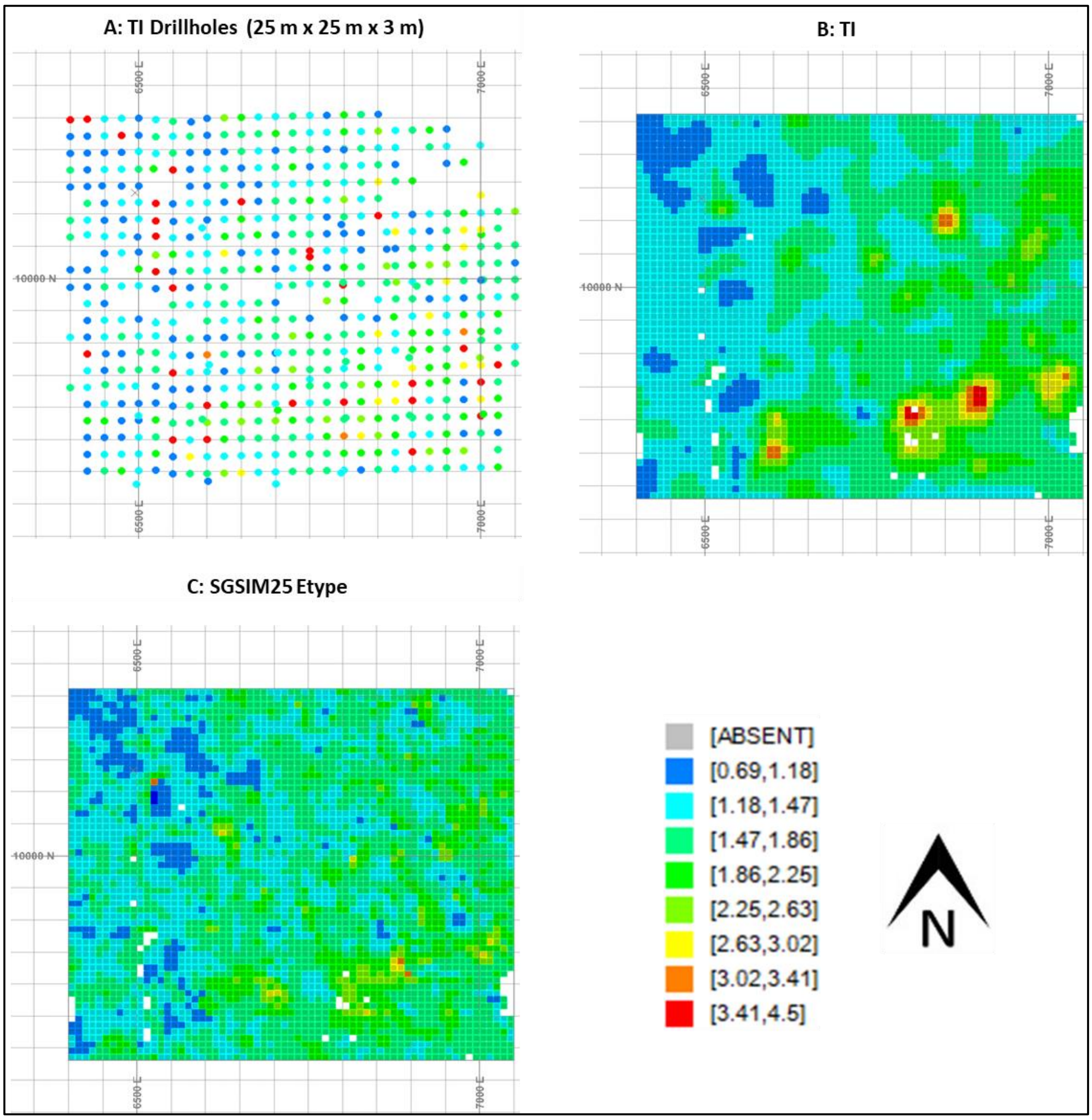

Figure 4.20 : Plan view of the spatial distribution of grades for the 25 m x 25 m x 3 m samples, TI and SGSIM25 etype estimates in the TI Area (10 m x 10 m x 3 m blocks)

Figure 4.21 shows a comparison of cross-sections through the TI and SGSIM25 etype estimates. The cross-sections were taken randomly in the north-south (N-S) and east-west (E-W) directions. There is a general resemblance between the TI and SGSIM25 etype estimate cross sections.

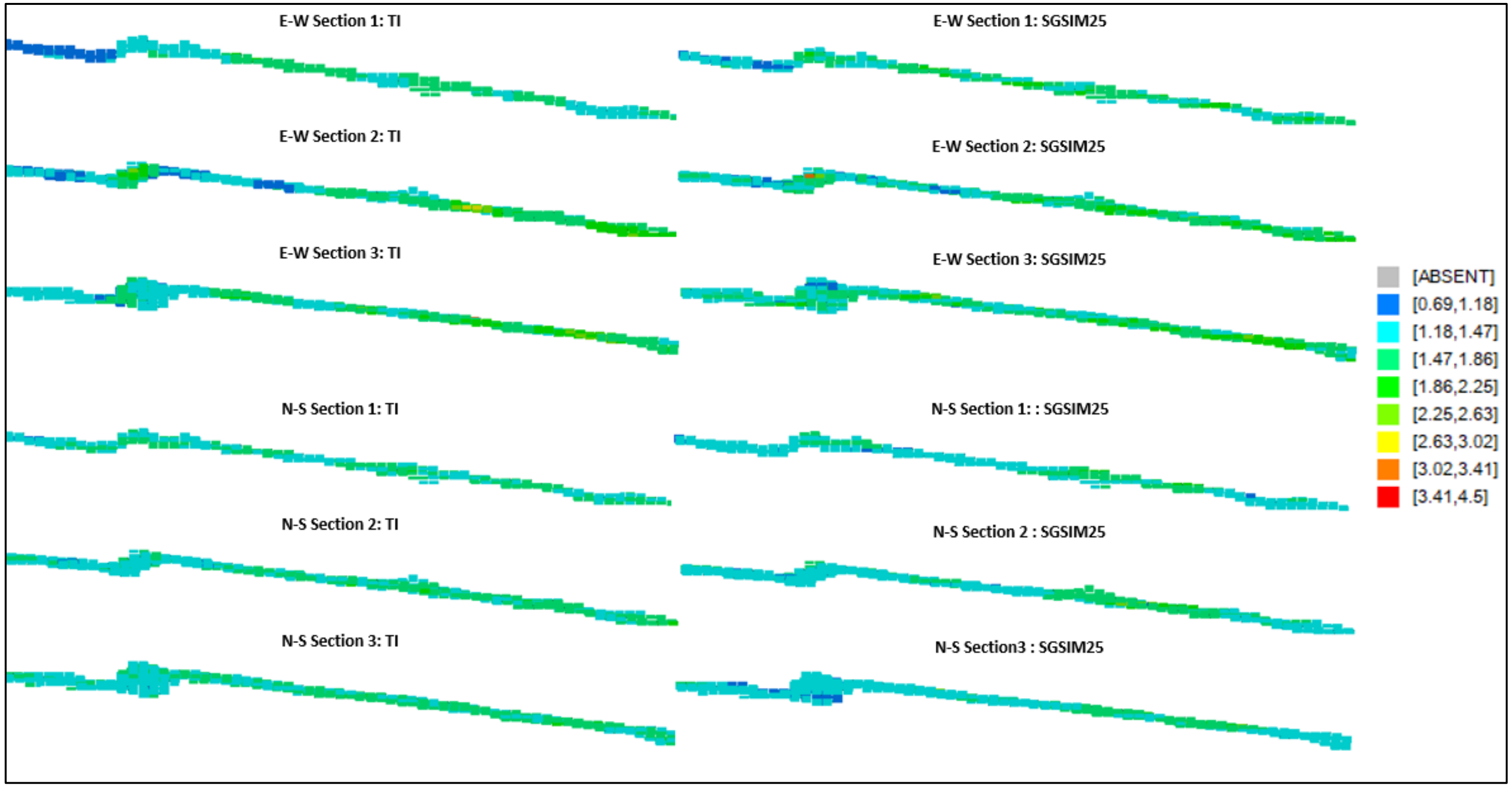

Figure 4.21 : Cross-sections through the TI and SGSIM25 etype estimate in the TI area (10 m x 10 m x 3 m blocks)

To quantify the differences between the results of the two techniques, the mean absolute percentage error (MAE%) of the blocks of the TI and SGSIM25 etype estimates at each location was calculated to be 15%. Although the means, cdfs, plans and sections between the TI and SGSIM25 etype estimate are generally similar; the high differences in their variance and the MAE of 15% is of concern. Perhaps, re-parametrisation of kriging inputs could reduce the over-smoothing of the TI blocks. Nonetheless, given the kriging efficiency of 89% and all other points considered; the TI was considered valid for the purpose of the study.

4.6. Application of DeeSse in TI Area Using 50 m x 50 m x 3 m Samples

The means and variances of the 50 DeeSse simulations and their etype estimate are summarised in Table 4.11. The mean and variance of the DeeSse etype estimate is 1.40 g/t and 0.07 $(g/t)^2$, respectively. The minimum average grade of the realisations is 1.37 g/t while the highest average grade of the simulations is 1.43 g/t. The variances around the means of the simulations range from 0.06 $(g/t)^2$ to 0.08 $(g/t)^2$.

Table 4.11 : Unweighted means and variances of 50 DeeSse realisations in the TI area (10 m x 10 m x 3 m blocks)

Simulation	Mean (g/t)	Variance $(g/t)^2$	Simulation	Mean (g/t)	Variance $(g/t)^2$
Etype estimate	1.40	0.07			
SIM1	1.42	0.07	**SIM26**	1.38	0.07
SIM2	1.40	0.07	**SIM27**	1.41	0.08
SIM3	1.40	0.06	**SIM28**	1.39	0.06
SIM4	1.39	0.06	**SIM29**	1.39	0.07
SIM5	1.38	0.07	**SIM30**	1.41	0.07
SIM6	1.40	0.06	**SIM31**	1.37	0.07
SIM7	1.38	0.07	**SIM32**	1.41	0.07
SIM8	1.40	0.07	**SIM33**	1.40	0.07
SIM9	1.42	0.07	**SIM34**	1.39	0.08
SIM10	1.43	0.07	**SIM35**	1.40	0.07
SIM11	1.39	0.07	**SIM36**	1.41	0.07
SIM12	1.37	0.07	**SIM37**	1.42	0.07
SIM13	1.39	0.07	**SIM38**	1.39	0.07
SIM14	1.38	0.07	**SIM39**	1.39	0.08
SIM15	1.39	0.07	**SIM40**	1.39	0.07
SIM16	1.41	0.08	**SIM41**	1.38	0.07
SIM17	1.39	0.07	**SIM42**	1.41	0.07
SIM18	1.39	0.07	**SIM43**	1.39	0.06
SIM19	1.40	0.07	**SIM44**	1.42	0.07
SIM20	1.39	0.07	**SIM45**	1.38	0.07
SIM21	1.40	0.06	**SIM46**	1.40	0.07
SIM22	1.40	0.06	**SIM47**	1.40	0.06
SIM23	1.39	0.07	**SIM48**	1.38	0.07
SIM24	1.40	0.06	**SIM49**	1.40	0.07
SIM25	1.38	0.07	**SIM50**	1.40	0.07

4.7. Validation of DeeSse in TI Area Using SGSIM (50 m x 50 m x 3 m Input Data)

The same NSCORE variogram of the 25 m x 25 m x 3 m in Table 4.8 was used for running SGSIM50 simulations. Hence, the relevant variography results will be like those described in Section 4.5. SGSIM50 was implemented to validate the DeeSse results which also had a similar input grid size of 50 m x 50 m x 3 m. The means and variances of the 50 SGSIM50 simulations and their etype estimate are summarised in Table 4.12.

The mean and variance of the SGSIM50 etype estimates are 1.47 g/t and 0.56 $(g/t)^2$, respectively. The minimum average grade of the realisations is 1.43 g/t while the highest average grade of the simulations is 1.51 g/t. The variances around the means of the simulations range from 0.48 $(g/t)^2$ to 0.62 $(g/t)^2$.

Table 4.12: Unweighted means and variances of 50 SGSIM50 realisations in TI area (10 m x 10 m x 3 m blocks)

Simulation	Mean (g/t)	Variance (g/t^2)	Simulation	Mean (g/t)	Variance (g/t^2)
Etype estimate	1.47	0.56	**SIM26**	1.48	0.60
SIM1	1.45	0.48	**SIM27**	1.49	0.59
SIM2	1.47	0.56	**SIM28**	1.45	0.56
SIM3	1.47	0.57	**SIM29**	1.47	0.55
SIM4	1.45	0.58	**SIM30**	1.46	0.56
SIM5	1.48	0.55	**SIM31**	1.48	0.58
SIM6	1.49	0.56	**SIM32**	1.46	0.58
SIM7	1.46	0.54	**SIM33**	1.50	0.54
SIM8	1.46	0.59	**SIM34**	1.48	0.54
SIM9	1.46	0.54	**SIM35**	1.47	0.55
SIM10	1.46	0.54	**SIM36**	1.44	0.57
SIM11	1.48	0.62	**SIM37**	1.45	0.53
SIM12	1.43	0.49	**SIM38**	1.43	0.50
SIM13	1.47	0.56	**SIM39**	1.51	0.60
SIM14	1.48	0.58	**SIM40**	1.44	0.52
SIM15	1.49	0.60	**SIM41**	1.47	0.55
SIM16	1.47	0.51	**SIM42**	1.46	0.53
SIM17	1.48	0.53	**SIM43**	1.50	0.56
SIM18	1.49	0.60	**SIM44**	1.46	0.52
SIM19	1.47	0.57	**SIM45**	1.47	0.60
SIM20	1.48	0.59	**SIM46**	1.51	0.58
SIM21	1.47	0.53	**SIM47**	1.47	0.55
SIM22	1.50	0.58	**SIM48**	1.45	0.54
SIM23	1.44	0.52	**SIM49**	1.48	0.58
SIM24	1.47	0.56	**SIM50**	1.50	0.57
SIM25	1.47	0.55			

Descriptive statistics, cdfs, block grade values, variograms, plans and sections between the DeeSse and SGSIM50 etype estimates are compared in order to validate the DeeSse results. Table 4.13 summarises the comparison of the descriptive statistics. From Table 4.13, it appears that SGSIM50 etype estimate produces a slightly higher global grade mean estimate than the DeeSse etype estimate (~5% higher). DeeSse's mean is also about 6% lower than the mean of sample data. However, the SGSIM50 etype estimates' variance differs significantly from the DeeSse's variance. There is significantly more inherent block-to-block variability within the SGSIM etype estimate than the DeeSse which tends to be smoother locally. DeeSse's range is much greater (~58%) than the SGSIM etype estimate. That means, DeeSse attempts to reflect lower and higher grades in the sample data better than SGSIM50. Although, the DeeSse range is intrinsically limited by the TI's spread as well. To investigate this difference in variability further, the cdfs for the DeeSse and SGSIM50 etype estimates were also analysed.

Table 4.13: Comparison of descriptive statistics between 50 m x 50 m x 3m input data, DeeSse and SGSIM50 etype estimates within the TI boundary (10 m x 10 m x 3 m Blocks)

Description	Count	Mean (g/t) (Unweighted)	Variance (g/t^2)	Minimum (g/t)	Maximum (g/t)	Range (g/t)
50 m x 50 m x 3 m samples	709	1.49	1.89	0.05	18.80	18.75
SGSIM50 etype estimate	6938	1.47	0.56	0.86	2.62	1.75
DeeSse etype estimate	6938	1.40	0.07	0.41	4.59	4.19

Figure 4.22 shows the cdf plots of the DeeSse and SGSIM50 etype estimates. From the cdfs, it can be observed that between cut-off grades of 1.05 g/t to 1.51 g/t some bias exists. That is, DeeSse mostly underestimates the proportion above cut-off grade. At cut-off grades below 1.05 g/t and above 1.51 g/t, the cdfs are generally similar. The cdfs also confirm that the spread of the DeeSse is greater than that of the SGSIM50 etype estimate.

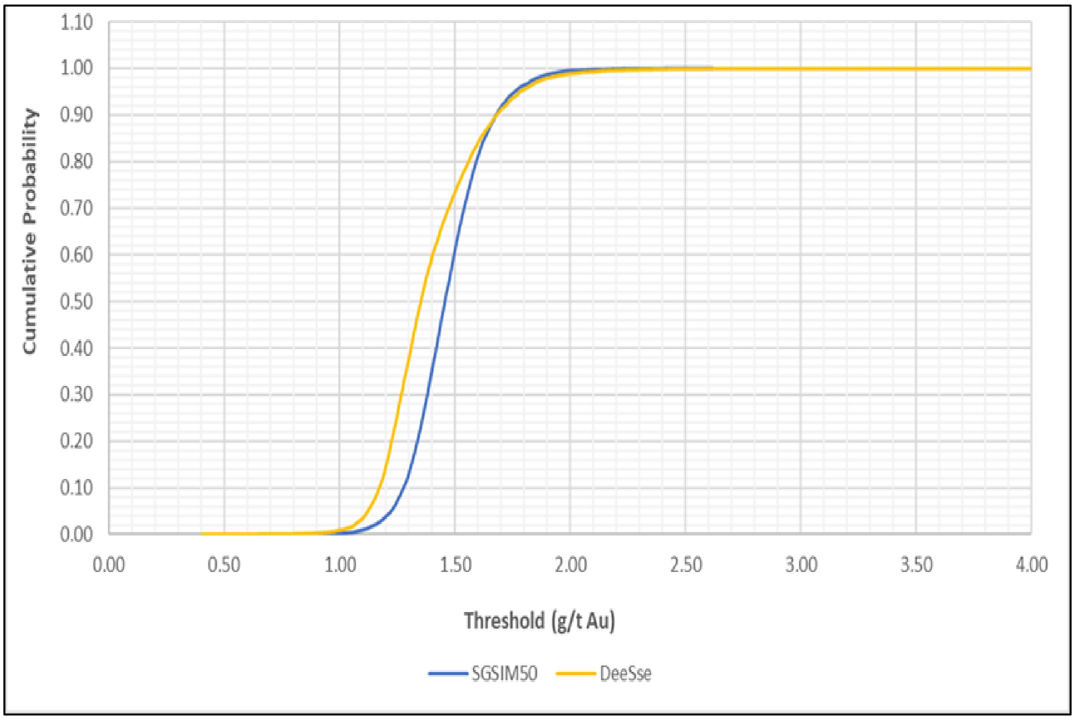

Figure 4.22: Cumulative distribution functions of DeeSse and SGSIM50 etype estimate grades for 10 m x 10m x 3 m blocks in the TI Area

In order to compare the spatial variability of DeeSse and SGSIM50 etype estimates, their NSCORE variograms were calculated and modelled as shown in Figure 4.23. The variograms also confirm that the SGSIM50 etype estimate has more spatial variability than the DeeSse etype estimate.

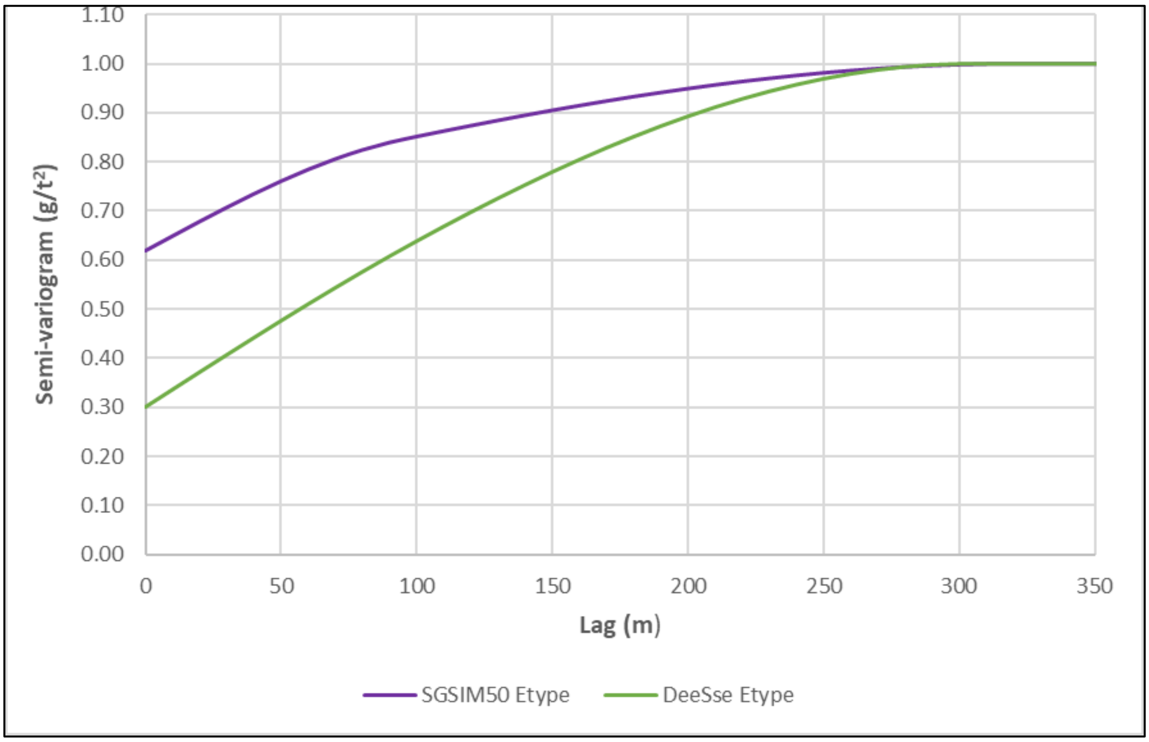

Figure 4.23 : NSCORE variograms of the DeeSse and SGSIM50 etype estimates in TI area (10 m x 10 m x 3 m blocks)

Figure 4.24 compares the plan views of the 50 m x 50 m x 3 m samples, DeeSse and SGSIM50 etype estimates. From Figure 4.24, it can be observed that the spatial grade distributions of the DeeSse and SGSIM50 etype estimate blocks are generally comparable. It should be noted how the DeeSse's map is more smoothed than the SGSIM50's plan. This confirms the deductions made from descriptive statistics, cdfs and NSCORE variograms.

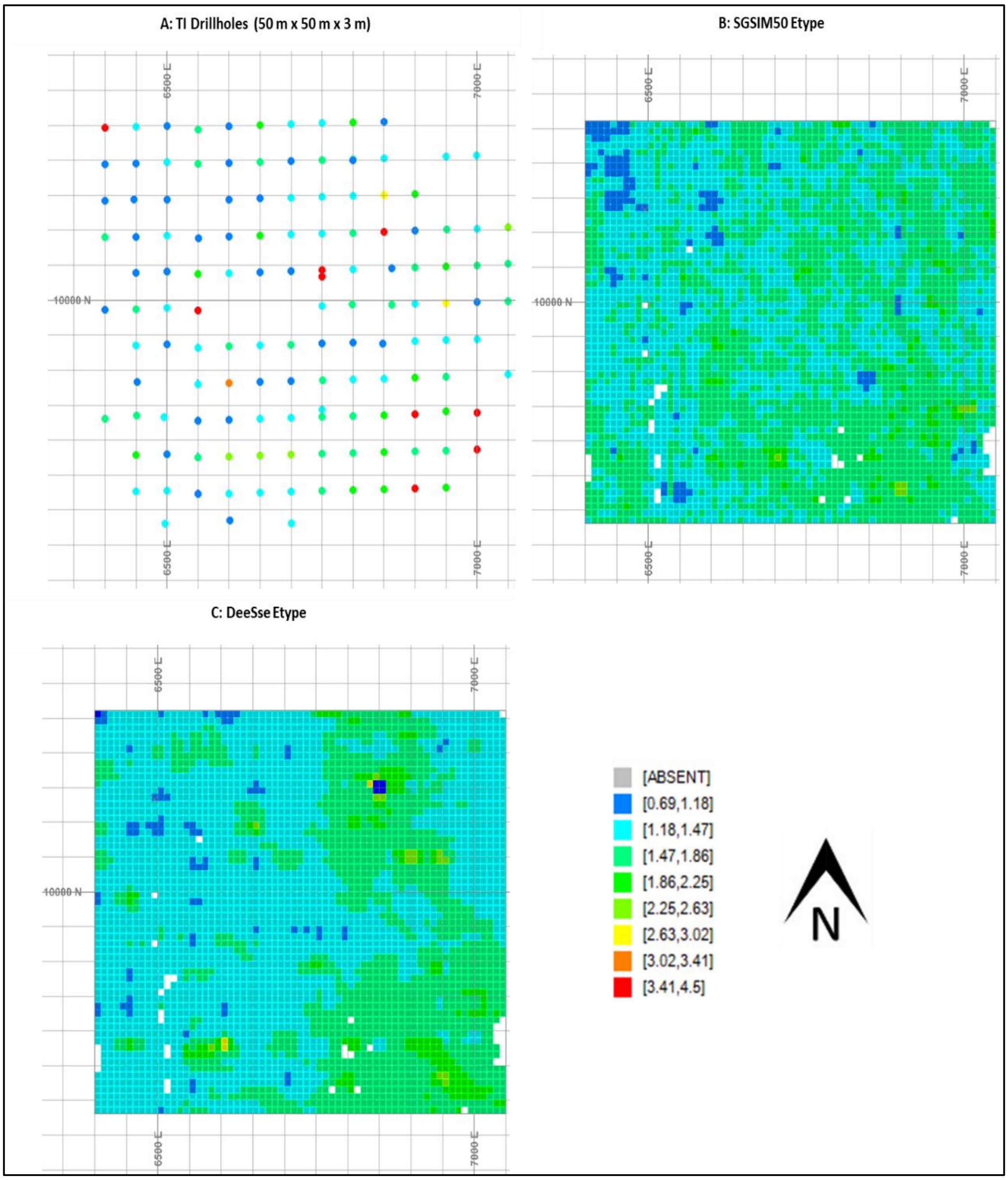

Figure 4.24 : Plan view of the spatial distribution of grades for the 50 m x 50 m x 3 m samples, DeeSse and SGSIM50 etype estimates in the TI Area (10 m x 10 m x 3 m blocks)

Figure 4.25: Cross-sections through the DeeSse and SGSIM50 etype estimates in TI area (10 m x 10 m x 3 m blocks) shows a comparison of cross-sections through the DeeSse and SGSIM50 etype estimates. The cross-sections were taken randomly in the north-south (N-S) and east-west (E-W) directions. There is general resemblance between the DeeSse and SGSIM50 etype estimates' cross sections with some occasional minor differences.

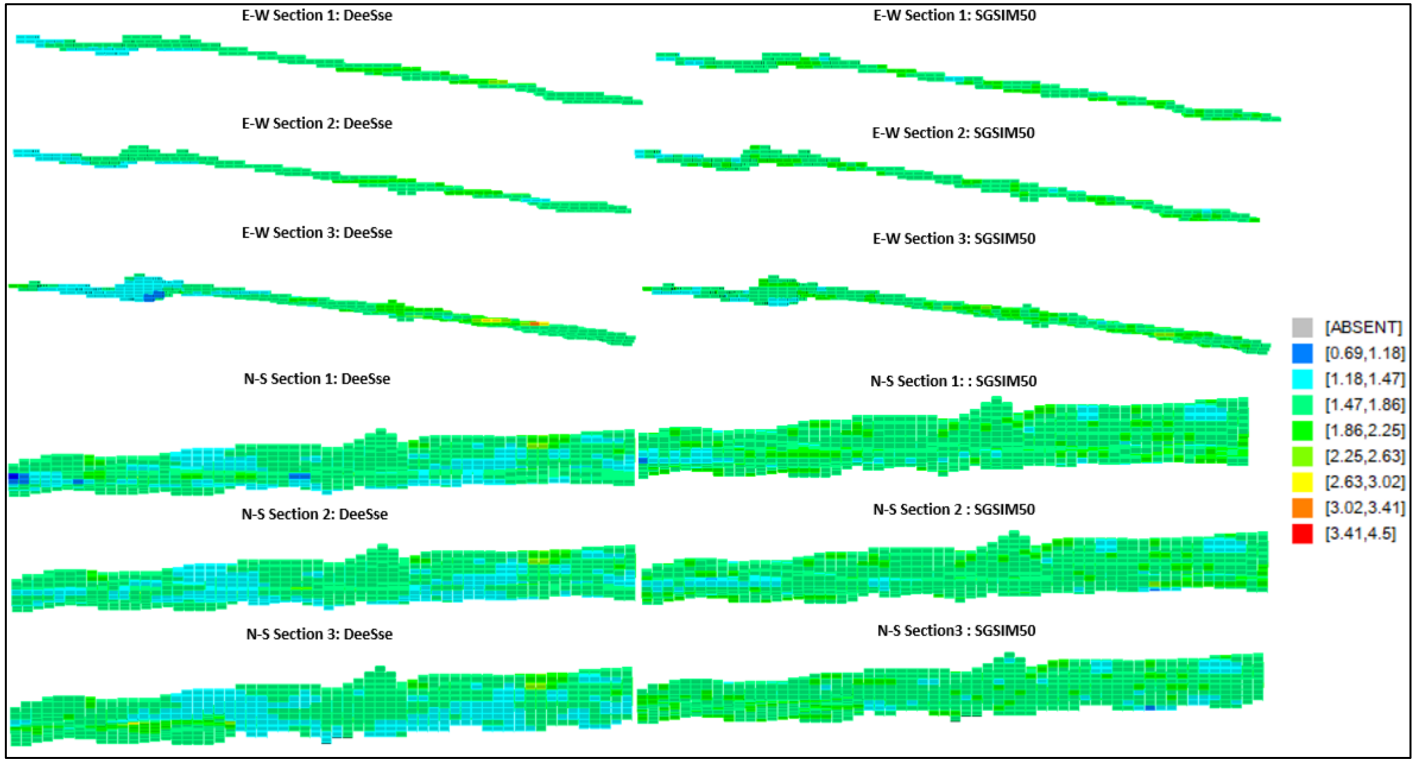

Figure 4.25: Cross-sections through the DeeSse and SGSIM50 etype estimates in TI area (10 m x 10 m x 3 m blocks)

To quantify the differences in the results of the two techniques, the mean absolute percentage error (MAE%) between the blocks of the DeeSse and SGSIM50 etype estimates at each location was calculated to be 13%. Although the means, cdfs, plans between the DeeSse and SGSIM50 etype estimates are generally similar; the high differences in their variance and the MAE of 13% is of concern. It is assumed that the same recommendations about the possible improvements to the TI suggested in Section 4.5 will result in better results. Nonetheless, all other points considered; the application of DeeSse seems plausible for the purpose of this study. Hence, DeeSse was then applied in the EA where the data is scarce.

4.8. Application of DeeSse in the Extension Area Using 200 m x 100 m x 3 m samples

The means and variances of the 50 DeeSse simulations and their etype estimate are summarised in Table 4.14: Unweighted means and variances of 50 DeeSse realisations in EA (10 m x 10 m x 3 m blocks). The mean and variance of the DeeSse etype estimate is 1.18 g/t and 0.05 $(g/t)^2$, respectively. The minimum average grade of the realisations is 1.11 g/t while the highest average grade of the simulations is 1.30 g/t. The variances around the means of the simulations range from 0.04 $(g/t)^2$ to 0.06 $(g/t)^2$.

Table 4.14: Unweighted means and variances of 50 DeeSse realisations in EA (10 m x 10 m x 3 m blocks)

Simulation	Mean (g/t)	Variance $(g/t)^2$	Simulation	Mean (g/t)	Variance $(g/t)^2$
Etype estimate	1.18	0.05			
SIM1	1.21	0.04	**SIM26**	1.19	0.04
SIM2	1.11	0.05	**SIM27**	1.24	0.04
SIM3	1.14	0.04	**SIM28**	1.16	0.05
SIM4	1.20	0.05	**SIM29**	1.13	0.05
SIM5	1.15	0.05	**SIM30**	1.17	0.05
SIM6	1.30	0.05	**SIM31**	1.17	0.04
SIM7	1.14	0.05	**SIM32**	1.19	0.04
SIM8	1.16	0.04	**SIM33**	1.14	0.04
SIM9	1.14	0.05	**SIM34**	1.23	0.04
SIM10	1.20	0.05	**SIM35**	1.21	0.04
SIM11	1.17	0.04	**SIM36**	1.23	0.04
SIM12	1.18	0.04	**SIM37**	1.11	0.04
SIM13	1.16	0.05	**SIM38**	1.17	0.05
SIM14	1.19	0.05	**SIM39**	1.11	0.05
SIM15	1.17	0.05	**SIM40**	1.24	0.05
SIM16	1.15	0.04	**SIM41**	1.16	0.06
SIM17	1.22	0.05	**SIM42**	1.15	0.05
SIM18	1.20	0.04	**SIM43**	1.23	0.04
SIM19	1.18	0.05	**SIM44**	1.19	0.04
SIM20	1.16	0.04	**SIM45**	1.25	0.06
SIM21	1.23	0.06	**SIM46**	1.14	0.05
SIM22	1.14	0.04	**SIM47**	1.25	0.05
SIM23	1.20	0.05	**SIM48**	1.22	0.04
SIM24	1.27	0.05	**SIM49**	1.13	0.04
SIM25	1.19	0.04	**SIM50**	1.15	0.05

4.9. Validation of DeeSse in the Extension Area Using SGSIM (200 m x 100 m x 3 m Input Data)

The same NSCORE variogram of the 25 m x 25 m x 3 m in Table 4.8 was used for running SGSIM200 simulations. Hence, the relevant variography results will be like those described in Section 4.5. SGSIM200 was implemented to validate the DeeSse results which also had a similar input grid size of 200 m x 100 m x 3

m. The means and variances of the 50 SGSIM200 simulations and their etype estimate are summarised in Table 4.15.

The mean and variance of the SGSIM200 etype estimate is 1.25 g/t and 0.38 $(g/t)^2$, respectively. The minimum average grade of the realisations is 1.19 g/t while the highest average grade of the simulations is 1.30 g/t. The variances around the means of the simulations range from 0.36 $(g/t)^2$ to 0.42 $(g/t)^2$.

Table 4.15: Unweighted means and variances of 50 SGSIM200 realisations in extension area (10 m x 10 m x 3 m blocks)

Simulation	Mean (g/t)	Variance $(g/t)^2$	Simulation	Mean (g/t)	Variance $(g/t)^2$
Etype estimate	1.25	0.38			
SIM1	1.25	0.39	**SIM26**	1.22	0.37
SIM2	1.24	0.38	**SIM27**	1.28	0.40
SIM3	1.26	0.38	**SIM28**	1.22	0.37
SIM4	1.27	0.40	**SIM29**	1.24	0.37
SIM5	1.26	0.39	**SIM30**	1.19	0.37
SIM6	1.24	0.38	**SIM31**	1.25	0.38
SIM7	1.25	0.38	**SIM32**	1.23	0.38
SIM8	1.24	0.37	**SIM33**	1.29	0.39
SIM9	1.24	0.39	**SIM34**	1.27	0.41
SIM10	1.24	0.36	**SIM35**	1.25	0.38
SIM11	1.23	0.36	**SIM36**	1.24	0.36
SIM12	1.28	0.40	**SIM37**	1.23	0.38
SIM13	1.29	0.39	**SIM38**	1.23	0.37
SIM14	1.26	0.40	**SIM39**	1.27	0.40
SIM15	1.29	0.41	**SIM40**	1.26	0.39
SIM16	1.26	0.38	**SIM41**	1.28	0.40
SIM17	1.24	0.37	**SIM42**	1.23	0.37
SIM18	1.24	0.37	**SIM43**	1.22	0.39
SIM19	1.24	0.37	**SIM44**	1.27	0.37
SIM20	1.28	0.40	**SIM45**	1.23	0.37
SIM21	1.30	0.41	**SIM46**	1.22	0.37
SIM22	1.21	0.37	**SIM47**	1.26	0.38
SIM23	1.26	0.38	**SIM48**	1.28	0.38
SIM24	1.29	0.41	**SIM49**	1.25	0.37
SIM25	1.23	0.37	**SIM50**	1.29	0.42

Descriptive statistics, cumulative distribution functions (cdf), block grade values, variograms, plans and sections between the DeeSse and SGSIM200 etype estimates are compared in order to validate the DeeSse results. Table 4.16 summarises the comparison of the descriptive statistics. From Table 4.16, it appears that SGSIM200 etype estimate produces a slightly higher grade mean estimate than the DeeSse etype estimate (~6% higher). The DeeSse's mean grade is also about 5% lower than the mean of the sample data. However, the SGSIM200 etype estimates' variance differs significantly from the DeeSse's variance. There is significantly more inherent block-to-block variability within the SGSIM etype estimate than the DeeSse which tends to be smoother locally. The DeeSse's range is much greater (~55%) than the SGSIM etype estimate. That means, DeeSse attempts to reflect lower and higher grades in the sample data better than SGSIM. It should be noted that the DeeSse's range is also intrinsically limited by the TI's spread. To investigate this difference in variability further, the cdfs for the DeeSse and SGSIM etype estimates were also analysed.

Table 4.16: Comparison of descriptive statistics between 200 m x 100 m x 3m input data, DeeSse and SGSIM200 etype estimates within the EA (10 m x 10 m x 3 m Blocks)

Description	**Count**	**Mean (g/t) Unweighted**	**Variance (g/t)^2**	**Minimum (g/t)**	**Maximum (g/t)**	**Range (g/t)**
200 m x 100 m x 3 m samples	102	1.24	0.98	0.03	4.98	4.95
SGSIM200 etype estimate	5798	1.25	0.38	0.69	1.85	1.16
DeeSse etype estimate	5798	1.18	0.05	0.19	2.80	2.61

Figure 4.26 shows the cdf plots of the DeeSse and SGSIM200 etype estimates in the EA. From the cdfs, it can be observed that between cut-off grades of 1 g/t to 1.5 g/t some bias exists. That is, DeeSse mostly underestimates the proportion above cut-off grade. At cut-off grades below 1 g/t and above 1.5 g/t, the cdfs are generally similar. The cdfs also confirm that the spread of the DeeSse is greater than that of the SGSIM200 etype estimate.

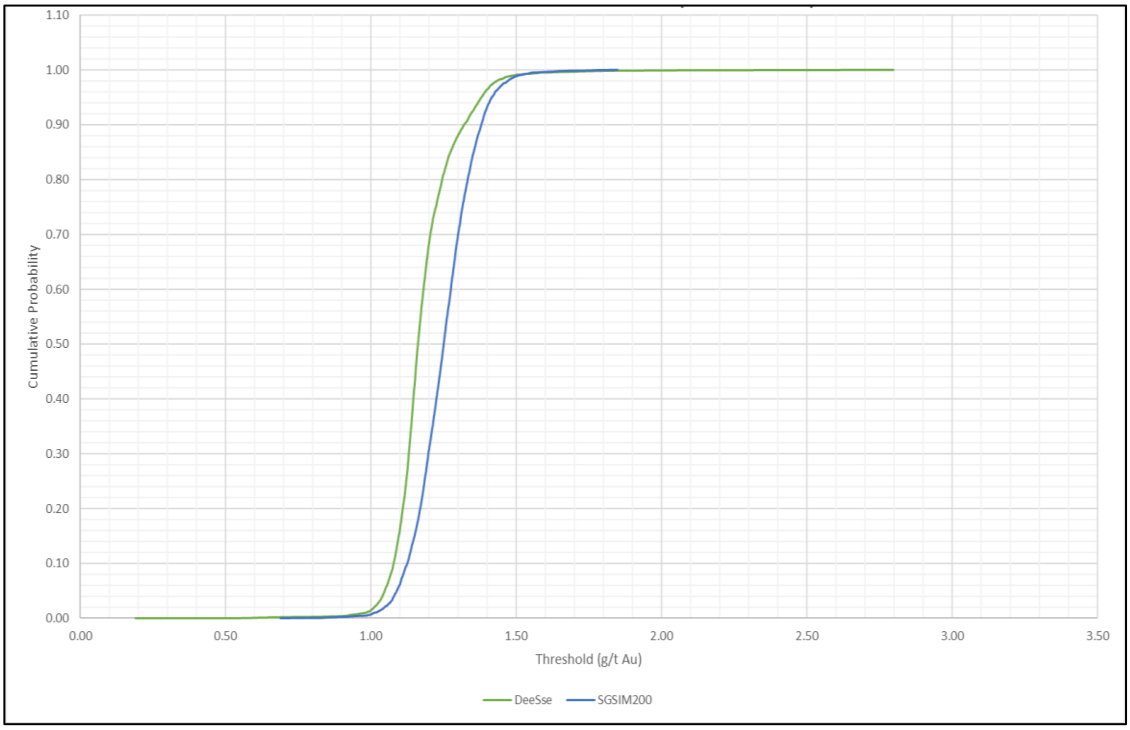

Figure 4.26: Cumulative distribution functions of DeeSse and SGSIM200 etype estimates grades for 10 m x 10m x 3 m blocks in the EA

In order to compare the spatial variability of DeeSse and SGSIM200 etype estimates, their NSCORE variograms were calculated and modelled as shown in Figure 4.27. The variograms also confirm that the SGSIM200 etype estimate has more spatial variability than the DeeSse etype estimate.

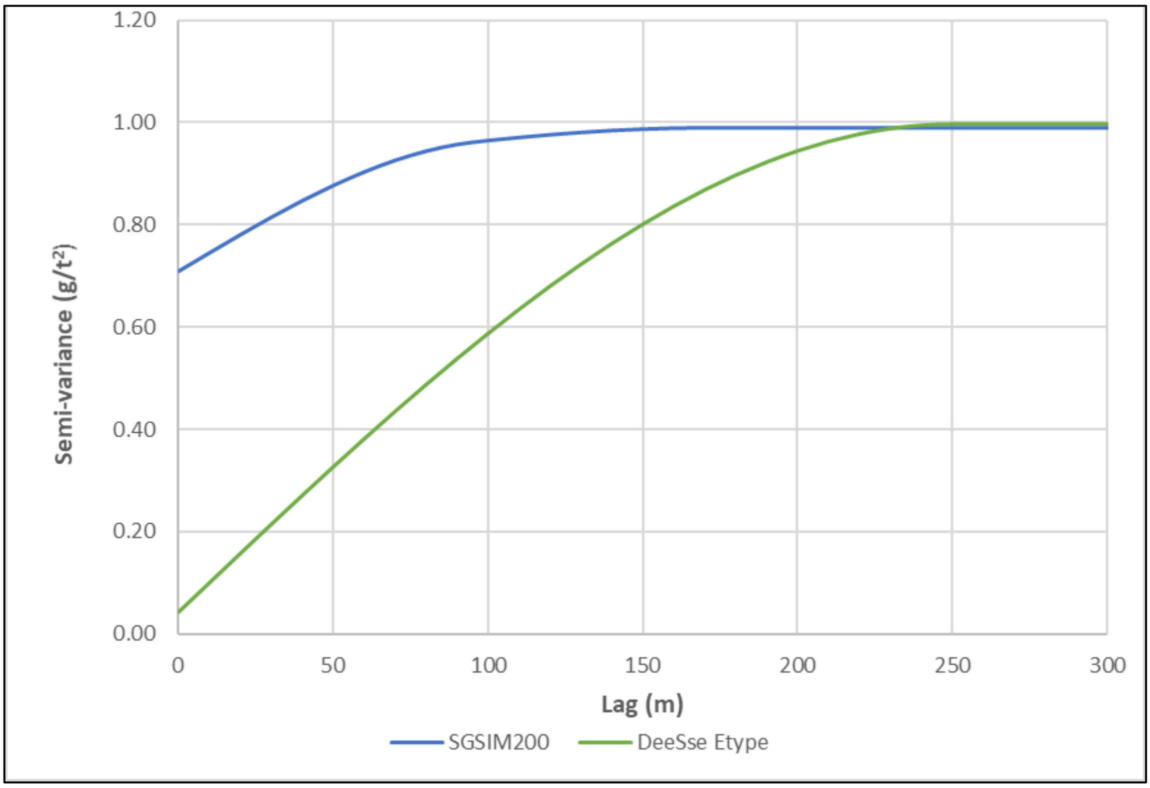

Figure 4.27 : NSCORE variograms of the DeeSse and SGSIM200 etype estimates in EA (10 m x 10 m x 3 m blocks)

Figure 4.28 compares the plan views of the 200 m x 100 m x 3 m samples, DeeSse and SGSIM200 etype estimates. From Figure 4.28, it can be observed that the spatial grade distributions of the DeeSse and SGSIM200 etype estimates' blocks are different. DeeSse etype estimate shows the expected decrease in the grades towards the north-western direction as discussed in Section 4.2.1 while SGSIM200 failed to capture the local connectivity. It should be noted that given the estimation blocks of 10 m x 10 m x 3 m from input data of 200 m x 100 m x 3m, it is expected that the SGSIM200 results would be inadequate. Further investigation on the impact of change of support will be beneficial. It should also be noted how the DeeSse's map is more smoothed than the SGSIM200 plan. This confirms the deductions made from descriptive statistics, cdfs and NSCORE variograms.

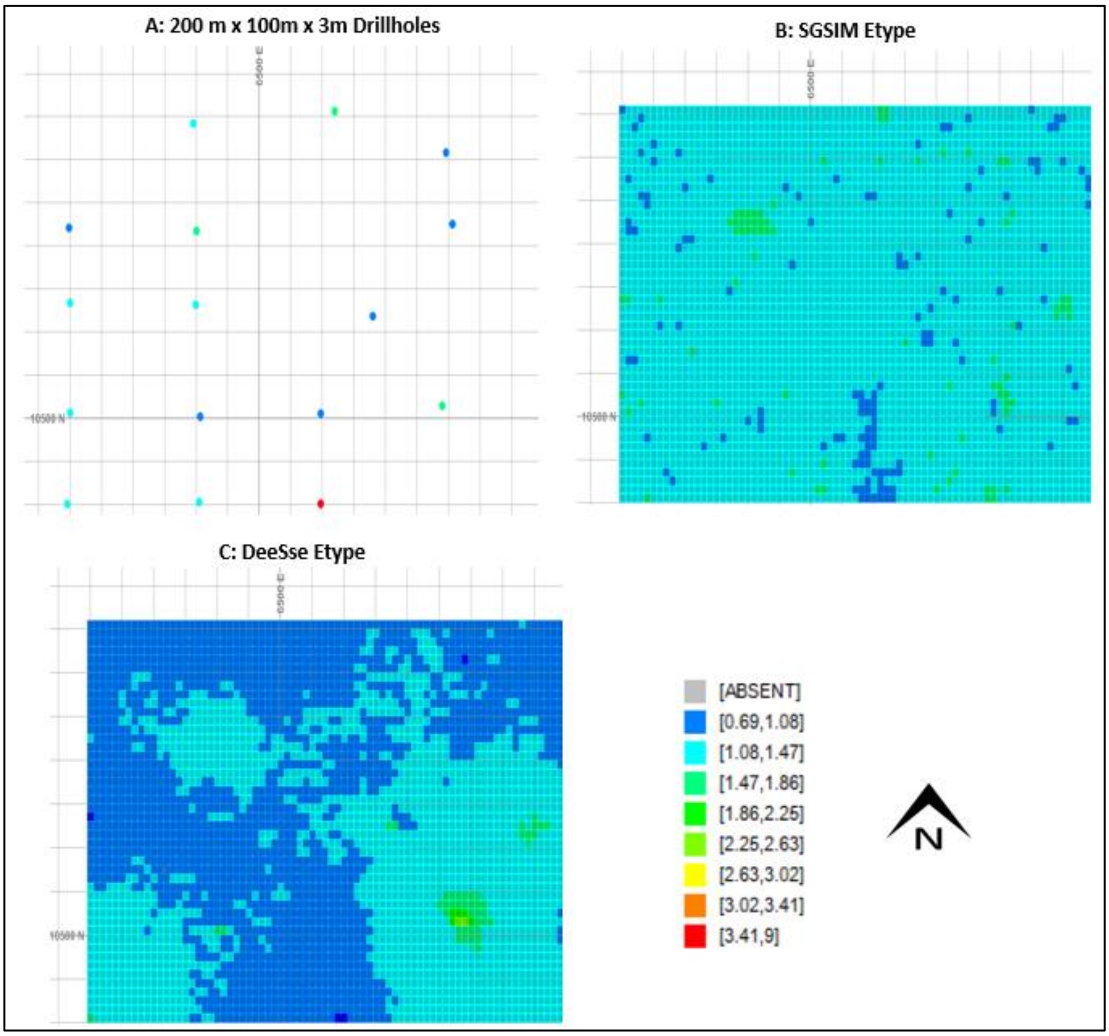

Figure 4.28 : Plan view of the spatial distribution of grades for the 200 m x 100 m x 3 m samples, DeeSse and SGSIM200 etype estimates in the EA (10 m x 10 m x 3 m blocks)

There was no need to compare cross sections as it was expected that they will not be comparable based on the deduction made from the plan views.

To quantify the differences in the results of the two techniques, the mean absolute percentage error (MAE%) between the blocks of the DeeSse and SGSIM200 etype estimates at each location was calculated to be 9%. Although the means and cdfs, DeeSse and SGSIM200 etype estimates are generally similar; the high differences in their variances, maps, and the MAE of 9% is of concern. In addition to possible improvements to the KE of the TI, an increase in block estimation sizes could improve the SGSIM200's results. Furthermore, it should be noted that the TI is primarily located in a high-grade area and was used to estimate within the EA which is mainly a low-grade area. This implies that a more representative TI could also significantly improve the results. Nonetheless, the DeeSse results were then used for stochastic reserve estimation and relevant results are discussed in the following section.

4.10. Stochastic Resource Estimation Using DeeSse in the Extension Area

4.10.1. Uncertainty around the estimates

Deterministic approaches report only one value for the estimated mean together with some confidence limits. However, stochastic estimation provided a more comprehensive description of the uncertainty around the estimates. Stochastic approaches allow for the reporting of possible minimum, maximum and quantile values for the estimated mean as shown in Table 4.17. This means that a more risk-based approach can be developed, e.g. simulations with minimum and maximum mean grades can be classified as downside and upside potential, respectively.

Table 4.17 : Stochastic estimation reporting on estimated mean grades for DeeSse blocks in the EA (10 m x 10 m x 3 m blocks)

Parameter	Mean
Mean (g/t)	1.18
Minimum(g/t) (Downside Potential)	1.11
Maximum (g/t) (Upside Potential)	1.30
Variance $(g/t)^2$	0.04 – 0.06
Q1 (g/t)	1.03
Median (g/t)	1.17
Q3 (g/t)	1.31

The mean of the simulations was reported to be 1.18 g/t with a confidence interval around the mean being between 1.178 g/t and 1.184 g/t. Instead of reporting one value for variance, the uncertainty in the variance can also be described as being between 0.04 $(g/t)^2$ and 0.06 $(g/t)^2$.

4.10.2. Probabilities above and below thresholds from the simulations

Figure 4.29 shows the probability above or below possible thresholds for the simulations' 10 m x 10 m x 3 m blocks. This provides another useful feature of stochastic modelling. For example, at the minimum average (downside potential) of the simulations which is 1.11 g/t, the probability of getting grades below and above this minimum mean grade can be estimated. From Figure 4.29, the probability of achieving grades above the mean of the downside potential is 0.88.

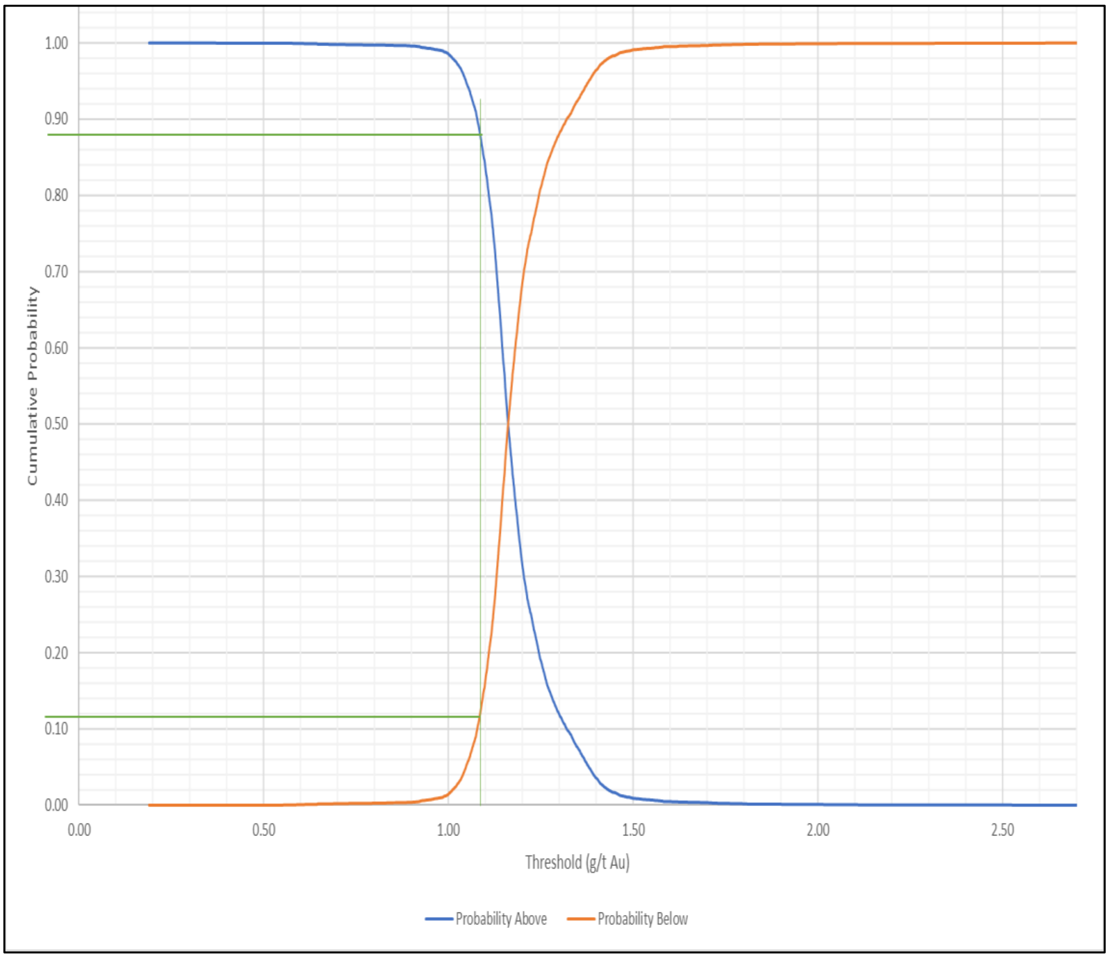

Figure 4.29: Probability below and above thresholds for DeeSse simulations in EA (10 m x 10 m x 3 m blocks)

4.10.3. Stochastic grade tonnage curves

Traditional approaches for constructing grade tonnage curves are based on one grade distribution of estimated blocks. Even when stochastic estimation methods such as SGSIM are used, grade tonnages curves would still be developed using only the etype estimate of the simulations as shown in Figure 4.30. Stochastic approaches should however be able to allow for the integration of the uncertainties from all simulations as shown in Figure 4.31 and Figure 4.32. By using relevant transfer functions, these different grade-tonnages curves can be integrated into reserve calculations and mine planning. To illustrate this, distributions of estimated metal content and projected revenues are calculated in this study instead of reporting single values for metal content or projected revenue. This provides a better understanding of the uncertainty in both metal content and revenue estimations as shown in Section 4.10.4 and 4.10.5.

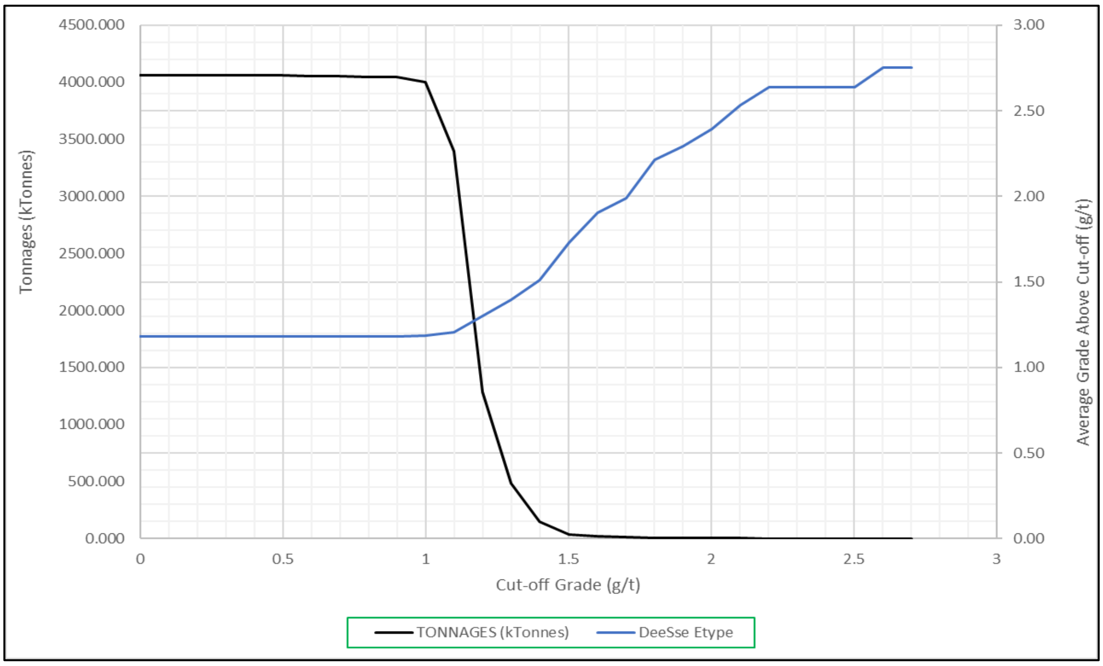

Figure 4.30 : Grade tonnage curves based on the etype estimate of the DeeSse simulations

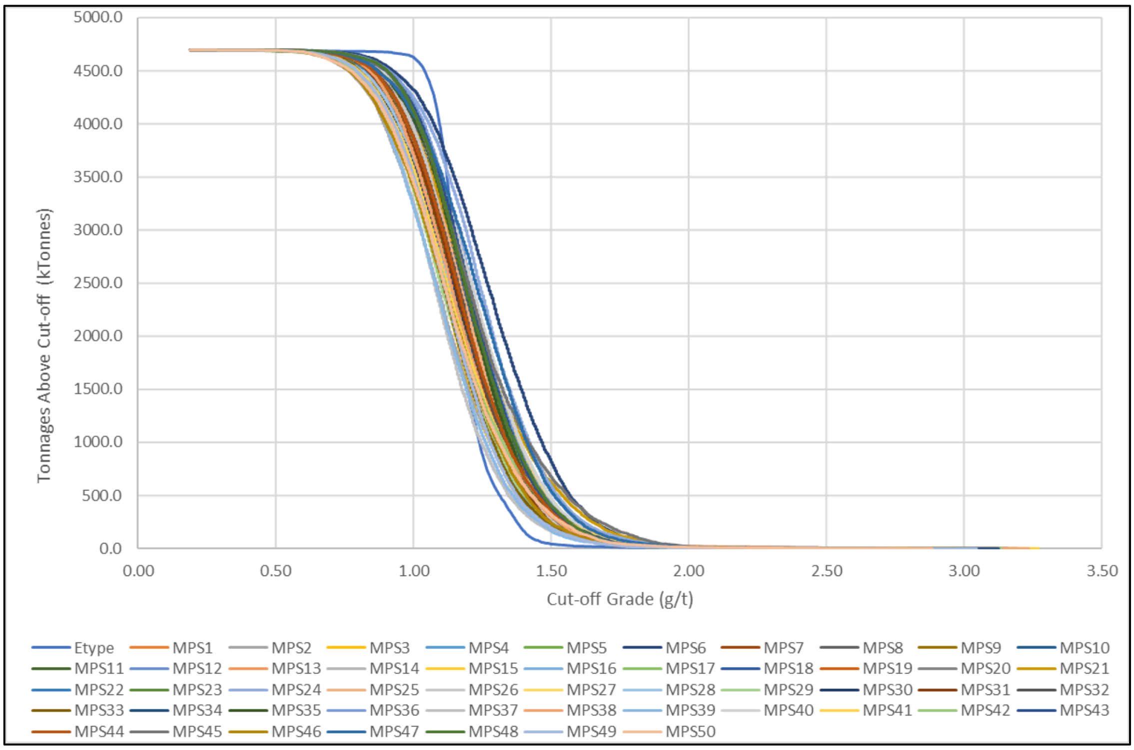

Figure 4.31 : Stochastic tonnage curves based on all 50 DeeSse simulations

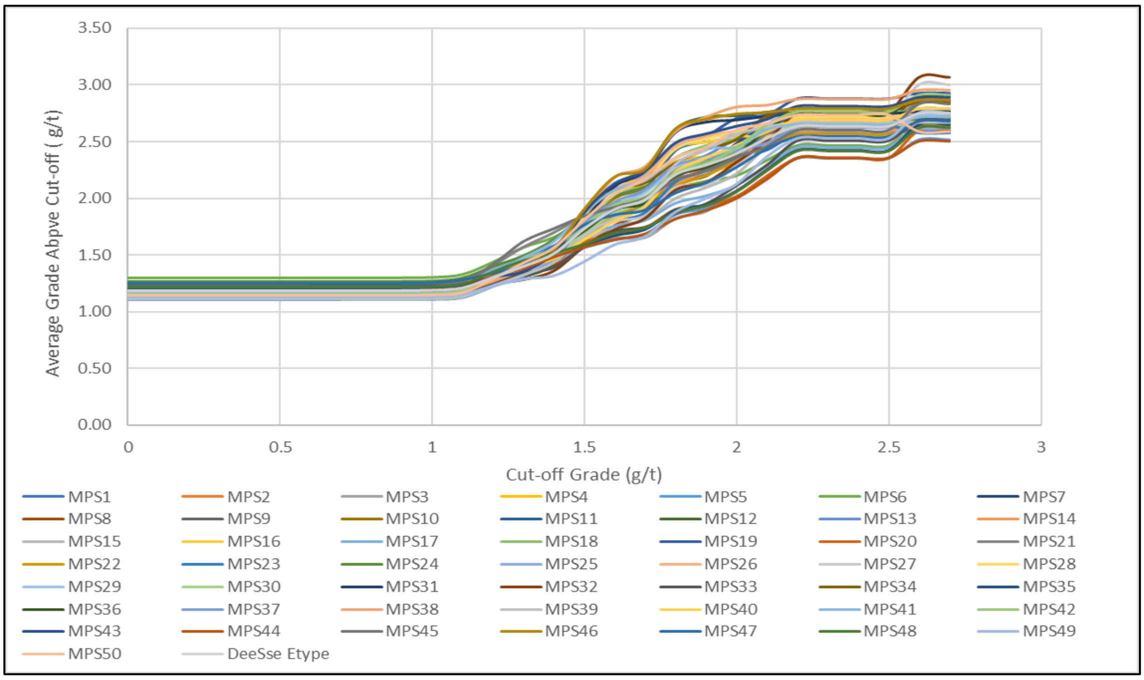

Figure 4.32: Stochastic grade curves based on all 50 DeeSse simulations

Another alternative to the approach shown in Figure 4.31 and Figure 4.32 is to identify the simulations with lowest and highest grades as the worst (downside)- and best (upside) - case scenarios, respectively. The etype estimate can then be regarded as the base (average) case. By so doing, grade tonnage curves can be constructed on a scenario basis as shown in Figure 4.33. Note: Dotted lines show tonnage curves and solid lines indicate associated grade curves.

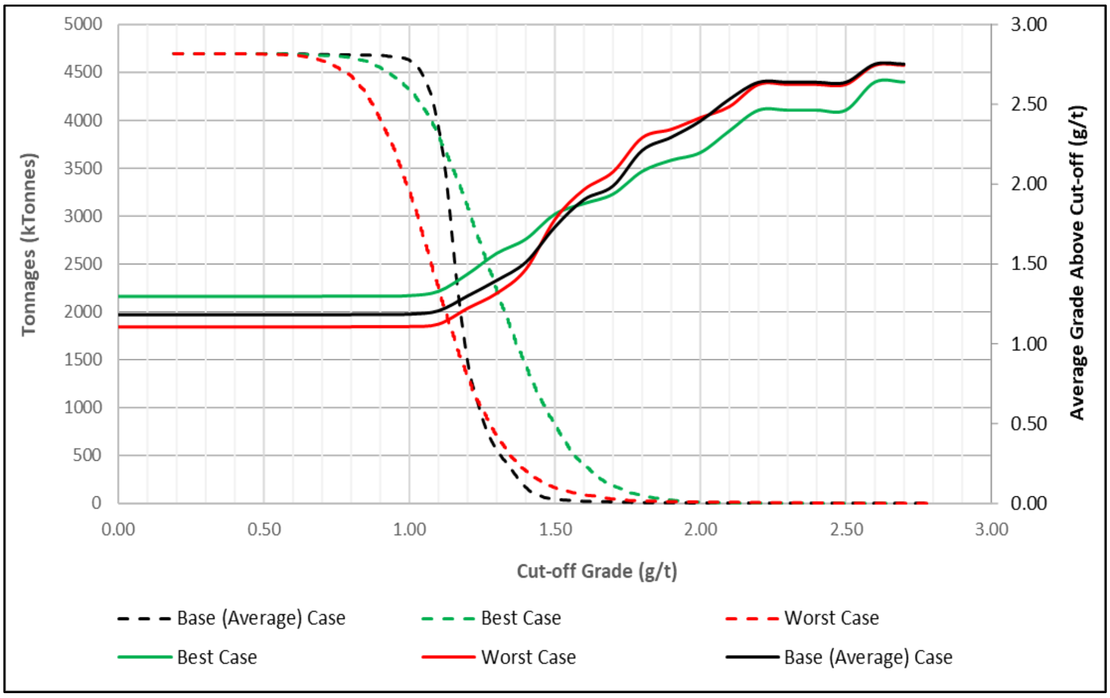

Figure 4.33 : Stochastic grade tonnage curves based on the worst-, best- and base -case scenarios

4.10.4. Uncertainty of metal content estimates

By applying a cut-off of 0.38 g/t, a mining recovery factor of 100%, dilution of 8.33%, plant recovery factor of 97.20 % and mine call factor (MCF) of 97 %; metal contents were calculated for the 50 DeeSse realisations. The modifying factors used to calculate metal content are taken or estimated from information provided in the Goldfields Mineral Resources and Mineral Reserves statement, (Goldfields, 2019). The resultant statistics and boxplot describing the uncertainties and distribution of the metal content estimates are shown in Table 4.18 and Figure 4.34 respectively. The mean of the estimated metal content from the 50 simulations is 4795.11 kg with confidence intervals between 4746.86 kg and 4843.36 kg. The minimum and maximum possible ounces are also reported as 4485.05 kg and 5261.86 kg.

Table 4.18 : Summary statistics of metal content based on the 50 DeeSse simulations

Parameter	Metal Content (koz)	Metal Content (kg)
Mean	169.14	4795.11
Standard deviation	6.05	171.55
Minimum	158.21	4485.05
Maximum	185.61	5261.86
Lower quartile	163.99	4649.13
Median	168.33	4772.18
Upper quartile	173.14	4908.44
Lower 95% CL for mean	167.44	4746.86
Upper 95% CL for mean	170.84	4843.36

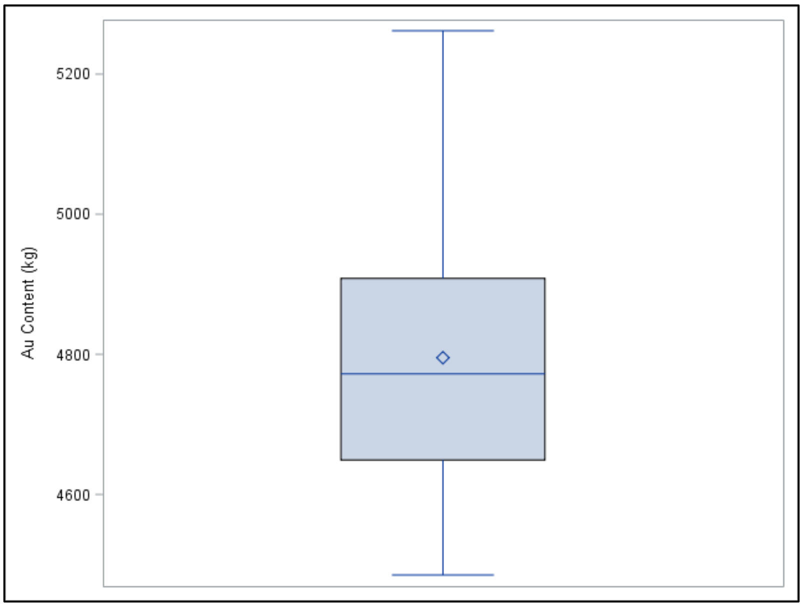

Figure 4.34 : Boxplot showing the distribution of metal content from 50 DeeSse simulations

4.10.5. Uncertainty of revenue estimates

By using an average gold price of 1200 US$/oz and Rand/US$ exchange (1US$=14.45 ZAR), similar to the price used in the Goldfields Mineral Resources and Mineral Reserves statement in the same year, expected revenues were estimated. The excepted revenues estimated were for each one of the 50 DeeSse realisations. The resultant statistics and boxplot describing the uncertainties and distribution of the revenue estimates are shown in Table 4.19 and Figure 4.35, respectively. The mean of the estimated revenues from the 50 simulations is ZAR 2.93 billion with confidence intervals between ZAR 2.90 billion and ZAR 2.96 billion. The minimum and maximum possible revenues are also reported as ZAR 2.74 billion and ZAR 3.22 billion.

Table 4.19 : Summary statistics of revenues based on the 50 DeeSse simulations

Parameter	Revenue (Million US$)	Revenue (Billion ZAR)
Mean	202.97	2.93
Standard deviation	7.26	0.11
Minimum	189.85	2.74
Maximum	222.73	3.22
Lower quartile	196.79	2.84
Median	202.00	2.92
Upper quartile	207.77	3.00
Lower 95% CL for mean	200.93	2.90
Upper 95% CL for mean	205.01	2.96

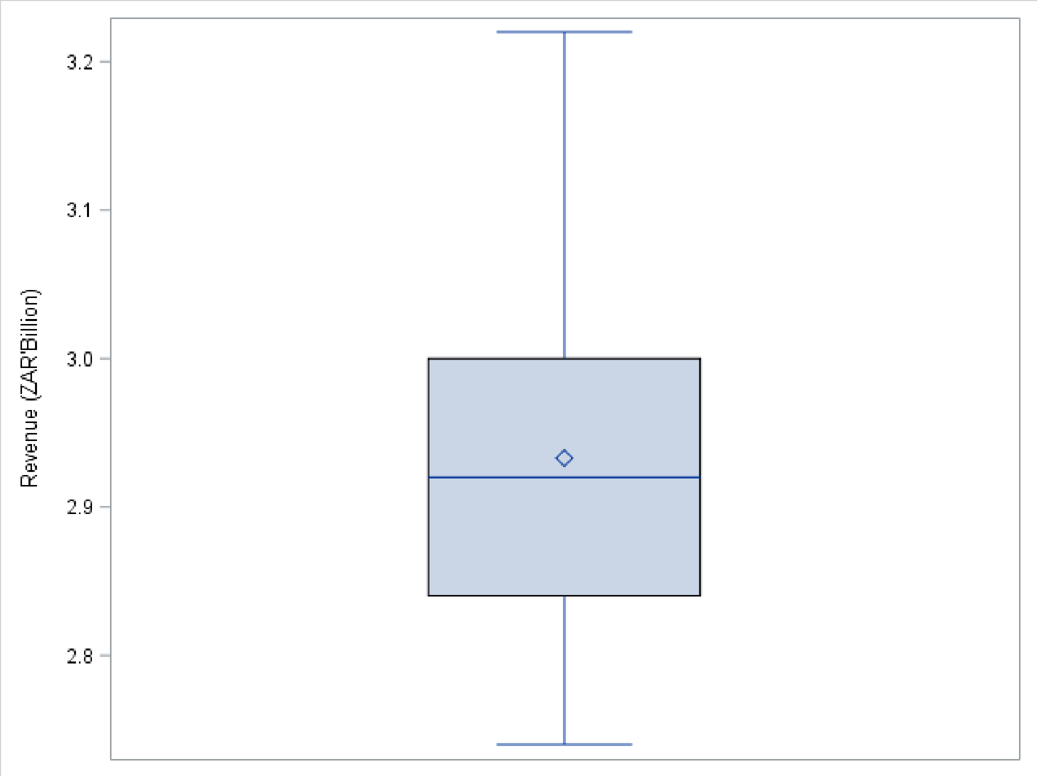

Figure 4.35 : Boxplot showing distribution of revenues from 50 DeeSse simulations

4.11. Chapter Summary

In this chapter, estimated statistics and underlying distributions for the three datasets used are discussed. The three datasets are the 25 m x 25 m x 3 m grade control samples, 50 m x 50 m x 3 m subset of the grade control data and the 200m x 100 m diamond drill hole composites. The underlying distributions of three datasets were found to be lognormal. The thickness and volume of the A1 reef domain was modelled within a domain and a subsequent block model produced. The block model parameters based on an SMU of 10 m x 10 m x 3 m were presented.

An SK TI was developed within a cuboid instead of a wireframe in order to meet the requirements of the algorithm in the Ar2Gems software. The use of a cuboid TI meant that the corresponding realisations would also be in cuboid form. As such, the SK cuboids and realisations would require splitting the cuboid and simulations with a wireframe during post processing and before analysis. The use of the cuboid and subsequent splits was tested and validated. The SK model was subsequently developed following variography and KNA.

Furthermore, DeeSse was implemented within the TI area together with SGSIM and the results from both approaches were comparable. However, possible improvements of the TI were identified. The TI and DeeSse were then applied in the extension area. Upon running DeeSse and SGSIM within the extension area, the subsequent results were compared. Although the results from both approaches were generally comparable, DeeSse provided a more robust approach that offered more confidence in the estimates.

The subsequent DeeSse simulations from the EA were used to quantify the uncertainty around the estimates, calculate probably plots for different thresholds and develop stochastic grade-tonnage curves. Furthermore, uncertainties and distributions of the metal content estimates, and revenue projections were determined.

5. CHAPTER V: DISCUSSION SUMMARY

5.1. Introduction

This chapter summarises the results and analysis carried out in CHAPTER IV: RESULTS AND ANALYSIS. The discussion will be summarised in relation to the research objectives and research questions discussed in Sections 1.7 and 1.8. The overall discussion culminates in expressing a proof of concept for the application of DeeSse for grade simulation by using a kriged model as a TI.

5.2. Development and Validation of a TI

An SK model was developed within the TI area using 25 m x 25 m x 3 m grade control data in order to test its ability to be used for DeeSse simulation. The estimation block sizes used were 10 m x 10 m x 3 m which is equivalent to the SMU. The SK model used for simulation was in the form of a cuboid instead of a commonly used block model estimated within a wireframe. The need to use a cuboid model was necessitated by the requirements of the DeeSse algorithm within the Ar2Gems software. The SK cuboid model's mean and variance were 1.53 g/t and 0.12 $(g/t)^2$, respectively. Post simulation, the SK model was split with a wireframe in order to retain only the blocks within the A1 geological boundary. The split SK model's mean and variance was found to 1.51 g/t and 0.15 $(g/t)^2$, respectively.

In order to validate the TI, it was compared to the SGSIM etype estimate developed from the same 25 m x 25 m x 3 m input data and equivalent NSCORE variogram. The TI and SGSIM etype estimate were generally comparable except that the variances differed significantly and the MAE% could be improved. It was concluded that the TI could be improved by optimising some of the variogram and kriging parameters. However, for the purpose of the study, the TI was deemed sufficient.

5.3. Application and Validation of DeeSse in the Pit Area with High Sampling Density (10 m x 10 m x 3 m blocks)

DeeSse simulations were run using 50 m x 50 m x 3 m input data and the TI in the TI area (pit area). The resultant DeeSse etype estimate's mean and variance were 1.40 g/t and 0.07 $(g/t)^2$, respectively. The comparative SGSIM etype estimate developed using the same input grid size of 50 m x 50 m x 3 m and a NSCORE variogram of 25 m x 25 m x 3 m samples had a mean of 1.47 g/t and a variance 0.56 $(g/t)^2$. The two etype estimates were generally comparable except the significant differences in variability and a MAE% that could be improved. SGSIM showed more local variability while DeeSse produced a greater range of grades. Similarly, it was noted that an improvement in the TI will improve the DeeSse results and that this could be achieved through re-parametrisation of the variogram and kriging inputs. Nonetheless, DeeSse's results were still plausible. It should be noted that DeeSse attempted to reflect the range of input data better than SGSIM, even though this was already limited by the smoothing in the TI.

5.4. Application and Validation of DeeSse for Grade Simulation within the Pit Extension Area with Low Sampling Density (10 m x 10 m x m blocks)

Simulation using DeeSse within the extension area yielded an etype estimate with a mean of 1.18 g/t and a variance of 0.05 $(g/t)^2$. The SGSIM etype estimate had a mean of 1.25 g/t and a variance of 0.38 $(g/t)^2$. There were significant differences in the variability of the DeeSse etype estimate and SGSIM etype estimate. SGSIM still showed more local variability while DeeSse gave a greater range of grade values. However, SGSIM results could not be relied on given the relatively small support size of 10 m x 10 m x 3m as compared to the input grid of 200 m x 100 m x 3 m. In this case, DeeSse is more reliable as it is also dependent on the TI which is at a grid size of 10 m x 10 m x 3 m in addition to the input data. A further investigation of how change of support will affect the performance of DeeSse versus SGSIM would be useful. Of course, the observed over-smoothing of the TI as previous discussed should be considered. Re-parametrisation of the variogram and kriging inputs may be necessary to improve the KE of the TI. An improvement in the TI could result in better DeeSse estimates. The TI is primarily located in a high-grade area and was used to estimate within the EA which is mainly a low-grade area. This implies that a more representative TI could also significantly improve the DeeSse results.

5.5. Integration of Uncertainty Grade Models in the Calculations of Grade-Tonnage Curves, Metal Content and Revenues

The 50 DeeSse simulations allowed for the reporting of more than just a single value for the mean grade but 50 possible averages values for grades. Statistics around each simulation were calculated and analysed. The mean of the simulations was reported to be 1.18 g/t with a confidence interval around the mean being between 1.178 g/t and 1.184 g/t. Instead of reporting one value for variance, the uncertainty in the variance can also be described as being between 0.04 $(g/t)^2$ and 0.06 $(g/t)^2$. The minimum (downside potential) and maximum (upside potential) possible average grade values were determined to be 1.11 g/t and 1.30 g/t. Probabilities of achieving an average grade above or below a particular cut-off can also be determined and reported. This type of reporting enables a better understanding of the uncertainty of estimates.

Th estimates from the 50 simulations were then used to calculate 50 possible grade tonnage curves which in turn allowed for 50 possible metal content and revenue estimates. Alternatively, metal content and revenue estimates could be reported in a scenario-based format, i.e. worst-, best- and base -case scenarios. The mean of the estimated metal content from the 50 simulations is 4795.11 kg with confidence intervals between 4746.86 kg and 4843.36 kg. The minimum and maximum possible ounces are also reported as 4485.05 kg and 5261.86 kg

The mean of the estimated revenues from the 50 simulations is ZAR 2.93 billion with confidence intervals between ZAR 2.90 billion and ZAR 2.96 billion. The minimum and maximum possible revenues are also reported as ZAR 2.74 billion and ZAR 3.22 billion.

5.6. Benefits of DeeSse

DeeSse enabled the estimation of grade in an area with sparsely drilled holes. Alternative methods are limited in areas where sample data is scarce. By using a representative TI together with conditioning data, DeeSse's estimation provides more confidence since it is based on more sampling information than just drill hole data. In this case, the TI was on the same support as the estimation block sizes, thus providing more precision. The stochastic estimation allows for better understanding of uncertainty which can be integrated into grade-tonnage calculations, metal content estimations and revenue projections. Probabilities of achieving a particular grade above a cut-off can also be determined. This will allow for risk profiling of ounces. DeeSse's ability to reproduce not only the mean grade but its variability provides for a more robust estimation approach.

5.7. Limitations of DeeSse

The choice of a representative training image is difficult. Ensuring that the TI patterns are repetitive and large enough to represent the variability in the SG requires significant testing prior to simulation. The TI used in this study is primarily in a high-grade area and does not fully represent the connectivity of low grades. The choice of the DeeSse input parameters involves extensive trial and error while making judgment on whether the resultant outcomes are realistic before selecting them. The use of a kriged model as a TI means that all the limitations of kriging such as smoothing are transferrable during simulation. For example, the TI used for simulation had a range of 3.09 g/t while the range of original data set used to create it was 22.6 g/t. The requirement for a cuboid model for DeeSse means that a large number of unnecessary blocks are included in the simulation. This would be very problematic when simulating a large orebody as it will increase computing costs and simulation time. It is still not clear if DeeSse will still outperform SGSIM in sparsely spaced areas if the support was increased.

5.8. Research Questions

The following research questions were answered:

- *How can the use of direct sampling MPS techniques enhance resource modelling for the extension area of the Akontansi pit at Tarkwa mine?*
  DeeSse was shown to enhance resource modelling in the extension area by providing a more robust approach for estimating grades in areas with low sampling density. The use of TI and conditioning data provides more confidence on the DeeSse estimates as they are based on abundant "sampling' information. DeeSse, being a stochastic method, then allows for uncertainty quantification around the estimates.
- *How can stochastic resource estimation be integrated into grade-tonnage curves, metal content calculations and revenue projections?*
  By calculating grade-tonnage curves for each DeeSse simulation, stochastic or scenario-based grade-tonnages can be calculated. The distributions of metal content estimates and revenue projections can be determined and reported instead of reporting single values.

5.9. Proof of Concept

A proof of concept has been developed for the application of DeeSse for grade simulation, particularly in areas with limited sampling information. DeeSse seems to provide a more robust estimation approach with more confidence than the alternative when sampling density is low. However, improvement on the TI is necessary.

5.10. Chapter Summary

In this chapter, results presented and analysed in CHAPTER IV: RESULTS AND ANALYSIS were discussed in order to link them together to the research objectives. The outcomes of the TI creation process and its validation as well as the results from the application of DeeSse in the extension area were discussed. The validation of DeeSse results using SGSIM was summarised.

6. CHAPTER VI: CONCLUSIONS AND RECOMMENDATIONS

6.1. Conclusions

Stochastic resource modelling has become of paramount importance in improving reserve modelling and mine planning decisions. The application of the current stochastic approaches such as SGSIM is sub-optimal in areas where the number of samples is scarce. This lack of sufficient data is generally the case in extension areas such as the one at Tarkwa where diamond drill holes are at a 200 m x 100 m x 3 m spacing. However, the abundant availability of closely spaced grade control samples next to these extension areas is not uncommon. At Tarkwa, these grade control drill holes are spaced at 25 m x 25 m x 3 m intervals. These samples provided an opportunity to create TIs using traditional kriging approaches. It was expected that kriging results and hence the TIs would be more robust when sampling density is high. As a result, an SK model was developed as a TI at a support of 10 m x 10 m x 3 m blocks. All simulations were subsequently carried out using the same support size as the TI.

The resultant TI was compared to the SGSIM etype estimate (SGSIM25) developed from the same 25 m x 25 m x 3 m input data and equivalent NSCORE variogram. The mean and variance of the TI was found to be 1.51 g/t and 0.15 $(g/t)^2$, respectively. While the mean and variance of the SGSIM25 etype estimate was estimated to be 1.54 and 0.63 $(g/t)^2$, respectively The TI and SGSIM25 etype estimates were generally comparable except that the variances differed significantly and the MAE% needed some improvements. SGSIM showed more local variability while the TI provided a wider range of grade values. Nonetheless, the TI was deemed sufficient for the purposes of the study but may require improvements for further studies. Following validation of the TI, DeeSse simulations were then run in the TI area using a 50 m x 50 m x 3 m input grid. The subsequent results were validated using SGSIM at the same grid size (SGSIM50) but using a NSCORE variogram of the 25 m x 25 m x 3 m data. The mean and variance of the DeeSse etype estimates were found to be 1.40 g/t and 0.07 $(g/t)^2$, respectively. Additionally, the mean and variance of the SGSIM50 etype estimate was estimated to be 1.47 g/t and 0.56 $(g/t)^2$, respectively. The results of DeeSse and SGSIM etype estimate also were generally comparable except that SGSIM showed more local variability while DeeSse provided a wider range of grade values.

DeeSse was then implemented in the EA where the sampling density is low at a 200 m x 100 m x 3 m grid size. The subsequent results were then compared with the SGSIM's outcomes within the same area (SGSIM200). The SGSIM input grid size was also 200 m x 100 m x 3 m with the NSCORE variogram of the 25 m x 25 m x 3 m data. The mean and variance of the DeeSse etype estimates were found to be 1.18 g/t and 0.05 $(g/t)^2$, respectively. While the mean and variance of the SGSIM50 etype estimates were estimated to be 1.25 g/t and 0.38 $(g/t)^2$, respectively. However, SGSIM200 results could not be relied on given the relatively small support size of 10 m x 10 m x 3 m as compared to the input grid of 200 m x 100 m x 3 m. In this case, DeeSse was more reliable as it was also dependent on the TI which is at a grid size of 10 m x 10 m x 3 m in addition to the input data. Further possible improvements on the TI and DeeSse were identified. These included re-parametrising the variogram and kriging inputs in order to reduce the over-smoothing in the TI and developing a more representative TI.

The subsequent DeeSse simulations from the EA were then used to quantify the uncertainty around the estimates, calculate probably plots for different thresholds and develop stochastic grade-tonnage curves. Furthermore, uncertainties and distributions of the metal content estimates, and revenue projections were determined. The two research questions in this study are answered as follows:

- DeeSse was shown to enhance resource modelling in the extension area by providing a more robust approach for estimating grades in areas with a low sampling density. The use of TI and conditioning data provided more confidence on the DeeSse estimates as they were based on abundant "sampling' information. DeeSse also allowed for uncertainty quantification around the estimates.

- Stochastic resource estimation was integrated into grade-tonnage curves calculation, metal content estimation and revenue projections by calculating averages about cut-offs for all 50 simulations. The distributions of metal content estimates and revenue projections can then be determined and reported instead of reporting single values. Alternatively, the grade-tonnage curves, metal content, and revenues can be classified and reported according to worst-, best - and base- case scenarios.

Although the application of DeeSse was successful, challenges around the smoothing of low and high grades within the TI were apparent. Volumetric uncertainty (i.e. uncertainty of the thickness of the reef zone) was not considered in the study. Therefore, it would be sub-optimal to follow the methodology described herein if the thickness within the selected domain was not known to be fairly constant. The need to use a cuboid model for DeeSse also meant that a large number of unnecessary blocks were included in the simulation. This would be very problematic when simulating large orebodies as it will increase computing costs and simulation time.

6.2. Recommendations

The following recommendations are suggested for further study:

- In order to improve the limitation brought about by kriging in the TI, it is recommended that a number of TIs be investigated. These TIs should include alternatives which will have a lesser smoothing effect when modelling the TI.

- Different sizes of TIs should also be considered and analysed to get a better understanding of the effect of the size of the TI on the quality of the simulations.

- The use of a secondary variable such as geophysical data together with the training image and drill hole samples should be considered.

- In addition to the grade uncertainty, the uncertainty of the geology should be integrated by simulating reef thickness or contacts between different lithologies.

- Instead of just comparing the SGSIM and DeeSse etype estimates in the EA; compare them to other approaches which would normally be used in areas where sampling density is low.

- Investigate the effect of change of support when using DeeSse in sparsely spaced areas and how that compares to SGSIM.

- Consider using a more comprehensive software designed with the entire value chain of Mineral Resource estimation and mine planning in mind. This will ensure that software integration issues are avoided and perhaps the need to estimate within a cuboid is illuminated.

- Instead of just calculating overall reserves, the grade and geological uncertainty can be introduced at the pit optimisation stage. At this stage, other uncertainties around operational parameters and financial aspects can be introduced.

REFERENCES

Aboagye, M., 2019. *Personal Communication (Unit Manager Resource Estimation Tarkwa Mine)* [Interview] (November 2019).

Abzalov, M., 2016. *Applied Mining Geology: Modern Approaches in Solid Earth Sciences.* 1st ed. Basel: Springer International Publishing.

Albor Consuegra, F.R., & Dimitrakopoulos, R., 2010. Algorithmic approach to pushback design based on stochastic programming: method, application and comparisons. *Transactions of the Institutions of Mining and Metallurgy: Section A,* 119(2), pp. 88-101.

Amarante, F.A.N , Rolo, R.M & Costa, J.F.C.L, 2019. Assessing Geologic Model Uncertainty - A Case Study Comparing Methods. *REM - International Engineering Journal,* 72(4), pp. 643-653.

Armstrong, M., 1998. *Basic Linear Geostatistics.* Berlin: Springer -Verlag.

Arpat, G.B. & Caers, J., 2007. Conditional Simulation with Patterns. *Mathematical Geology,* 39(2), pp. 117-203.

Bardossy, A., 2002. *Introduction to Geostatistics,* 2002: Institute of Hydraulic Engineering at the University of Stuttgart.

Bardossy, G. & Fodor, J., 2001. Traditional and New Ways to Handle Uncertainty in Geology. *Natural Resources Research,* 10(3), pp. 179-187.

Boisvert, J.B., Pyrcz, M.J. & Deutsch, C., 2007. Multiple-Point Statistics for Training Image Selection. *Natural Resources Research ,* Volume 16, pp. 313–321.

Boucher, A., Dimitrakopoulos, R. & Vargas-Guzmán, J., 2004. Joint Simulations, Optimal Drillhole Spacing and the Role of the Stockpile. In: O. Leuangthong & Deutsch. C.V, eds. *Geostatistics Banff.* Dordrecht: Springer, pp. 35-44.

Chanderman, L., 2017. *Application of Stochastic Orebody Simulation Techniques to assess Geological Volume and Grade Uncertainty for Gold Reef Deposits,* Johannesburg: University of the Witwatersrand (Msc. Thesis).

Chilès, J. & Delfiner, P., 1999. *Geostatistics: Modeling Spatial Uncertainty.* 2nd ed. New York: John Wiley & Sons .

Clark, I., 1986. *The Art of Cross Validation in Geostatistical Applications.* Littleton, 19th Application of Computers and Operations Research in the Mineral Industry, Society of Mining Engineers.

Clark, I., 2015. Regression revisited (again). *Journal of The Southern African Institute of Mining and Metallurgy,* Volume 115, pp. 45-50.

Clark, I. & Harper, B., 2000. *Practical Geostatistics 2000.* Ecosse: Geostokos.

Collings, P., Khosrowshahi, S. & Ness, P., 2001. Geological Modelling and Geostatistical Resource Estimation of the Hope North Deposit. In: A. Edwards, ed. *Mineral Resource and Ore Reserve Estimation – The AusIMM Guide to Good Practice.* Melbourne: The Australasian Institute of Mining and Metallurgy , pp. 269–284.

Cressie, N., 1990. The Origins of Kriging. *Mathematical Geology,* 22(3), pp. 239-252.

Dagasan, Y., Erten, O., Renard, P., Straubhaar, J.; Topal, E., 2019. Multiple-Point Statistical Simulation of the Ore Boundaries for a Lateritic Bauxite Deposit. *Stochastic Environmental Research and Risk Assessment Volume,* Volume 33, p. 865–878.

Datamine, 2020. *Datamine StudioRM Product* . Datamine.

David, M., 1977. Theoretical Basis of the Approach: The Theory of Regionalized Variables. In: M. David, ed. *Geostatistical Ore Reserve Estimation.* Amsterdam: Elsevier Scientific Publishing Company, pp. 91-114.

de Carvalho, J. & Dimitrakopoulos, R., 2019. Effects of High-Order Simulations on the Simultaneous Stochastic Optimization of Mining Complexes. *Minerals,* 9(4:210), pp. 1-15.

De Souza, L., Felipe J, Costa, J.F.C.L. & Koppe, J., 2004. Uncertainty Estimate in Resources Assessment: A Geostatistical Contribution. *Natural Resources Research,* 13(1), pp. 1-15.

Deutsch, C.V. & Deutsch, J., 2015. *Introduction to Choosing a Kriging Plan.* [Online] Available at:
http://www.geostatisticslessons.com/pdfs/introkrigingplan.pdf
[Accessed 25 September 2020].

Deutsch, C.V. & Journel, A., 1997. *GSLIB Geostatistical Software Library and User Guide.* 2nd ed. New York,: Oxford University Press.

Deutsch, J., Szymanski, J. & Deutsch, C.V., 2014. Checks and measures of perfomance for kriging estimates. *The Journal of the Southern African Institute of Mining and Metallurgy,* Volume 114, pp. 223 - 230.

Dimitrakopoulos, R., 2011. Stochastic Optimization for Strategic Mine Planning: A Decade of Developments. *Journal of Mining Science,* 47(2), pp. 138-150.

Dimitrakopoulos, R. & Godoy, M., 2014. Grade control based on economic ore/waste classification functions and stochastic simulations: Examples, comparisons and applications. *Institute of Materials, Minerals and Mining; Mining Technology,* 123(2), pp. 90-106.

Dohm, C., 2004. Quantifiable Mineral Resource Classification - A Logical Approach. In: O. Leuangthong & C. Deutsch, ed. *Geostatistics Banff.* Springer, pp. 333-342.

Dohm, C., 2019. *MINN 7006 Geostatistical Evaluation of Mineral Resources Course Notes.* Johannesburg: University of the Witwatersrand.

Emery, X. & Lantuéjoul, C., 2014. Can a Training Image Be a Substitute for a Random Field Model?. *Mathematical Geosciences,* Volume 46, pp. 133–147.

Emery, X., Ortiz, J.M. & Rodriguez, J.J., 2006. Quantifying Uncertainty in Mineral Resources by Use of Classification Schemes and Conditional Simulations. *Mathematical Geology ,* 38(4), pp. 445-464.

Ersoy, A. & Yunsel, T.Y, 2006. Geostatistical Conditional Simulation for the Assessment of the Quality Characteristics of Cayırhan Lignite Deposits. *Energy Exploration and Exploitation,* 24(6), pp. 391-416.

Eskandari, K. & Srinivasan, S., 2008. Reservoir Modelling of Complex Geological Systems--A Multiple-Point Perspective. *Journal of Canadian Petroleum Technology,* 49(8), pp. 59-68.

Everett, J.E. & Grobler, F., 2013. Optimised ore selection from conditionally simulated block models. *Transactions of the Institutions of Mining and Metallurgy: Section B, Applied Earth Science,* 122(4), pp. 207-216.

Garcia, M., 2016. *Stochastic Orebody Modelling and Stochastic Long-Term Production Scheduling for an Iron Ore Deposit, in Northern Quebec (MSc. Thesis).* Montreal: McGill University.

Glacken, I.M, 1996. *Change of Support by Direct Conditional Block Simulation, MSc Thesis,* Stanford: Stanford University.

Glacken, I.M. & Snowden, D., 2001. Mineral Resource Estimation. In: A. Edwards, ed. *Mineral Resource and Ore Reserve Estimation - The AusIMM Guide to Good Practice.* Melborne: The Australasian Institute of Mining and Metallurgy, pp. 189-198.

Godoy, M. & Dimitrakopoulos, R., 2011. A Risk Quantification Framework for Strategic Mine Planning: Method and Application. *Journal of Mining Science,* 47(2), pp. 235-246.

Goldfields, 2019. *Mineral Resources and Mineral Reserves Supplement,* Johannesburg: Goldfields.

Goovaerts, P., 1999. Impact of the Simulation Algorithm, Magnitude of Ergodic Fluctuations and a Number of Realizations on the Spaces of Uncertainty of Flow Properties. *Stochastic Environmental Research and Risk Assessment,* Volume 13, pp. 161–182.

Guardiano, F. & Srivastava, R., 1992. *Multivariate Geostatistics: Beyond Bivariate Moments.* Dordrecht, Geostatistics Troia ’92, Quantitative Geology and Geostatistics, vol 5., Springer.

Guibal, D., 2001. Variography, a Tool for the Resource Geologist. In: A. Edwards, ed. *Mineral Resource and Ore Reserve Estimation – The AusIMM Guide to Good Practice.* Melbourne: The Australasian Institute of Mining and Metallurgy, pp. 85–90.

Hashemi, S., Javaherian, A., Ataee-pour, M. & Khoshdel, H., 2014. Two-Point Versus Multiple-Point Geostatistics: The Ability of Geostatistical Methods to Capture Complex Geobodies and Their Facies Associations — An Application to a Channelized Carbonate Reservoir, Southwest Iran. *Journal of Geophysics and Engineering,* 11(6), p. 065002.

Holland, N., 2020 "2019 Results Presentation". *Gold Fields Full Year 2019 Results Presentation.* Johannesburg: Gold Fields.

Hosseini, S., Asghari, O. & Emery, X., 2017. Direct Block-Support Simulation of Grades in Multi-Element Deposits: Application to Recoverable Mineral Resource Estimation at Sungun Porphyry Copper-Molybdenum Deposit. *The Journal of the Southern African Institute of Mining and Metallurgy,* Volume 117, pp. 577-585.

Hu, L. & Chugunova, T., 2008. Multiple-Point Geostatistics for Modeling Subsurface Heterogeneity: A Comprehensive Review. *Water Resources Research,* 44(11), p. W11413.

Isaaks, E.H., 2005. The Kriging Oxymoron: A Conditionally Unbiased and Accurate Predictor (2nd Edition), *Geostatistics Banff 2004: Quantitative Geology and Geostatistics .* Dordrecht: Springer, pp. 363-374.

Isaaks, E.H. & Srivastava, I.M., 1989. *An Introduction to Applied Geostatistics.* 1st ed. New York: Oxford University Press.

Jara, R.M, Couble, A, Emery, X, Magri, E.J, Ortiz, J.M, 2006. Block Size Selection and Its Impact on Open-pit Design and Mine Planning. *Journal of The South African Institute of Mining and Metallurgy,* Volume 106, pp. 205-211.

Johnson, T., 2001. Structural Block Modelling at BHP Iron Ore's Mt Whaleback Mine. In: A. Edwards, ed. *Mineral Resource and Ore Reserve Estimation – The AusIMM Guide to Good Practice.* Melbourne: The Australasian Institute of Mining and Metallurgy, pp. 169-186.

Journel, A.G., 1974. Geostatistics for Conditional Simulation of Ore Bodies. *Economic Geology,* Volume 69, pp. 673-687.

Journel, A.G., 1989. *Fundamentals of Geostatistics in Five Lessons.* Washington, D.C., American Geophysical Union.

Journel, A.G., 2003. *Multiple-point Geostatistics: A State of the Art,* Stanford: Stanford Center for Reservoir Forecasting.

Journel, A.G. & Deutsch, C.V., 1993. Entropy and Spatial Disorder. *Mathematical Geology,* 25(3), pp. 329-355.

Journel, A.G. & Huijbregts, C., 1978. Simulation of Deposits. In: *Mining Geostatistics.* London: Academic Press Limited, pp. 500-554.

Journel, A. G. & Zhang, T., 2005. *The Necessity of a Multiple-Point Prior Model,* Stanford: Department of Geological and Environmental Science Stanford University.

Khosrowshahi, S. & Shaw, W., 2001. Conditional Simulation for Resource Characterisation and Grade Control—Principles and Practice. In: A. Edwards, ed. *Mineral Resource and Ore Reserve Estimation – The AusIMM Guide to Good Practice.* Melbourne: The Australasian Institute of Mining and Metallurgy, pp. 285-292.

Kitts, D., 1976. Certainty and Uncertainty in Geology. *American Journal of Science,* Volume 276, pp. 29-46.

Krige, D.G., 1951. *A statistical approach to some mine valuation and allied problems on the Witwatersrand,* Johannesburg: University of the Witwatersrand.

Krige, D.G., 1960. On the departure of ore value distributions from the lognormal model in South African gold mines. *Journal of the Southern African Institute of Mining and Metallurgy,* 61(4), pp. 231 - 244.

Krige, D.G., 1996. *A Practical Analysis of the Effects of Spatial Structure and of Data Available and Accessed, on Conditional Biases in Ordinary Kriging.* Wollongong, International Geostatistics Congress.

Krige, D.G., 1999. Essential Basic Concepts in Mining Geostatistics and their Links with Geology and Classical Statistics. *South African Journal of Geology,* 102(2), pp. 147-151.

Leite, A. & Dimitrakopoulos, R., 2007. Stochastic Optimisation Model for Open Pit Mine Planning: Application and Risk Analysis at a Copper Deposit. *Mining Technology,* 116(3), pp. 109-118.

Leuangthong, O., McLennan, J. & Deutsch, C.V., 2004. Minimum Acceptance Criteria for Geostatistical Realizations. *Natural Resources Research ,* Volume 13, pp. 131-141.

Leuangthong, O. & Nowak, M., 2015. Dealing with High-grade Data in Resource Estimation. *The Journal of The Southern African Institute of Mining and Metallurgy,* Volume 115, pp. 27-36.

Lochbühler, T., Pirot, G., Straubhaar, J. & Linde, J., 2014. Conditioning of Multiple-Point Statistics Facies Simulations to Tomographic Images. *Mathematical Geosciences,* Volume 46, pp. 625–645.

Mann, C.J., 1993. Uncertainty in Geology. In: J. Davis & J.C Hersfeld, eds. *Computers in Geology - 25 years of Progress.* New York: Oxford University Press , pp. 247.

Mariethoz, G., 2018. When Should We Use Multiple-Point Geostatistics? In: 1st, ed. *Handbook of Mathematical Geosciences: Fifty Years of IAMG.* Cham: Springer, pp. 645-653.

Mariethoz, G. & Caers, J., 2014. *Multi-point Geostastics: Stochastic Modeling with Training Images.* 1st ed. Hoboken: Wiley Publishers, pp. 155-171.

Mariethoz, G., Renard, P. & Straubhaar, J., 2010. The Direct Sampling Method to Perform Multiple-Point Geostatistical Simulations. *Water Resources Research,* 46(11), pp. 1-14.

Matheron, G., 1971. *The Theory of Regionalised Variables and Its Application,* Fontainebleau: Ecole Nationale Superieure des Mines de Paris.

Matheron, G. & Kleingeld, W., 1987. The Evolution of Geostatistics. *Journal of the Southern African Institute of Mining and Metallurgy,* Volume 3, pp. 9-12.

Meerschman, E, Pirot, G, Mariethoz, G, Straubhaar, J, Van Meirvenne, M, Renard, P, 2013. A Practical Guide to Performing Multiple-Point Statistical Simulations with the Direct Sampling Algorithm. *Computers & Geosciences,* Volume 52, pp. 307-324.

Menabde, M., Froyland, G., Stone, P. & Yeates, G., 2018. Mining Schedule Optimisation for Conditionally Simulated Orebodies. In: R. Dimitrakopoulos, ed. *Advances in Applied Strategic Mine Planning.* Cham: Springer International Publishing, pp. 91-100.

Mustapha, H. & Dimitrakopoulos, R., 2011. HOSIM: A high-order stochastic simulation algorithm for generating three-dimensional complex geological patterns. *Computers and Geosciences,* 37(9), pp. 1242-1253.

Oriani, F, Mehrotra, R, Mariethoz, G, Straubhaar, J, Sharma, A, & Renard, P, 2018. Simulating Rainfall Time-Series: How to Account for Statistical Variability at Multiple Scales?. *Stochastic Environmental Research and Risk Assessment,* Volume 32, pp. 321–340.

Ortiz, J.M. & Deutsch, C.V., 2004. Indicator Simulation Accounting for Multiple-Point Statistics. *Mathematical Geology,* 36(5), pp. 545-565.

Peredo, O. & Ortiz, J.M., 2011. Parallel Implementation of Simulated Annealing to Reproduce Multiple-point Statistics. *Computers and Geosciences,* Volume 37, pp. 1110-1121.

Perez, C., Ortiz, J. & Boucher, A., 2015. Geological Resources Modelling in Mining. In: G. Mariethoz, ed. *Multiple-Point Geostastistics; Stochastic Modeling with Training Images.* Sussex: John Wiley & Sons, pp. 329-343.

Pérez-Díaz, L., Alcalde, J. & Bond, C.E, 2020. Handling Uncertainty in the Geosciences: Identification, Mitigation and Communication. *Solid Earth,* 11(3), pp. 889-897.

Pluyaud, P, D'Or, D, David, E, Walgenwitz, A, Renard, P, & Straubhaar, J., 2019. *3D Geological Modeling Using Cutting-Edge Multiple-Point Statistics Technology (White paper),* Geneva: Ephesia Consult.

Renard, P., Julien Straubhaar, J. & Madani, N., 2019. *Introduction to Facies Modelling using PluriGaussian Simulations and Multiple-Point Statistics (Course Presentations),* Neuchatel: University of Neuchatel.

Rivoirard, J., 1987. Computing Variograms on Uranium Data. In: G. Matheron & M. Armstrong, eds. *Geostatistical Case Studies.* Dordrecht: D. Reidel Publishing Company, pp. 1-22.

Rongier, G., Collon, P. & Renard, P., 2017. A Geostatistical Approach to the Simulation of Stacked Channels. *Marine and Petroleum Geology,* Volume 82, pp. 318 - 335.

Rossi, M.E., 2003. *Practical Aspects of Large-Scale Conditional Simulations.* Johannesburg, Application of Computers and Operations Research in the Minerals Industries, South African Institute of Mining and Metallurgy.

Rossi, M.E. & Alvarado, S., 1998. *Conditional Simulations Applied to Recoverable Reserves.* London, APCOM '98 Conference, Institution of Mining and Metallurgy.

Rossi, M.E. & Camacho, J.E., 2004. Application of conditional simulations to resource classification schemes. *CIM Bulletin,* 97(1079), pp. 62-68.

Rossi, M.E. & Deutsch, C.V., 2014. *Mineral Resource Estimation.* 1st ed. Dordrecht: Springer.

SAMREC, 2016. *The South African Code for the Reporting of Exploration Results, Mineral Resources and Mineral Reserves,* Johannesburg: SAMCODES Standards Committee [Online]. Available at:
https://www.samcode.co.za/codes/category/8-reporting-codes? download= 231 :202001_SAMREC%20Code%20with%20Table%201
[Accessed 20 October 2020].

Shaw, W. & Khosrowshahi, S., 1997. *Grade Control Sampling and Ore Blocking: Optimisation Based on Conditional Simulation.* Launceston, Mining Geology Conference, The Australasian Institute of Mining and Metallurgy.

Spatial Analysis Lab, 2005. *Notes on Introduction to Spatial Autocorrelation,* Seattle: School of Oceanography at the University of Washington.

Srivastava, R.M., 2013. Geostatistics: A Toolkit for Data Analysis, Spatial Prediction and Risk Management in the Coal Industry. *International Journal of Coal Geology,* Volume 112, pp. 2-13.

Srivastava, RM., 2018. The Origins of the Statistics (MPS) Algorithm. In: B. Daya Sagar, Q. Cheng & F. Agterberg, eds. *Handbook of Mathematical Geosciences.* Cham: Springer International Publishing, pp. 665-672.

Straubhaar, J., Renard, P. & Mariethoz, G., 2016. Conditioning Multiple-Point Statistics Simulations to Block Data. *Spatial Statistics,* Volume 16, pp. 53-71.

Straubhaar, J, Renard, P, Mariethoz, G, Froidevaux, R & Besson, O, 2011. An Improved Parallel Multiple-point Algorithm Using a List Approach. *Mathematical Geosciences,* Volume 43, pp. 305–328.

Strebelle, S., 2002. Conditional Simulation of Complex Geological Structures Using Multiple-Point Statistics. *Mathematical Geology,* Volume 34, pp. 1–21.

Strebelle, S., 2012. *Multiple-Point Geostatistics: From Theory to Practice. 9th International Geostatistics Congress,* Oslo, Chevron ETC.

Sunday, C. & Deutsch, C., 2020. *Choosing the Discretization Level for Block Property Estimation.* [Online]
Available at: http://geostatisticslessons.com/pdfs/discretization.pdf
[Accessed 20 October 2020].

Tahmasebi, P., 2017. Structural Adjustment for Accurate Conditioning in Large-Scale Subsurface Systems. *Advances in Water Resources ,* Volume 101, pp. 60-74.

Tahmasebi, P., 2018. Multiple Point Statistics: A Review. In: D. Sagar, Q. Cheng & F. Agterberg, eds. *Handbook of Mathematical Geosciences: Fifty Years of IAMG.* Cham: Springer Open, Chapter 30, pp. 613-643.

Tahmasebi, P., Hezarkhani, A. & Sahimi, M., 2012. Multiple-point Geostatistical Modeling Based on the Cross-Correlation Functions. *Computational Geosciences ,* Volume 16, pp. 779–797.

Van der Grijp, Y. & Minnitt, R.C.A, 2015. Application of Direct Sampling Multi-Point Statistic and Sequential Gaussian Simulation Algorithms for Modelling

Uncertainty in Gold Deposits. *The Journal of The Southern African Institute of Mining and Metallurgy,* Volume 115, pp. 73-85.

van der Westhuizen, R., Searra, J. & Hugo, L., 2011. *Tarkwa Gold Mine Technical Report,* Houghton: Goldfields.

Vann, J., Bertoli, O. & Jackson, S., 2002. *An Overview of Geostatistical Simulation for Quantifying Risk.* Fremantle, Geostatistical Association of Australasia.

Vann, J. & Guibal, D., 2001. Beyond Ordinary Kriging — An Overview of Non-Linear Estimation. In: A. Edwards, ed. *Mineral Resource and Ore Reserve Estimation - The AusIMM Guide to Good Practice .* Melbourne: The Australasian Institute of Mining and Metallurgy, pp. 249–256.

Vann, J., Jackson, S. & Bertoli, O., 2003. *Quantitative Kriging Neighbourhood Analysis for the Mining Geologist — A Description of the Method With Worked Case Examples.* Bendigo, 5th International Mining Geology Conference.

Vargas, A.M., 2017. Optimizing Grade-Control Drillhole Spacing with Conditional Simulation. *Minería y Geología,* Volume 33, pp. 1-12.

Wackernagel, H., 2013. *Geostatistical Structure Analysis: The Variogram,* Paris: MINES ParisTech.

Wawruch, T.N. & Betzhold, J.F., 2005. Mineral Resource Classification Through Conditional Simulation. In: *Geostatistics Banff 2004, Quantitative Geology and Geostatistics.* Dordrecht: Springer, pp. 479-489.

Yin, Y. & Feng, W., 2017. A Location-Based Multiple Point Statistics Method: Modelling the Reservoir with Non-Stationary Characteristics. *Open Geosciences,* 9(1), pp. 635–649.

Zhang, T., Switzer, P. & Journel, A.G., 2006. Filter-Based Classification of Training Image Patterns for Spatial Simulation. *Mathematical Geology,* 38(1), pp. 63-80.